Development of active tilt control for a three-wheeled vehicle

Drew, Benjamin William

Award date:
2006

Awarding institution:
University of Bath

DEVELOPMENT OF ACTIVE TILT CONTROL FOR A THREE-WHEELED VEHICLE

Submitted by Benjamin William Drew
for the degree of
Doctor of Philosophy
of the University of Bath
December 2006

ProQuest LLC
789 East Eisenhower Parkway
P.O. Box 1346
Ann Arbor, MI 48106-1346

Contents

List of Figures

List of Tables

Summary

The CLEVER Project was a European Union funded research project to design and develop a low emission alternative vehicle for city environments, which aimed to combine the comfort and safety of a conventional car with the small road footprint and high efficiency of a motorcycle. The project comprised nine industrial companies and academic institutions from across Europe who collaborated to prove the concept. The project resulted in the construction of five prototypes: three were used for crash testing, one was used for chassis development, and one was a show vehicle.

This thesis focuses on the design, development and testing of the novel tilting system that was the focus of the research at the University of Bath. The role of the chassis of CLEVER is to provide safe and predictable handling while satisfying the requirements of the project. Due to the narrow wheel track, the CLEVER vehicle needs to bank into corners in a similar manner to a motorcycle to maintain stability. The requirement of car-like controls necessitates an active, automatic tilting system.

The two primary components of the tilting chassis are an active control system, which controls an actuation system that performs the tilting action. While previous work includes modelling and simulation of active control systems, none have taken the steps to develop an actuation system with which to tilt a vehicle, and none have developed a system appropriate for a serious means of transport.

Through evaluation and assessment of simulation and modelling work for both the active control system and the hydraulic actuation system, the tilting system was developed. Following detailed design work of the chassis systems, a development prototype was constructed, including the implementation of the tilting system in

hardware. The vehicle achieves the targets of the project with the results showing an acceptable correlation with the simulation work.

It is proved that a tilting three-wheeled vehicle with one front wheel and a cabin that tilts, which uses direct tilt control as its tilting strategy, can achieve a balanced cornering condition. Good results for steady state handling were achieved, however, as predicted in the simulation work, transient performance is limited. A high control gain value required to provide fast response also increases the moment applied between the upright rear unit and the tilting cabin. Aggressive steering inputs from the driver allows the vehicle to generate cornering force significantly before the tilting system reaches the balanced point, leading to a dangerous condition and possible rollover.

While the CLEVER vehicle offers a tangible glimpse of an alternative vehicle concept, which has achieved very positive public attention, further work, including the investigation of alternative control strategies and more sophisticated control, is required to enable the concept to succeed.

Notation

Symbol	Description	Units
a	Distance from front wheel axle to CoG	m
A	Pivot point location	
AD0–AD5	Analogue inputs into controller	bits or Volts
A_p	Actuator piston area	m^2
AR	Amplitude ratio	
a_{per}	Perceived lateral acceleration	m/s^2
A_{side}	Side area of vehicle	m^2
a_y	Lateral acceleration	m/s^2
$a_{y,\text{max}}$	Maximum lateral acceleration	m/s^2
b, b_1, b_2	Lever arm	m
b_{max}	Maximum lever arm	m
B_p	Viscous damping in actuator	Ns/m
c	Damping in tilt mechanism	Ns/rad
C	Linear damping in actuator	Ns/m
C_d	Coefficient of drag	
C_e	Valve coefficient	
CoG	Centre of gravity	
C_x	Flow gain	
C_{x1}	Flow gain for actuator one	
C_{x1}	Flow gain for actuator two	
C_p	Flow pressure gain	
C_{p1}	Flow pressure gain for actuator one	
C_{p2}	Flow pressure gain for actuator two	
db	Valve deadband (15% valve opening)	bits
d_{cyl}	Actuator piston diameter	m
d_{hose}	Flexible hose diameter	m
F_a	Force provided by actuator	N
F_L	Load force	N
F_w	Wind force	N
F_{YL}	Lateral force on left hand wheel	N
F_{YR}	Lateral force on right hand wheel	N
F_{ZL}	Vertical force on left hand wheel	N

Symbol	Description	Units
F_{ZR}	Vertical force on right hand wheel	N
g	Gravitational constant	$9.81\,\mathrm{m/s^2}$
G	Proportional constant (gain) relating T_{act} to θ_e	Nm/rad
G_1	Transfer function relating x_v to x_p	
G_2	Transfer function relating F_L to x_p	
G_{min}	Minimum value for G	Nm/rad
h	Distance from ground/tilting axis to CoG	m
g_i	Integer value of gravitational constant used in controller	bits
$\Im$	Imaginary part	
I_x	Tilting cabin roll inertia about tilt axis	$\mathrm{kgm^2}$
J	Total cabin inertia ($I_x + mh^2$)	$\mathrm{kgm^2}$
k	Scaling factor used in controller	
K_A	Amplifier gain	A/V
k_d	Derivative gain	
k_p	Proportional gain	
K_T	Position transducer gain	V/m
K_V	valve gain	m/A
$k_\theta, k_{\theta 1}, k_{\theta 2}$	Gain relating actuator extension with tilt angle	m/rad
l	Wheelbase	m
l_{hose}	Length of flexible hose	m
l_i	Integer value of wheelbase used in controller	bits
m	Mass of tilting cabin	kg
M_{cog}	Moments around CoG	Nm
M_{t}	Moment applied between tilting body and base	Nm
$M_{\mathrm{t,max}}$	Maximum moment applied between tilting body and mass	Nm
P	Power	kW
ΔP	Pressure drop across one side of valve	$\mathrm{N/m^2}$
P_1, p_1	Pressure in actuator one	$\mathrm{N/m^2}$
P_2, p_1	Pressure in actuator two	$\mathrm{N/m^2}$
P_m	Load pressure ($P_1 - P_2$)	$\mathrm{N/m^2}$
P_{max}	Maximum system pressure	$\mathrm{N/m^2}$
P_s	Supply pressure	$\mathrm{N/m^2}$
Q/q	Flow	$\mathrm{m^3/s}$
Q_1, q_1	Flow into chamber one	$\mathrm{m^3/s}$
Q_2, q_1	Flow out of chamber two	$\mathrm{m^3/s}$
Q_{compl}, Q_c	Flow due to compliance	$\mathrm{m^3/s}$
Q_{displ}, Q_d	Flow due to displacement	$\mathrm{m^3/s}$
$\Re$	(Real) part	
R	Corner radius	m
R	Log modulus of amplitude ratio (Chapter 4)	dB

Symbol	Description	Units
s	Laplace operator	
t	Wheel track	m
t	Time	s
T	Torque	Nm
T_{act}	Torque generated by actuators	Nm
T_{dist}	Torque generated by disturbances	Nm
T_{max}	Maximum torque generated by actuators	Nm/rad
V	Forward velocity	m/s
V_1	Volume of actuator one	m^3
V_2	Volume of actuator two	m^3
V_i	Command valve voltage	V
V_o	Voltage feedback from tilt position	V
VA	Analogue output from controller to control valve	bits or Volts
VB	Analogue output from controller to unloading valve	bits or Volts
V_{compl}	Differential change in volume	m^3
V_i	Integer value of speed used in controller	bits
V	Total volume of actuator and hoses	m^3
X	Valve input	percent
x_p	Actuator extension	m
x_{p1}	Piston displacement for actuator 1	m
x_{p2}	Piston displacement for actuator 1	m
x_v	Valve input	%/Volts/bits

Symbol	Description	Units
β	Bulk modulus	N/m^2
β_e	Effective bulk modulus	N/m^2
δ	Steer angle	deg or rad
δ_i	Integer value of steer angle used in controller	bits
δ_{ic}	Centralised integer value of steer angle used in controller	bits
θ	Tilt angle	deg or rad
θ_d	Demand tilt angle	deg or rad
θ_e	Tilt angle error $(\theta_d - \theta)$	deg or rad
θ_i	Integer value of tilt angle used in controller	bits
θ_{ic}	Centralised integer value of tilt angle used in controller	bits
θ_{ss}	Steady-state tilt angle	deg or rad
ρ	Density of air	kg/m^3
τ	First order lag time constant	s
ϕ	Phase angle	deg
ω	Rotational velocity	rad/s
ω_n	Natural frequency	rad/s
ζ	Damping ratio	

Acknowledgements

Firstly, I would like to thank my supervisors, Dr Jos Darling, Prof Kevin Edge and Dr Geraint Owen, for their support, guidance, help and patience throughout the project, and Prof Andrew Plummer for his additional help. In addition, I must express my gratitude towards my colleague and friend, Matt Barker.

I also appreciate the support and encouragement I received from my other colleagues, peers, friends and family. In particular, I thank my parents for proof-reading this thesis, and Chris Lamming for his friendship, and for inspiring and encouraging a curious engineering mind.

My thanks also extend to the project partners across Europe, who, through their support for the project, enabled me to travel and experience a wide range of cultures and places during the work.

I gratefully acknowledge the European Commission for the funding they provided for the CLEVER Project under contract reference number G3RD-CT-2002-00815. I also acknowledge the additional contribution that BMW AG made towards the project, enabling the manufacture and construction of the development prototype.

Finally, I thank my wife, Elizabeth, for her everlasting love and support.

Chapter 1

Introduction

The need for personal mobility in urban environments has led to traffic congestion and increased pollution. One solution is to increase the number of people per vehicle through the use of public transport or car sharing. It is evident, however, that most people prefer individual transport whenever possible. While conventional cars provide high levels of passive safety and comfort, they have a large road footprint and produce high emissions. Motorcycles consume minimal urban space and are generally more fuel efficient per seat, but are considered unsafe and offer no protection from the elements. The development of an alternative vehicle concept aiming to marry the comfort and passive safety of cars with the minimal urban space requirements and efficiency of motorcycles is the objective of the EU-funded research project, CLEVER [1, 2]. One of the unique features of this vehicle concept is a narrow wheeltrack. As such, a tilting chassis is required to maintain stability. The subject of this thesis was the development, implementation and initial testing of the active tilting control system and its actuation system.

1.1 Project Overview

The CLEVER Project is a collaborative research project comprising nine partners from industry and academia. CLEVER is an acronym standing for 'Compact Low Emission VEhicle for uRban transport'. The role of the University of Bath is the

definition, development and design of the chassis and the chassis systems, including the steering, suspension, transmission and braking systems, with the tilting mechanism being the main focus. The target of the project was the production of a proof-of-concept prototype that highlights new technologies that could be employed in similar vehicles of the future. It is suggested that by 2012 in the UK, there will be up to 20,000 vehicles in this 'sub-car' bracket [3].

One of the main focuses of the project is to produce an environmentally friendly vehicle with low fuel consumption and carbon dioxide (CO_2) emissions. A target of 60 g/km was set (equating to an equivalent gasoline consumption of 2.4 l/100 km (108 miles per gallon)), accompanied with the aim of reducing other hydro carbon and nitrous oxide emissions to 10% of current Euro IV legislation [4]. (To put these figures in perspective, a Ford Focus with a 1.6/,l gasoline engine produces CO_2 emissions of 161 g/km, and has a combined fuel consumption of 6.7 l/100 km (42 miles per gallon) [5].) One method of achieving these targets is by using an 'alternative' fuel. Compressed Natural Gas (CNG), while having a lower calorific value than conventional gasoline, produces significantly less CO_2 than gasoline or diesel fuel. The use of CNG as an automotive fuel is growing, but large areas exist where the supply infrastructure is poor, so a new refuelling technology with exchangeable gas cylinders is required.

In order to provide similar comfort levels to conventional cars, the cabin of CLEVER must be fully enclosed. Occupant protection must also be comparable to current city oriented cars which achieve a three star rating in the Euro NCAP tests. To achieve this passive safety rating, a full safety frame is required including crash elements and crumple zones that help reduce the high decelerations experienced in an accident and prevent any intrusion into the occupant space. In addition to occupant protection, a high level of pedestrian protection is required.

CLEVER must also appeal to a large proportion of motorists, and as such, must have conventional car-like controls. Preliminary market research conducted by one of the project partners [6] determined that the vehicle must look good, be safe, offer weather protection and not require further training or development of skills, as is currently required to ride motorcycles. Another reason supporting the need for car-like controls in CLEVER is vehicle classification. Current legislation classifies such novel concepts on a case-by-case basis, categorising a vehicle as

either a car or a motorcycle. Car manufacturers have a commitment to reduce their overall fleet emissions to reach 140 g/km by 2009, and to 120 g/km by 2021 [7, 8]—motorcycles are excluded—and for CLEVER type vehicles to be included in these calculations, the vehicle must be seen to replace conventional cars. One of the outputs of the project is a proposal of a vehicle category situated between motorcycles and cars.

Another target of CLEVER is to reduce the consumption of road space in urban environments, as this would bring advantages with respect to parking and traffic congestion—two CLEVER vehicles could fit in the space provided for one conventional car. To achieve this, the external dimensions of CLEVER are fixed at 1 metre wide, 3 metres long and less than 1.4 metres high. To accommodate two occupants within the vehicle, a tandem seat arrangement is proposed, with the passenger seated behind the driver. This small vehicle size is also necessary to achieve low fuel consumption; the reduced frontal area of such a narrow vehicle reduces the aerodynamic drag [9].

1.2 Tilting Chassis Concept

The role of the chassis of CLEVER is to provide safe and predictable handling while satisfying the requirements set out above. The important requirements having a large effect on the chassis arrangement of CLEVER are its external size and its requirement for car-like controls.

Due to the narrow width of CLEVER, the wheeltrack is correspondingly small. Vehicles have a tendency to roll out of corners, and those with a narrow wheel track with respect to the height of the centre of mass could unload the inner wheel, leading to roll-over. In order to maintain stability, a tilting chassis is one possible solution.

In order to provide car-like controls in a narrow vehicle, the tilting system cannot be controlled in a similar manner to motorcycles. Motorcycle control requires rider skill in order to balance the lateral acceleration forces with the gravitational forces acting on the vehicle and the motorcyclist. In addition, motorcyclists employ a subtle counter-steering input to enter and exit a steady state

corner, whereas drivers of the CLEVER vehicle are not expected to input a similar counter-steering input with a steering wheel. For this reason, an active control system must be employed to monitor the vehicle states and actively tilt the vehicle automatically towards the centre of the turn. This tilting system must also include an energy efficient actuation system to provide the tilting torque without significantly impacting on the fuel consumption and emissions of the vehicle.

The objective of this research is the design and development of the control and actuation systems employed in this tilting chassis for the CLEVER vehicle. An initial investigation of previous and existing tilting vehicles is undertaken to establish the state of the art. From this research, the tilting system is designed, and using simulation models, the active control system is developed. The actuation system is also designed, and models were developed to evaluate the complete tilting system. The system was then constructed in hardware including the implementation on a realistic dedicated prototype vehicle which was tested and tuned to provide a stable, safe and agreeable driving characteristic, meeting the targets of the CLEVER Project.

1.3 CLEVER Specifications

Table 1.1 is a summary of the initial target specifications for the CLEVER vehicle.

* indicates that these are drivers' subjective assessments, on a scale from 0–10, with 10 being an 'excellent' rating.

Figure 1.1 shows illustrations of the initial styling concepts for the CLEVER vehicle.

Item	Description
Length	3 m
Width	1 m
Height	1.4 m
Wheelbase	2.4 m
Wheeltrack	0.84 m
Top speed	100 kph
Acceleration 0–60 kph	7–8 sec
Driving range	200 km
C_D·A value	0.4–0.5 m^2
Unladen mass	250–350 kg
CO_2 emissions	60 g/km
Handling	7–8 (> 6 better than Carver [10]*)
Turning circle	8–9 m
Controls	Steering wheel and pedals (car-like)
Comfort	3–4 (> 6 better than Smart [11]*)
Refuelling convenience	4–5 (> 6 better than Smart*)
Occupants	2 in 1+1 tandem seating arrangement
Luggage	40–50 litres
Construction	Lightweight metal frame with plastic body panels
Passive safety	3 stars EuroNCAP
Retail cost	€7000–8000 (series production)

Table 1.1: CLEVER Vehicle specifications

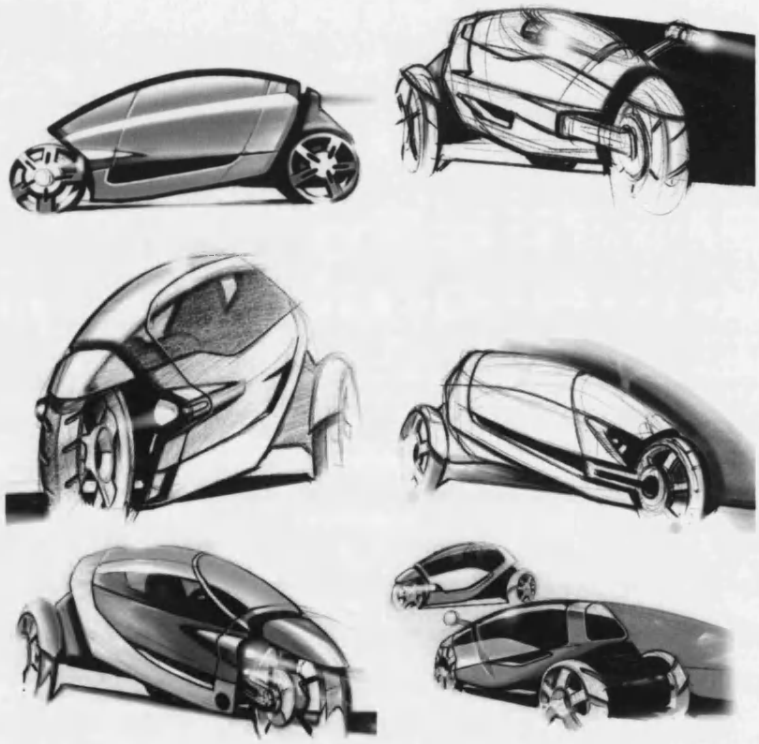

Figure 1.1: Initial styling concepts of the CLEVER Vehicle

Chapter 2

Review

2.1 Tilting Vehicles

2.1.1 Narrow Vehicles

Narrow track vehicles have been identified as a possible solution to the problems of congestion and emissions within a city environment [12]. The main issue with narrow vehicles is their instability in corners. In general, vehicles with a narrow wheel track relative to the centre of mass height are prone to rolling over in a corner [13]—narrowness and reluctance to rollover are mutually exclusive traits in narrow non-tilting 3- or 4-wheeled vehicles [14].

Figure 2.1 shows the rear of a narrow vehicle with the forces acting upon the vehicle during a steady state turn to the right. Although the wheels have a width in the diagram, this is shown for clarity; the contact patch is assumed to be infinitessimally small at the centre point of the tyre.

Assuming that the tyres will not slide, the maximum lateral acceleration application before roll over can be calculated when the vehicle is on the limit of rollover,

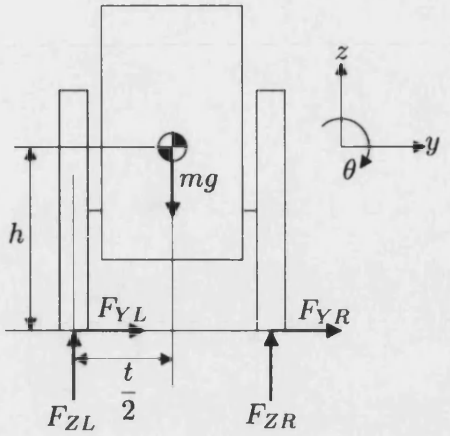

Figure 2.1: Forces acting a non-tilting narrow vehicle in a steady state turn

when $F_{ZR} = F_{YR} = 0$. Taking moments around the centre of gravity:

$$\sum M_{cog} = \frac{F_{ZL}t}{2} - F_{YL}h = 0 \tag{2.1}$$

In this limiting condition, the weight of the vehicle is on the left tyres:

$$F_{ZL} = mg \tag{2.2}$$

and the cornering force on the left tyres is equivalent to the lateral acceleration force:

$$F_{YL} = m\omega^2 R = \frac{mV^2}{R} = ma_y \tag{2.3}$$

So combining equations 2.1, 2.2 and 2.3, the maximum lateral acceleration, $a_{y,\max}$, is governed by equation 2.4.

$$a_{y,\max} = \frac{gt}{2h} \tag{2.4}$$

Thus, for a four-wheeled vehicle (with equal front and rear tracks), the margin of safety against rollover is determined by the ratio of half the wheel track and the height of the centre of mass. To achieve a lateral acceleration of 1 g, the height of the centre of mass must be less than half the wheel track. With a vehicle with a 1 metre wide wheel-track, this would result in a centre of gravity height maximum of 0.5 m. Having such a low centre of gravity height would result in the occupants being positioned very low within the vehicle, impeding accessibility and reducing visibility. The vehicle would also consequently have little ground clearance.

By tilting the centre of mass towards the centre of the curve, this tendency to overturn is reduced. If the tilt axis were at ground level, the lateral force due to cornering in a steady turn combined with the force due to gravity results in no overturning tendency at all [15]. This frees the restriction on the maximum height of the centre of gravity in a narrow vehicle. Figure 2.2 shows a similar narrow vehicle, now tilting (with the tilt axis at ground level), in a steady state right hand corner. Again the forces acting upon the vehicle mass are shown. The non-tilting components are assumed to have no mass.

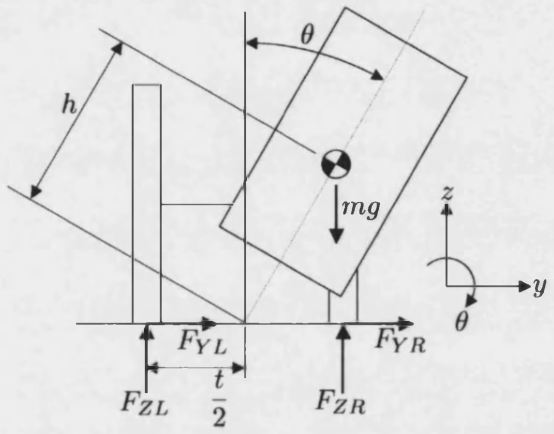

Figure 2.2: Forces acting a tilting narrow vehicle

Again, taking moments about the centre of gravity, we can see that the maximum lateral acceleration is now governed by equation 2.5.

$$\sum M_{cog} = F_{ZL}\left(h\sin\theta + \frac{t}{2}\right) - F_{YL}h\cos\theta = 0 \quad \rightarrow \quad a_{y,\max} = \frac{g(h\sin\theta + \frac{t}{2})}{h\cos\theta} \tag{2.5}$$

The lateral acceleration, $a_{y,\max}$ is now a function of the tilt angle, θ. (Indeed, if $\theta = 0$, we arrive at equation 2.4.) With tilting vehicles, the maximum lateral acceleration before roll over is limited by tyre adhesion and tilt angle limitations.

The above applies to three-wheeled vehicles with one small difference: the line around which the vehicle will roll over is is not the contact point of one of the paired wheels. If the vehicle does roll, it will roll about the line joining the contact patch of the single wheel and one of the paired wheels. As the vehicle

is symmetrical, half the track width is reduced proportionally dependent on the longitudinal position of the centre of gravity [16]. Figure 2.3 is a plan view of a three wheeled vehicle with one front wheel. The dimension a is the longitudinal distance from the front wheel axle to the centre of gravity, and l is the wheelbase.

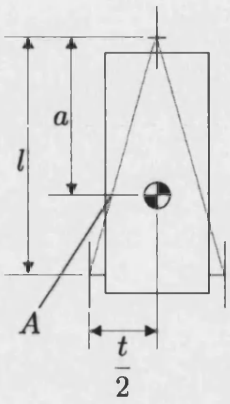

Figure 2.3: Plan view of three-wheeled vehicle

Now, equation 2.4 becomes:

$$\sum M_A = mg\frac{t}{2}\left(\frac{a}{l}\right) - a_{y,\max}mh = 0 \quad \rightarrow \quad a_{y,\max} = \frac{gt}{2h}\left(\frac{a}{l}\right) \tag{2.6}$$

Similarly, equation 2.5 becomes:

$$\begin{aligned} \sum M_A &= mg\left(h\sin\theta + \frac{t}{2}\left(\frac{a}{l}\right)\right) - ma_{y,\max}h\cos\theta = 0 \\ \rightarrow \quad a_{y,\max} &= \frac{g\left(h\sin\theta + \frac{t}{2}\left(\frac{a}{l}\right)\right)}{h\cos\theta} \end{aligned} \tag{2.7}$$

In general, a is less than l, so therefore a three-wheeled vehicle's resistance to rollover is less than that for a four-wheeled vehicle. This effect is emphasised when a three-wheeled vehicle with a single front wheel is braking in a corner. The lever arm about which the acceleration vector acts is reduced further (it becomes less than $\frac{ta}{2l}$), so supporting the common belief that three-wheelers are more unstable than four wheeled vehicles with an equivalent track.

2.1.2 Motorcycles

The most common tilting road vehicle is the bicycle or motorcycle. As motorcycles have effectively zero-wheel-track, motorcycles *must* tilt in order to remain stable. The method in which motorcycles remain stable involves significant rider skill and the use of a subtle counter-steering input (see section 2.2.1 for more details). It is for this reason that when learning to drive a car, one simply has to master the controls to direct, accelerate and decelerate. Learning to ride a motorcycle requires more extensive training to acquire the necessary skills to control a motorcycle. Rice [17] demonstrated that skill plays an important role in motorcycle stability by conducting a study to determine the influences of rider skill and experience on motorcycle manoeuvring. Significant differences between the riders' results illustrates this.

2.1.3 Trains

Considerable research focusing on tilting trains was conducted during the 1960s and 1970s [18]. The main motivation for this development was to maintain passenger comfort while enabling higher cornering speeds. One method to reduce the lateral acceleration felt by passengers is to lay new track with banking in corners and less curvature. The problem with this approach is that while the banking may be suitable for newer high-speed trains, it would be over-tilted for slower-speed and freight trains which share the track. This was overcome in France and Japan by building dedicated lines, but for many other countries, economic and infrastructure reasons associated with an established railway network meant that this was not a viable option. This justifies the attention on tilting trains.

Two methods were investigated: using a high roll axis with the carriage acting as a pendulum that naturally rolls outward, thereby banking passengers to the inside of the curve; or using a low roll axis with the cabin that is actively tilted inwards using an actuation system. Note that a pendulous system actually increases the lateral instability. Initial challenges included the slow response offered by traditional servo systems which caused nausea associated with the unnatural tilting action, but with the advent of the latest digital signal processing technology which can 'read' the line ahead, tilting trains are starting to become more

mainstream [19]. Many European countries now operate active tilting trains. Both passive pendulous and active trains have also reached commercial use in Japan [20].

2.1.4 Tilting Three-Wheeler Chassis Arrangement

Despite their reduced resistance to roll-over, three wheeled vehicles offer significant advantages in chassis design flexibility when incorporating a tilting system. Additionally, three-wheelers also offer advantages in terms of weight savings, since the chassis is not subjected to torsional loads in the case of one-wheel bumps [3, 16]. For this reason, most examples of multi-wheeled tilting vehicles have three wheels.

Many existing tilting three-wheeled vehicles are designed and built by enthusiasts [21]; established car or motorcycle manufacturers have not fully embraced the concept—there are very few examples in mass production largely due to cost and safety concerns.

A number of wheel and tilting arrangements for such vehicles exist, and can be classified into those with one front wheel (delta arrangement), and those with two front wheels (tadpole arrangement).

One Front Wheel

There are two possibilities for tilting three-wheeled vehicles with one front wheel: those with a main tilting structure and separate rear module, or those with a single vehicle frame. With the former, the rear wheels attached to the rear module remain upright with respect to the road at all times, and the cabin tilts independently. The latter has rear wheels that remain in line with the vehicle when tilting. These systems are referred to as 1F1T (one front wheel, one wheel tilting) or 1F3T (one front wheel, three wheels tilting), respectively.

Delta tilting three-wheeler vehicles have the advantage of a simple steering system: a standard motorcycle based system can be employed. The 1F1T design

also facilitates easy power train integration. The rear module can contain the engine and transmission necessary to drive both rear wheels. The whole rear module can be part of the unsprung mass or each rear wheel can be suspended independently. Figure 2.4 shows the tilt joint and the rear traction module of the Honda Gyro Canopy, which contains the complete engine and transmission necessary to drive the vehicle. In this case, the traction module is part of the unsprung mass of the vehicle.

Figure 2.4: Honda Gyro tilt joint

Another merit of the 1F1T design is simple packaging, since the cabin and drive train elements are two separate entities with a single tilt joint. The design also aids implementation of direct tilting system: actuators can be positioned between the two units that rotate the cabin of the vehicle with respect to the upright rear unit.

A disadvantage of such a design is that the rear module of the vehicle does not tilt, and therefore the associated lateral acceleration causes it to roll outwards in a corner. The extent of this problem can be reduced by minimising the rear unit weight and centre of gravity height.

Unlike 1F1T vehicles, 1F3T vehicles do not have two discrete modules. Instead the tilting mechanism is integrated into the vehicle chassis and all wheels camber in turns. In comparison with the 1F1T arrangement, the design has the advantage that the whole vehicle tilts to the balanced position. With the tilt axis on the ground, the design offers handling most like a motorcycle. There are some disadvantages however: transmitting power to both rear wheels is more difficult—drive shafts fitted directly to the wheels require joints that can accommodate the large relative wheel travel. Using a swing arm arrangement requires a differential to be placed between the swing arm mounting points directing drive to the wheels using chains or belts. However, in order to achieve high tilt angles,

space for long swing arms and wheel travel are required. Another possible rear suspension arrangement is a double wishbone type, but again, packaging and power transmission issues arise. Figure 2.5 shows the basic concept of a 1F3T vehicle employing rear swing arms and a prototype vehicle based on this concept.

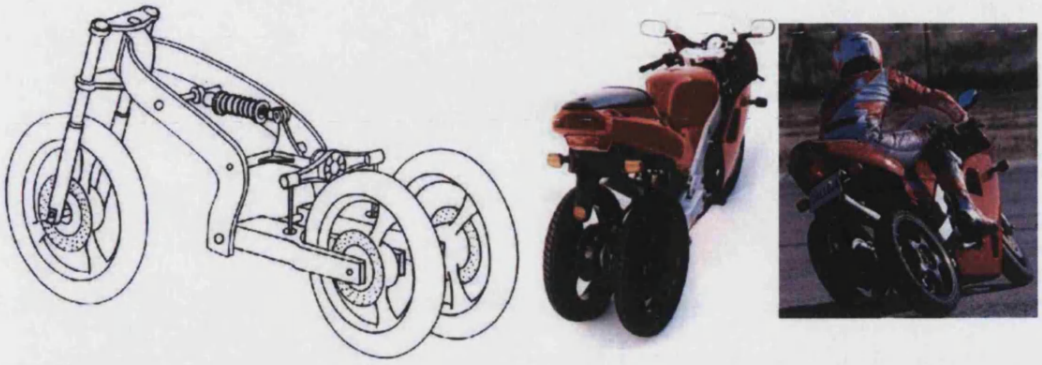

Figure 2.5: A 1F3T concept (left) and prototype vehicle (right) [22]

A merit of a 1F3T design is that by having all wheels tilted, the whole vehicle is balanced. The major limiting factor is the packaging of the rear wheels.

Two Front Wheels

The integration of steering is more complex on three-wheeled vehicles with two front wheels—a car-like system has to be adopted as opposed to a simpler motorcycle setup. This poses further difficulties when integrating a tilting mechanism; the front wheels have to steer, and the geometry has to allow for both a suspension system and a tilting mechanism. However, as a consequence, the drive to the single rear wheel is simple; no differential is needed (assuming rear wheel drive), and a simple motorcycle style trailing swing arm design can be employed as the suspension system.

Existing Concepts

Many concepts of tilting three-wheeled vehicles have been designed and constructed. In the early 1980s, General Motors built a 1F1T tilting three-wheeled vehicle concept dubbed the Lean Machine, owing to its ability to lean in corners and its high fuel efficiency [14]. Foot pedals in the cabin actuated the tilting

system and allowed the tilt angle to be determined by the driver; it did not aim to balance lateral acceleration forces. In addition, the vehicle was also low to the ground, so the tilting mechanism was not used to increase the permissible height of the vehicle [23]. The maximum tilting angle was ±55°. An image of this vehicle is shown in figure 2.6.

Figure 2.6: The General Motors Lean Machine [14]

Although only sold in Japan, the Honda Gyro (figure 2.7) represents an example of a production 1F1T tilting three-wheeled vehicle. Owing to a large carrying capability relative to the vehicle size they are typically used as fast food delivery vehicles. The tilting system is a completely passive design and the vehicle is controlled in the same way as a motorcycle using the counter-steer technique. When stationary, the driver must stabilise the vehicle manually.

Figure 2.7: The Honda Gyro [24]

The Vandenbrink Carver (figure 2.8) is another example of a production 1F1T tilting three-wheeled vehicle. The Carver differs from the Honda Gyro in that it employs a fully active control system, dubbed 'Dynamic Vehicle Control', and thus has car-like controls [25]. The active control system is a hydro-mechanical system that tilts the vehicle body as a result of the steering wheel input, but

also provides an element of steer control via tilt angle feedback [26]. The Carver employs hydraulics to actuate the tilt system. The rear module contains the full power-train. In emergency situations, such as during an emergency stop or failure of the tilting system, and at speeds below 5 mph, the Carver is reported to lock in the upright position [27].

In the Carver, two hydraulic actuators are positioned between the non-tilting rear unit and the tilting cabin, and this hydraulic system is controlled by the driver steering. The steering moment acts on the front wheel and this torque controls a hydraulic valve that then generates a pressure difference over the two tilting cylinders. A study conducted at TNO Road Vehicles Research Institute in the Netherlands reveals that optimal (motorcycle) tilting angle is not reached with the Carver [28] reducing the stabilising effect of tilting the vehicle. It is argued [29] that the Vandenbrink Carver was designed as an expensive, 'niche' road going vehicle that has the 'fun' and 'dynamic' driving characteristic of tilting in corners [30].

Figure 2.8: The Vandenbrink Carver

An example of a 2F3T vehicle is the Mercedes-Benz F300 Life-Jet, a concept vehicle revealed by the manufacturer in 1997 [31]. Its objective was to combine the safety and comfort of a car with the 'fun' driving dynamics of a motorcycle. The vehicle was one of the first three-wheeled vehicles employing an active tilt control system—hydraulic actuators applied to the front axle and allowed the vehicle to lean into corners. It is reported that the electronic control system took measurements from sensors and calculated the optimum roll angle [32]. How this 'optimum' angle was calculated is unknown. A photograph of the vehicle is shown in figure 2.9. The large camber angle at the front wheels, as seen in the photograph, helps generate the lateral tyre forces required for handling manoeuvres.

Figure 2.9: The Mercedes-Benz F300 Life Jet [32]

By employing the tilt system between the front wheels, the combination of tilt control, steering and suspension is complicated. Despite its wide front wheel track, the maximum tilting angle was limited to $\pm 30°$. The vehicle width limits the advantages in urban environments and highlights another disadvantage with the design: in order to have large tilting angles, the wheel track has to be wide in comparison to the width of the body. This is to allow the necessary vertical relative wheel travel to achieve the required tilt angle (as per 1F3T). This wide track with respect to body width also results in compromised vehicle packaging. This issue is illustrated in figure 2.10.

Figure 2.10: Narrow body of 2F3T [33]

It is possible to have a 2F1T vehicle where only the rear wheel tilts. Like 1F1T vehicles described above, the vehicle would comprise two discrete units, with the front module non-tilting. Such a vehicle would be difficult to construct since a mechanical connection between the steering and the tilting cabin is difficult to implement; a steer-by-wire system could be employed. No examples of a vehicle with this arrangement exist.

2.2 Vehicle Dynamics

2.2.1 Motorcycle Dynamics

To develop an appropriate control system for a tilting three-wheeled vehicle, it is important to consider the passive vehicle behaviour. Similarities exist between these vehicles and motorcycles, and as such, the dynamic principles applied to motorcycles also apply to tilting three-wheeled vehicles, especially those with one front wheel.

Front-end Geometry

The steering axis of a motorcycle is inclined at a rake angle to produce trail between the steering axis and the front tyre contact patch. This is shown in figure 2.11. The primary function of this rake angle, and the corresponding trail, is to build in a certain amount of steering stability. Because the tyre contact point is behind the steering axis, when the handlebars are turned to the left, the front tyre contact patch moves to the right. This produces a self-aligning moment at the front wheel tending to return the wheel to point in the direction in which the vehicle is travelling. Such an arrangement (often referred to as caster) is also used in automotive systems to encourage self-centring [34, 35].

Figure 2.11: Motorcycle front-end geometry

This lateral movement of the front tyre contact patch also causes the axis on which the vehicle is balanced to shift away from the vehicle centre-line. The

front wheel also leans as well as turning. This is shown in plan view in figure 2.12.

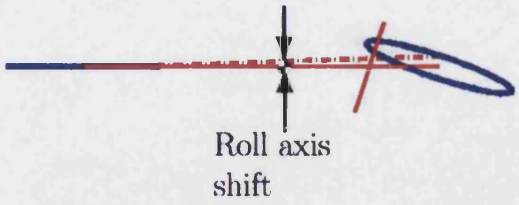

Figure 2.12: Trail creating shift in roll axis

The rake angle and the corresponding trail also help to stabilise the vehicle. With a forward velocity, as the motorcycle leans to one side, the contact patch moves around the crown of the tyre. This, combined with the trail, turns the handlebars in the same direction of the lean, causing a centripetal reaction force out of the corner, tilting the motorcycle to an upright position. A higher rake angle, while making the steering heavier, provides increased stability; likewise, a small rake angle lightens the steering and provides a faster but less stabilising response [36].

Low Speed Control

When the front wheel is turned at low speeds (less than ~1 m/s), the centre of gravity is no longer directly above the axis on which the bike is balancing, creating a moment causing capsize [37]. To keep the motorcycle upright, this moment is countered by the rider shifting body weight [38, 39], or by increasing the centripetal reaction force by either increasing the vehicle speed, or increasing the steering angle. At low speeds, the steering moment due to weight is high and the stabilising gyroscopic forces are low. Motorcycles and passive tilting three-wheeled vehicles with one front wheel are controlled at low speed using a direct steer technique: the vehicle corners in the direction the handlebars are turned.

High Speed Control

At high speed, motorcyclists have to lean into the bend to balance the centripetal reaction force with gravity. In steady state, this can be represented by an inverted

pendulum, as in figure 2.13. This is true for large radius corners, neglecting vehicle yaw. The vehicle can be seen to be accelerating laterally.

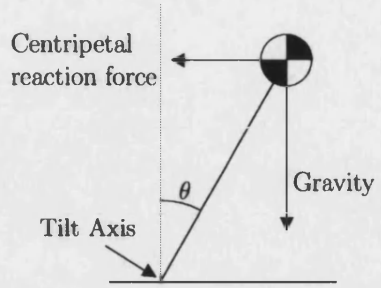

Figure 2.13: Steady state cornering

Here, θ is the vehicle tilt angle. Turns at higher speeds are initiated by the subtle and often subconscious technique of counter steering [36, 40]. When the rider wants to go around a right-hand corner, the handlebars are moved initially to the left. The vehicle begins turning to the left, causing a centripetal reaction force large enough to tilt the vehicle to the right. As the vehicle leans, the rider follows the action by turning the handlebars to the right [17].

In addition to this centripetal reaction force, at higher speeds, there is the gyroscopic torque at the front wheel. A torque which tries to turn the wheel to the left will cause the wheel to lean to the right [37]. These two forces mean that a slight left turn of the handlebars has the immediate effect of making the vehicle lean to the right. The vehicle remains in a steady state corner until the steer angle or vehicle speed is changed. Counter steering is used to change the lean angle or exit the corner.

Karnopp and Fang [41] developed a simple motorcycle model that illustrates the necessity of counter steering to achieve a vehicle tilt angle. The input is demand lean angle, and the outputs are required steer angle and actual lean angle. These are shown in figure 2.14. The counter-steer occurs in the first quarter of a second at the beginning of the turn, and there is slight lag between the demand tilt angle and the steer angle (indicated at the zero angle position).

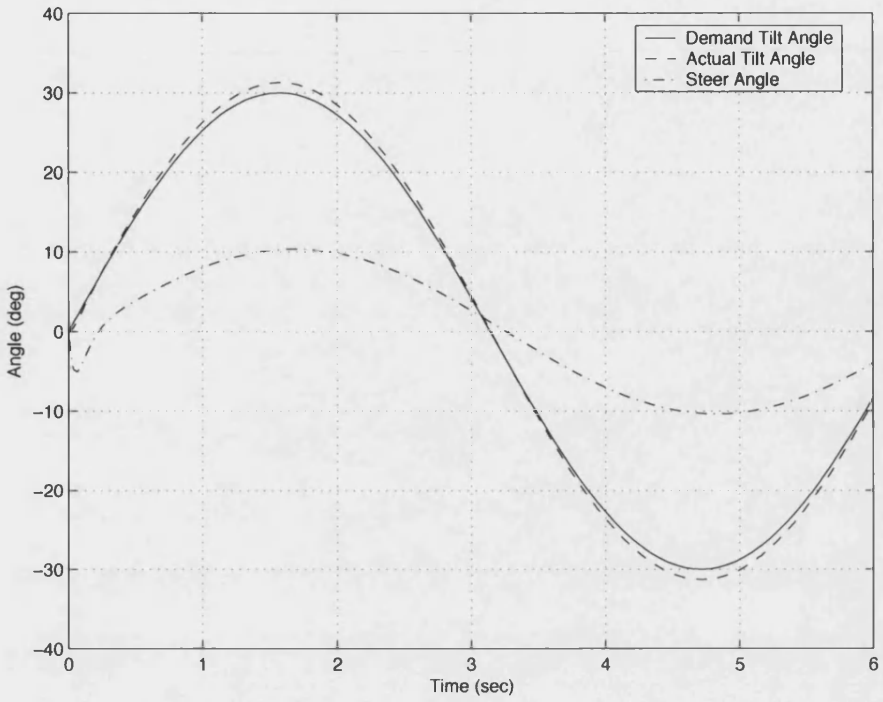

Figure 2.14: Simulation results demonstrating the necessity of counter-steering to balance vehicle [41]

2.2.2 Tilting Three-Wheeled Vehicle Dynamics

Roll Axis Position

A tilting three-wheeled vehicle can have its roll axis at ground level in a similar way to a motorcycle by having all wheels tilting (e.g. Calleja Three-Wheeler, figure 2.5 and Mercedes-Benz F300 Life Jet figure 2.9) or by having a four-bar linkage between two modules to create a roll axis approximately at ground level [42]. As explained above, practical implementation of these designs is limited.

A 1F1T vehicle with a simple bearing connection causes the roll axis to be positioned above ground level. The inclination of this axis and its height above the ground can result in an additional steer when the vehicle is tilting. Additionally, projection of the roll axis on the ground provides the actual axis about which moments of the whole vehicle are balanced, meaning that for instance, a 45° lean around the tilt axis does not balance the vehicle for a 1 g corner.

An inclined roll axis that intersects with the front wheel contact patch (figure 2.15

(a)) will introduce an additional steer effect at the front of the vehicle (the vehicle oversteers). An inclined roll axis that intersects directly between the rear wheel contact points introduces a steer effect at the rear (b) (the vehicle understeers). A horizontal roll axis above the ground will introduce both front and rear steer (c). An active control system has to take this into account when matching steer angle with corner radius and thus the calculation of an appropriate tilt angle demand.

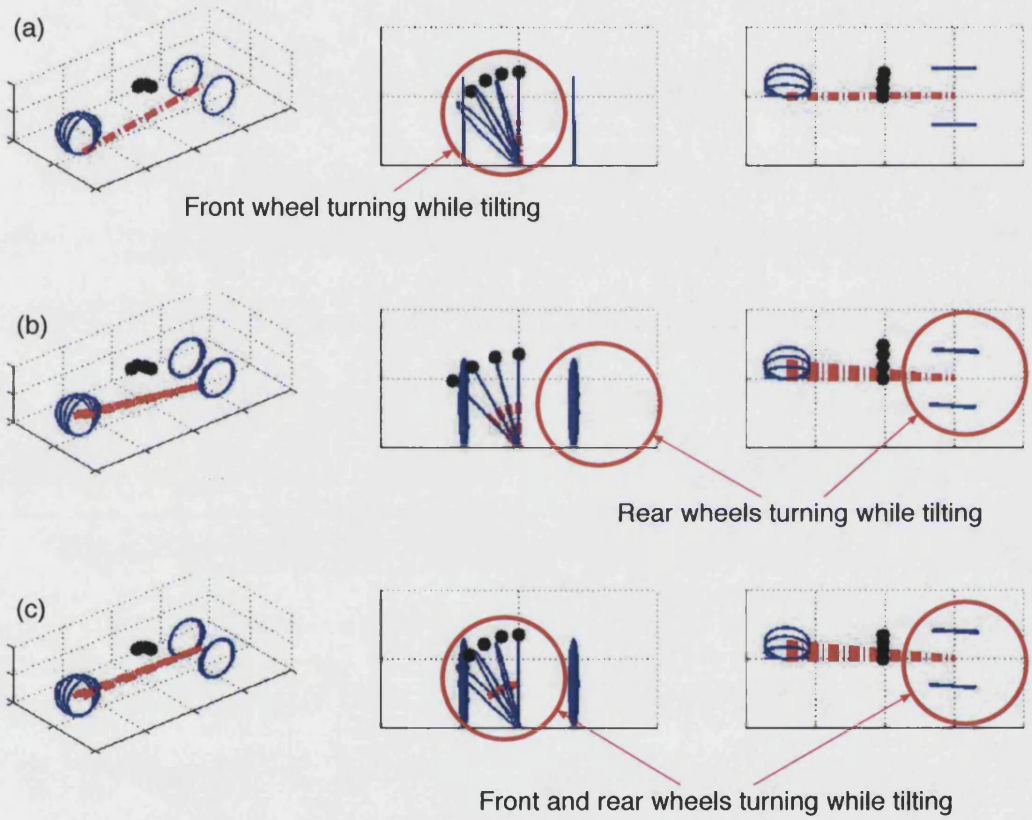

Figure 2.15: 1F1T chassis with different roll axis positions [43]

Additional Dynamics Considerations

In addition to the roll axis position, other factors have to be taken into account when developing a tilt control system. Two, identified here, are tyres and vehicle weight.

In simplified vehicle models, tyres can be represented by solid infinitely thin discs which neglect any slip angles. In reality, the non-linear behaviour of tyres

influences the 'feel' of the vehicle and the over-steer or under-steer behaviour, among other handling characteristics. This is documented in detail in [44]. These effects were taken into consideration during tilt control system tuning.

Since it is envisaged that such a vehicle will have an unladen weight of around 350 kg, the addition of a driver and passenger will add significantly to the mass of the vehicle. This will change the way in which a tilt control system responds, and, as such, the tilt actuation system must take this increased inertia into account.

2.3 Control

2.3.1 Passive Tilt Control

There are two methods of controlling the tilting action of the vehicle: passive and active control. One method of passive control is that similar to the control employed when riding a motorcycle, necessitating rider skill and counter steering. Advantages of such a system are simple integration and no complex control system. However, such a system requires motorcycle driving skill, suffers from poor performance in low speed conditions, generates no stabilising moment when stationary, and suffers under the influence of external disturbances such as side winds. These requirements of passive control also detract from the ojective of developing a vehicle intended to replace conventional cars.

2.3.2 Active Tilt Control

Active control, despite its inherent complexity, alleviates the requirement of the driver having to counter-steer, allowing direct steering inputs as expected when using car-like controls. A vehicle with a fully enclosed cabin is more susceptible to side winds, and an active control system has the advantage of keeping the vehicle upright in these situations, as well as maintaining stability in low speed or stationary conditions. This research focuses on active control.

There are three methods employed with active tilting systems: direct tilt control,

steer tilt control, or a dual mode system.

Direct Tilt Control

Direct tilt control (DTC) employs an actuation system connected between two parts of the body which, when activated, causes the vehicle or the tilting portion of the vehicle to tilt. One of the advantages of direct tilt control is simple implementation on a vehicle. On 1F1T vehicles such as the Vandenbrink Carver (figure 2.8) linear hydraulic actuators between the non-tilting rear module and the main vehicle cabin are used to tip the vehicle cabin to the calculated tilt angle. Another important advantage is that the tilt moment is applied directly to the tilting portion of the vehicle, and thus good stability can be maintained at every speed, including standstill.

The main challenge encountered with DTC is that a large moment is required to tilt the vehicle during the transition from a straight to a circular path. Passive chassis dynamics cause a centripetal moment to be applied about the roll axis when the front wheel is steered. A DTC system that follows the steering input has to overcome this initial moment in addition to providing a torque to rotate the tilting body if the counter steering technique is to be avoided.

This high peak in the tilt torque requirement is noted by most previous studies that deal with direct tilt control and various attempts have been made to reduce it. Hibbard and Karnopp [18] mention that with trains, preview capabilities could be employed, since the path of a train can be known in principle—indeed, current trains employ an element of lead in controlling the banking angle [19]. The train can therefore tilt simultaneously with the application of lateral forces. Karnopp [15] notes that cars are subjected to much higher lateral accelerations that may vary rapidly, even changing sign quickly, and the path is not known, limiting the scope of preview capabilities.

Li *et al* [45], who built an experimental vehicle incorporating an active tilt control system, also encountered this issue. The method they mention to overcome the problem of large tilt torque requirements is an automatic scheme in which the steering command is used to control the tilt mechanism directly while the direction control of the front wheel is slaved to the tilt angle through some delaying

action. They note that this scheme lacks reliability since there is no direct control of the steering. The system employed in the Vandenbrink Carver (figure 2.8) develops on this idea by mechanically connecting the steering with the hydraulic valve that controls the lean angle.

The problem of large tilt torque demand is related to the vehicle's tilt dynamics and a lag between the application of steer and generation of cornering forces. A method noted by Gohl *et al* [46] is to perfectly synchronise the yaw rate (which creates the initial outward lateral acceleration) and tilt. This would be analogous to the steady state, where the balanced tilt angle is reached and thus no tilt torque is required to maintain the position. With a simple vehicle model, this would be possible. However when implemented on a real vehicle, the relaxation length of the tyres would have to be relatively long to synchronise with the dynamics of the tilting system. The resulting vehicle would have unacceptable handling due to the extended delay between an input and the change in vehicle direction.

Snell [47], who looked at both DTC and STC to control a tilting three-wheeled vehicle, noted another problem with direct tilt control with a vehicle comprising two discrete modules. If the inertia of the tilting portion of the vehicle is large with respect to the inertia of the rear module, sudden steering inputs that require large roll moments may easily cause the inner wheel of the base to leave the ground. Despite DTC stabilising the vehicle during steady state high-g cornering, the vehicle may be prone to roll-over during transients when the lateral acceleration is generated before the necessary lean angle has been achieved.

Karnopp [23] also conducted a study of DTC when road surface friction is suddenly reduced and concluded that the tilt angle recovered to an appropriate value in a reasonable time, which demonstrates another advantage of a DTC system.

Steer Tilt Control

A vehicle employing steer tilt control (STC) is free to tilt but is balanced by the use of counter steering in a similar manner to that employed on a motorcycle. When entering a corner, the driver would steer to follow the intended path, but the control system would initially turn the front wheel in the opposite direction, causing the vehicle to topple towards the centre of the corner. The system would

then steer into the corner until a balanced tilt position was reached. To exit the corner, the system would initially steer deeper into the corner, causing the centripetal reaction force to increase and overcome the gravitational force, tilting the vehicle to an upright position.

As mentioned above, Karnopp and Fang [41] derived a model of tilting dynamics by relating steering angles to the body tilt angle. Their simple model illustrates the necessity of counter steering before a turn (see 2.2.1) and highlighted the basic control problems associated with turning, banking and balancing. Despite neglecting tyre slip angles, camber thrust and suspension movement, the simulation results followed the trend demonstrated by experimental measurements conducted by Rice [17].

The problem of balancing a vehicle using STC is analogous to that of a constrained inverted pendulum [46, 47]. Examined by Golten and Verwer [48], the controller must use negative gain (i.e. positive) feedback which cancels the inherent negative system gain. If the cabin starts dropping to the right, the base must move to the right as well to catch up to balance the tilting cabin. In order to tilt the cabin from one position to another, the base must first be moved away from the desired location, causing the cabin to topple towards the goal. This similarity to the inverted pendulum problem is highlighted by the equation governing roll dynamics (equation 3.1): it also represents the planar dynamics of an inverted pendulum.

The main advantage with STC is that large roll moments can be generated efficiently and with no risk of rollover during transients since there is no moment between the base and the upper body. However, this leads to the main disadvantage of STC: at low speed there is little possibility of generating high enough tyre cornering forces (and hence lateral acceleration) to balance against the gravitational force, thus high steering gains are required. Additionally, at zero speed, balancing may not be possible because the only moment the STC system can generate is through shifting the front tyre contact patch (figure 2.12). This moment is likely to be smaller than others acting on the system.

In [23], Karnopp claims that STC would feel more natural to the driver at high speeds. Snell agrees with this [47], stating that the vehicle rotates about a point above the tilt axis, closer to the centre of mass (and consequently closer to the

occupants' heads) so the component of acceleration caused by angular roll acceleration is less than that felt during transients with a DTC system.

A fundamental problem with STC is the integration of the steering system. One possibility is to use a steer-by-wire system with no direct mechanical link between the steering wheel inside the cabin and the steered front wheel. Sensors would read the direct-steering inputs at the steering wheel and control the front wheel in an appropriate counter-steering manner. One problem with steer-by-wire is providing acceptable and reliable driver feedback at the steering wheel together with the lack of mechanical connection, which contravenes current legal requirements for safety. Although an electrical system may be used for steering, it must be possible to steer the vehicle in the event of total or partial failure of the by-wire system [49]. With steer-by-wire, the driver receives no steering feel other than that produced artificially.

An alternative possibility for steering integration is active steering or active pinion, which is a recent development in the automotive industry [50]. Such a system would allow a driver independent steering input without having to disconnect the mechanical linkage between the steering wheel and the front axle [51]. Employed in a STC system, the driver's input is that normally associated with driving a car, but the steering system initially counteracts this input and steers the opposite direction, providing the counter steer necessary to tilt the vehicle. Currently, active steering systems are available commercially on premium brand cars to reduce the steering effort required in low speed conditions. For low speed driving, the steering ratio is low (i.e. lock-to-lock in one steering wheel rotation), while higher speed driving increases this ratio. This delivers quick and agile steering at lower speeds, with more stability at higher speeds [52].

Dual Mode Tilt Control

A tilting vehicle using a dual mode tilt control (DMTC) system aims to integrate the low-speed stability of DTC and the high-speed dynamics of STC. So and Karnopp [53, 54] studied a method of synthesising the two systems into one which changes control method as a function of speed. They note that although the same steady-state tilt angle can be reached using either method, the transient behaviour of the vehicle is very different. The main difficulty noted was having a

good transition between the two modes. By introducing smoothly varied control gains, smooth responses result between the two tilting modes.

Snell [47] also aimed to combine the desirable objective of high speed dynamics of STC with the low speed stability of DTC, and discussed the difficulty of blending the two systems. Unlike So and Karnopp [53] whereby the vehicle is either controlled by STC or DTC, in simulation, Snell aimed to marry the two systems by combining both steering and direct moment control to tilt the vehicle.

DMTC systems highlight one of the major differences in the behaviour of the two control methods. Although the tilting mass of the vehicle rotates around the same axis with respect to the non-tilting mass, when looking at the vehicle as a whole, with STC and the associated counter steer, the vehicle actually rotates around an higher axis in the tilting body. For example, when turning to the right, the base of the vehicle will initially move to the left causing the top of the tilting mass to move to the right. The point of rotation lies on the line joining the centre of the top of the tilting mass and the mid-point of the base (when viewed from the rear).

The main challenges associated with a DMTC system include the same implementation issues with STC, and that of integrating the two control methods. Additionally, multiple actuators would be required to directly tilt the vehicle and steer the vehicle, adding expense and complexity.

Control Signal

One method of calculating the desired lean angle of an actively controlled tilting vehicle is by using an accelerometer mounted on a non-tilting portion of a vehicle measuring lateral cornering acceleration. From this, the desired bank angle can be calculated. The main problem associated with this method is that the measurement is affected by the road camber, one sided bumps and general road noise. Hibbard and Karnopp [55] suggest two different control methods to overcome this problem: an accelerometer on the tilting body measuring the perceived lateral acceleration—the lateral acceleration perpendicular to the tilt angle—or measuring the torque requirement by examining the pressure differential across the actuators. These solutions are logical since both signals are independent of

road camber and both become zero in the desired steady state tilt position. They have success in simulating the use of perceived lateral acceleration as a control signal; the road camber angle is simply a disturbance to the system. With actuator torque as a control signal, they note a non-minimum phase reverse action type of response to a sudden change in lateral acceleration encountered when entering a turn—the body will lean to the outside of the turn before the controller can begin to pull the vehicle inwards. Although this works, they acknowledge that it may be less satisfactory than the responses of alternative control schemes.

2.3.3 Steer Torque and Driver Feel

An area requiring consideration is the feedback that the driver receives from any active control system. Bortoluzzi *et al* [56] identify the importance of driver psychological effects in the definition of acceptable handling characteristics. Considering the simplest case of DTC, when the driver first turns the steering wheel the self-aligning torque generated at the front wheel works against his input. As the machine begins to lean, the contact patch rolls around to the edge of the tyre, and the torque reduces, eventually starting to work in the opposite direction. The point at which this occurs is dependent on the geometry of the vehicle, in particular the position and inclination of the tilt axis.

In conventional cars, an element of self-centring is engineered into the steering system by castoring the steering wheels so that if no steering torque is applied by the driver, the car's steered wheels will self-centre. As stated earlier, a vehicle with passive tilt control and normal steering geometry is also stable, and will return to the upright condition if the steering wheel is released. Depending on the geometry, on a vehicle with active direct tilt control with no steering input from the driver, the applied torque will turn the steering wheel further into the corner. If the control system uses steering wheel position as one of its inputs, then the vehicle will attempt to tilt further. This is not desirable if the driver wants to return to the upright position by releasing the steering wheel. Although steering torque could be used as a control input, this poses problems since it changes signs and could go to zero during transient stages between steady states. The use of active steering or steer-by-wire is likely to emphasise this issue. The successful combination of driver feel and the vehicle's ability to self-right are important

considerations for successful control system development.

2.4 Actuation Systems

A vehicle employing active control requires a method of actuation. With steer tilt control, one actuator is required to provide the additional steering input if an active steering system is used, or two actuators are required if a steer-by-wire system is used (one for the steering input, and one for feedback to the driver). It is likely that these would be simple electric servo motors that provide high speed response and accurate positioning. The main difficulty in implementing steer tilt control using steer-by-wire is being able to maintain car-like control if the power supply fails. With an active steering system, the driver would have to suddenly switch from the direct-steer to the counter-steer technique to balance the vehicle.

Active direct tilt control vehicles need to have an actuation system that can apply a moment between the non-tilting and tilting bodies. Based on a simple model, estimates of mechanical torque requirements were found for what is considered a worst case manoeuvre: a sinusoidal tilt between maximum left and maximum right tilt positions at 0.33 Hz. This is equivalent to a series of fast lane changes or a slalom test. It must be noted that in steady state, the required tilt torque goes to zero. The tilt torque is shown in figure 2.16 for a ± 1 g lateral acceleration sinusoidal manoeuvre. For initial estimated masses and inertias of the CLEVER vehicle, the torque required is approximately 1670 Nm, and the peak mechanical power requirement is approximately 1.7 kW with a peak power during cycle of 750 W. The large tilt moment required at the start of a turn when using direct tilt control can be noted at the beginning of the manoeuvre.

The calculation assumes a perfect controller resulting in a perfect dynamic response, and does not take into account any inefficiencies within the actuation system, so the power requirement on the real vehicle is likely to be higher.

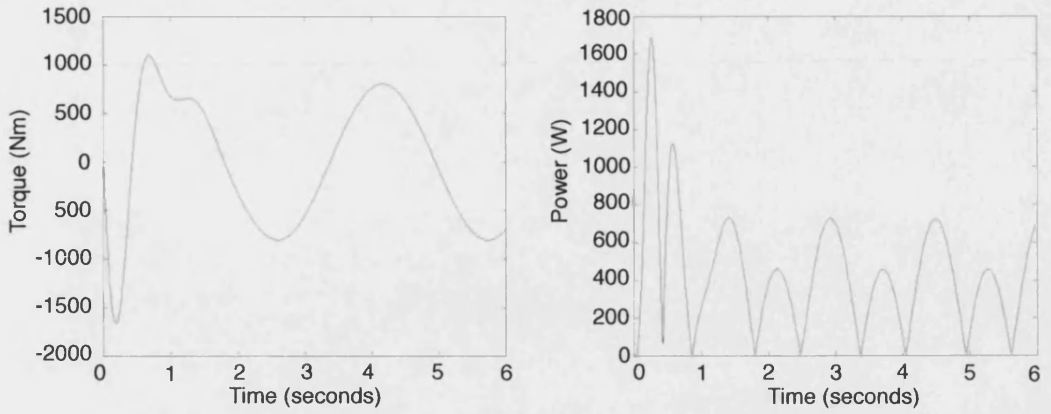

Figure 2.16: Required tilt torque and power at actuator

2.4.1 Electric Actuation

In order to provide the torque and power required with a standard 12 volt vehicle electrical system, a high current (150–200 A) servo-drive would be necessary. An electric motor supplying the necessary high power operating at low voltages requires large windings in the motor to handle the high current leading to increased motor weight and size. One way to overcome this issue is to operate the system at a higher voltage, with a high speed-low torque motor running through a gear box. A gear box to transfer the required power is likely to be very heavy.

The advantages of electric actuation are convenient power supply and storage, and research has shown that a suitable motor and servo drive are available [57]. High efficiency (~95%) is also a benefit. The main disadvantages are that the chosen system is expensive with respect to the target cost of the vehicle, and the size of the motor to handle the high currents seriously compromises the vehicle packaging.

2.4.2 Hydraulic Actuation

A hydraulic system can offer high power in a compact solution, despite the efficiency being less than an electric actuation system (generally 60-80%). The flexibility of installation that a hydraulic system enables is also an advantage in terms of packaging. A preliminary circuit is shown in figure 2.17.

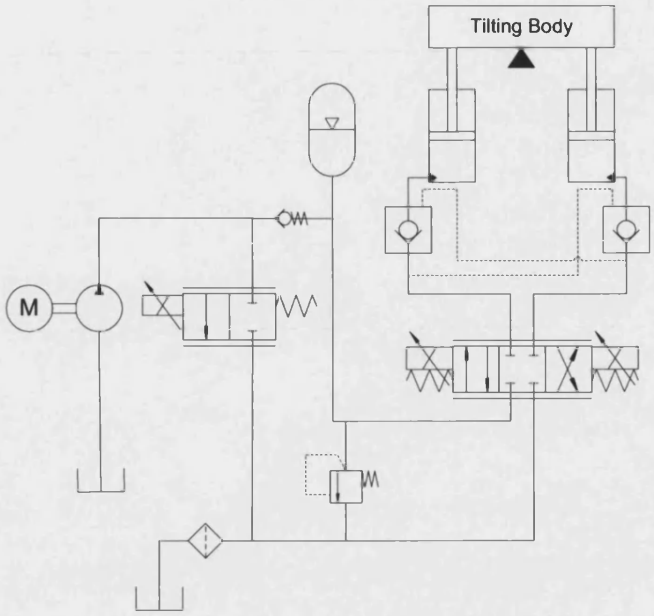

Figure 2.17: Preliminary Hydraulic Circuit Design Proposal

In order to provide the flow to fulfil the tilt speed requirement, yet provide an efficient system, the engine of the vehicle would directly drive a positive displacement gear pump. A gear pump is a suitable option owing to its compact and light weight characteristics. A hydraulic solution where the pump is driven by an electric motor poses similar issues to direct electric tilt actuation in terms of current requirements for the electric motor.

In order to increase the efficiency of the system, an accumulator would be implemented within the circuit primarily as an energy storage device, so that the pump can be unloaded when the flow requirement is small and the accumulator is charged. One consideration with such an arrangement is the characteristic of the unloading valve; to prevent a sudden load on the engine, soft-start valves [58] could be considered, but a solution using a proportional relief valve controlled electronically would provide increased flexibility concerning the loading and unloading cycles.

An alternative to a standard pump with an unloading valve is a variable displacement pump. These pumps are however very expensive. The lower cost digital displacement pump-motor, which can vary displacement from maximum to zero capacity within one revolution of the pump [59] could be an alternative. This technology, however, is currently under development and is not yet mature

enough for this application.

In addition to energy storage, the accumulator serves two further purposes: it would supplement the flow of the pump during peak flow requirement conditions so allowing the use of a smaller pump, and would provide flow in the event of a pump or engine failure.

A proportional directional control valve would be employed to direct flow to either linear actuator, positioned between the front and rear frames.

2.5 Solution for the CLEVER Vehicle

Following the background research covered in this chapter, design decisions were made concerning the overall chassis layout of the CLEVER vehicle and its tilting system. The chosen solution for CLEVER is a tilting three-wheeled vehicle with one front wheel (delta arrangement) that tilts with the cabin, and rear module that remains upright with respect to the ground (1F1T). Despite 1F3T vehicles offering better characteristics in terms of balancing the mass in corners, a 1F1T design offers a solution that facilitates manufacture, construction and maintenance; eases the integration of the complete drivetrain and tilting systems within a compact rear unit; allows for a motorcycle derived steering system; and as large relative suspension movements are not required, this concept fits within the styling constraints.

Due largely to the necessity of car-like controls and an enclosed cabin, a direct tilt control (DTC) system is implemented, controlling a hydraulic actuation system with linear actuators positioned between the front tilting cabin and the non-tilting rear unit. This configuration was chosen as it offers good stability at all speeds, and offers the best prospect of achieving the technical requirements of the project supported by robust engineering design. A hydraulic actuation system is used owing to its high power density, engineering feasibility with standard vehicle electrics and flexibility of installation.

Figure 2.18 shows illustrations of the initial styling proposal for the CLEVER vehicle, and figure 2.19 shows photographs of a quarter scale styling model of

CLEVER with the finalised styling.

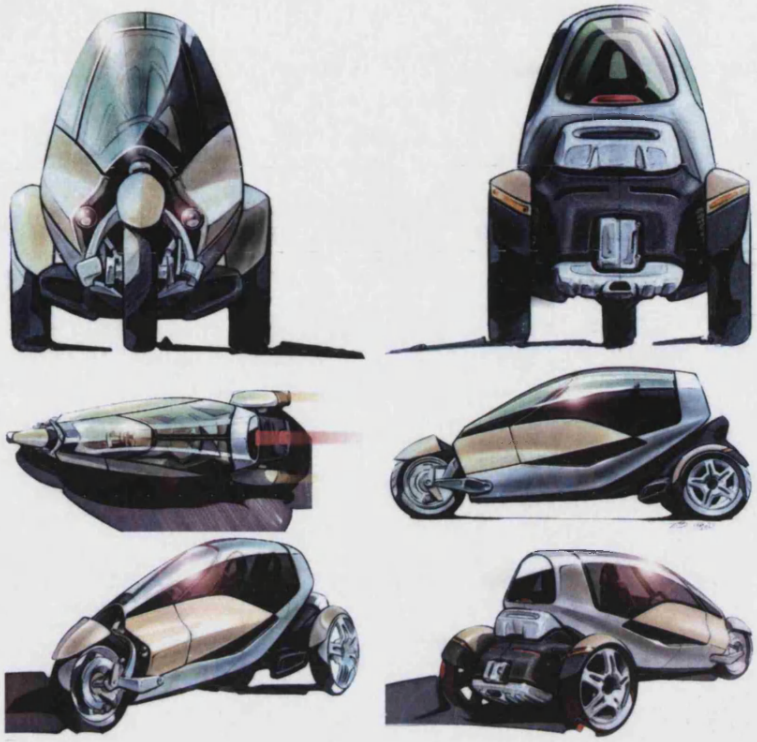

Figure 2.18: Initial styling illustrations of the CLEVER Vehicle

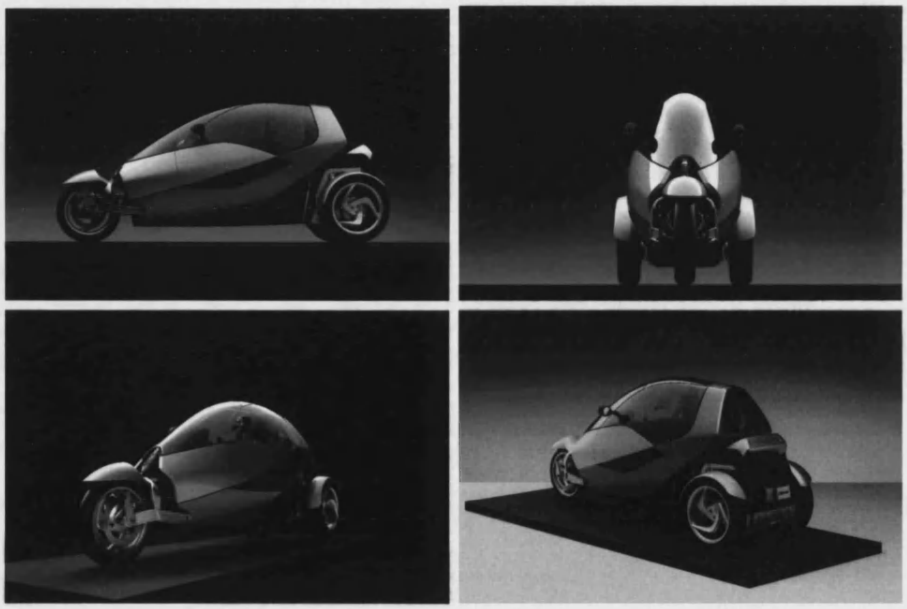

Figure 2.19: Quarter scale styling model of the CLEVER Vehicle

Chapter 3

Control

3.1 Introduction

In chapter 2, a system providing direct tilt control was proposed as the solution for the CLEVER vehicle. The objective of this controller was to monitor the system dynamics and generate a command signal to the hydraulic actuation system to tilt the vehicle cabin to the necessary angle in order to maintain stability in corners by balancing the lateral acceleration with gravity.

This direct tilt control system was to be implemented electronically, with sensors measuring driver inputs and vehicle dynamics. These measurements formed the inputs to a micro-controller which determined the tilt position demand and calculated the necessary valve opening to tilt the cabin to the correct angle.

To evaluate the performance of the direct tilt control system, a simple model of the vehicle is developed. An inverted pendulum, representing the tilting vehicle cabin, is used as the basis of this model. This model is used to assess the initial parameters in the controller before implementation in hardware on the prototype.

In order to implement the control system on the vehicle, the system must be constructed in hardware. A controller and sensors are selected, and a signal conditioner box is designed and built to regulate the input and output signals to

and from the controller.

The software for the micro-controller is developed in two stages. Firstly, the overall program structure is designed and built, and the LCD display and keypad interfaces are incorporated into this initial code. The direct tilt control system is then programmed (based on the calculations used in simulation) to determine the demand tilt angle, and from this step, calculate the necessary valve opening to tilt the vehicle to the correct tilt angle.

3.2 Simulation

3.2.1 Inverted Pendulum Model

To establish the fundamental dynamics of the tilting system, the tilting cabin of CLEVER is represented as an inverted pendulum as shown in figure 3.1. The inverted pendulum is mounted on a massless base, which rotates about pivot point A, the tilt axis. An external moment, M_t may be applied to the inverted pendulum about the tilt axis in order to rotate the tilt axis.

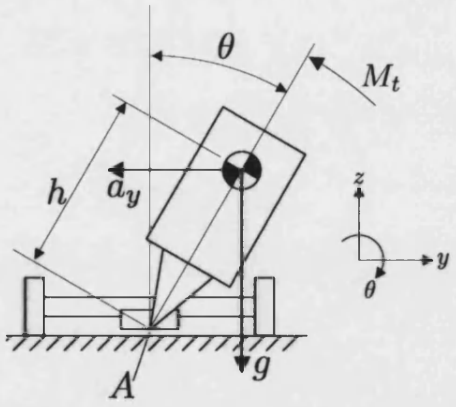

Figure 3.1: The tilting cabin represented as an inverted pendulum

This model gives rise to the equation of motion for the inverted pendulum.

$$\sum M_A = (I_x + mh^2)\ddot{\theta} = mgh\sin\theta - ma_y h\cos\theta + M_t \tag{3.1}$$

It is important to note that if the values of M_t and a_y were set to zero, equation 3.1 represents the dynamics of an inverted pendulum. The gravitational term is destabilising. If θ is slightly positive (i.e. leaning to the right), a moment is created in the positive direction increasing the tilt angle.

When a_y is positive, the tilting cabin has a tendency to follow the acceleration and lean to the right. It is desirable, however, to tilt the vehicle to the left so that in steady state, the gravity and the acceleration terms on the right hand side of equation 3.1 cancel. In this steady-state tilt position no stabilising moment is required, so M_t reduces to zero. This steady state case exists when:

$$\theta = \theta_{ss} = \tan^{-1}\left(\frac{a_y}{g}\right) \tag{3.2}$$

The goal of the active tilting system is to position the tilting cabin such that $\theta = \theta_{ss}$, which is exactly what motorcyclists must achieve to prevent roll over. In reality, the base of CLEVER's tilting system is the rear unit, which of course has a mass and its own roll mode out of the bend. The method used to compensate for this was to overlean the tilting cabin beyond the 'balance' point. This is covered in more detail in section 3.4.2.

The benefits of tilting the cabin to this position are three-fold:

- The vehicle is balanced in the steady state; there is no overturning tendency, irrespective of vehicle track.
- With a constant value for a_y, and with no external disturbances such as side wind loads, no moment is required to maintain this position ($M_t = 0$).
- The perceived lateral acceleration felt by the occupants within the tilting cabin is zero.

3.2.2 Direct Tilt Control

As discussed in section 2.5, the chosen solution for the active control system is direct tilt control, where the steering wheel is directly connected to the front

wheel, and the control system is used to control the proportional control valve which directs the hydraulic flow to either cylinder, providing the necessary torque between the front and rear units to tilt the cabin.

In order to simulate the control system, a transfer function was developed relating the input demand, θ_d, with the actual tilt angle, θ, based on the inverted pendulum model presented above. Tilt actuation system dynamics are neglected, allowing the focus to be placed on the control system. In addition, yaw dynamics, base mass and vertical motion of the base are not considered in this initial controller development stage.

With direct tilt control, the purpose of the controller is to tilt the vehicle such that $\theta_d = \theta_{ss}$, as shown in equation 3.2, where a_y is developed by the driver steering the vehicle.

In this initial case, the tilting motion is governed by equation 3.1. As the controlling moment, M_t will be provided by the actuators, this is replaced by T_{act}, which is the torque provided from the actuators. This results in:

$$\sum M_A = (I_x + mh^2)\ddot{\theta} = mgh\sin\theta - ma_y h\cos\theta + T_{act} \tag{3.3}$$

It is assumed for this simulation that the torque produced by the actuators is a function of the difference between demand and actual tilt angles, represented by equation 3.4.

$$T_{act} = G(\theta_d - \theta) \tag{3.4}$$

This equation represents the simplified tilt actuation system dynamics, with torque being the production of a proportional constant, G, and the difference between θ_d and θ.

From equation 3.2 the demand tilt angle is:

$$\theta_d = \tan^{-1}\left(\frac{a_y}{g}\right) \tag{3.5}$$

Combining equations 3.3, 3.4 and 3.5, linearising for small angles and rearranging results in equation 3.6.

$$(I_x + mh^2)\ddot{\theta} - mgh\theta = G(\theta_d - \theta) - mgh\theta_d \tag{3.6}$$

From this equation, a block diagram can be developed.

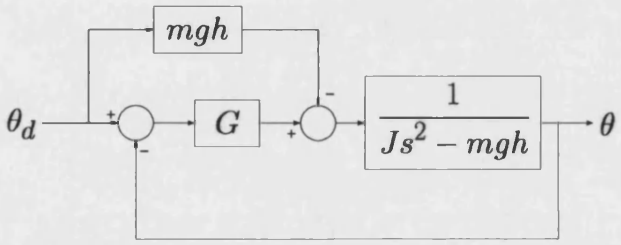

Figure 3.2: Block diagram of basic control model

where $J = I_x + mh^2$. Through block diagram manipulation, the transfer function in the s-domain is shown to be:

$$\frac{\theta}{\theta_d}(s) = \frac{G - mgh}{(I_x + mh^2)s^2 + (G - mgh)} \tag{3.7}$$

Clearly, for the vehicle to be stable, it is required that

$$G > mgh \tag{3.8}$$

since if G is less than mgh, the system has one pole on the right hand side of the s-plane diagram, indicating instability.

Initial designs indicate that $m = 295\,\text{kg}$, and $h = 0.5\,\text{m}$, therefore the minimum

value for G is

$$G_{\min} = mgh = (295)(9.81)(0.5) = 1447\,\text{Nm/rad} \tag{3.9}$$

Chapter 4 discusses the hydraulic actuation system in more detail, but the following values are drawn from it to use in this analysis:

$$\begin{aligned} P_{\max} &= 160\,\text{bar} = 160 \times 10^5\,\text{N/m}^2 \\ d_{\text{cyl}} &= 0.032\,\text{m} \quad \rightarrow \quad A_p = \frac{0.032^2\pi}{4}\,\text{m}^2 \\ b_{\max} &= 0.144\,\text{m} \end{aligned}$$

where $P_{\max}$ is the supply pressure, $b_{\max}$ is the maximum lever arm. A_p is the actuator piston area.

Therefore the maximum torque supplied by the hydraulic tilting system is:

$$\begin{aligned} T_{\max} &= P_{\max} A_{\text{act}} b_{\max} \\ T_{\max} &= (160 \times 10^5)(8.042 \times 10^{-4})(0.144) \\ T_{\max} &= 1853\,\text{Nm/rad} \end{aligned} \tag{3.10}$$

Setting the value of G to the value of $T_{\max}$ results in a stable system, because the quantity $(G - mgh)$ in the denominator in equation 3.7 is now guaranteed to be positive. This is reasonable since the only stabilising action that can be applied to the tilting cabin is from the actuation system.

Performing a root locus plot for the system shown in figure 3.3 reveals that it has two poles lying on the imaginary axis (at $s = \pm 1.81j$) of the s-plane diagram. The system is therefore neither stable nor unstable, with the transients neither decaying, nor increasing over time; the system is deemed marginally stable.

When this system is simulated, a step input demand produces a non-decaying oscillation, as shown by the blue trace in figure 3.4. One way to reduce this oscillation is to introduce an element of velocity based damping into the equation of motion. It is reasonable to assume that in the CLEVER tilt system, the velocity based damping will be introduced by several methods: actuator friction

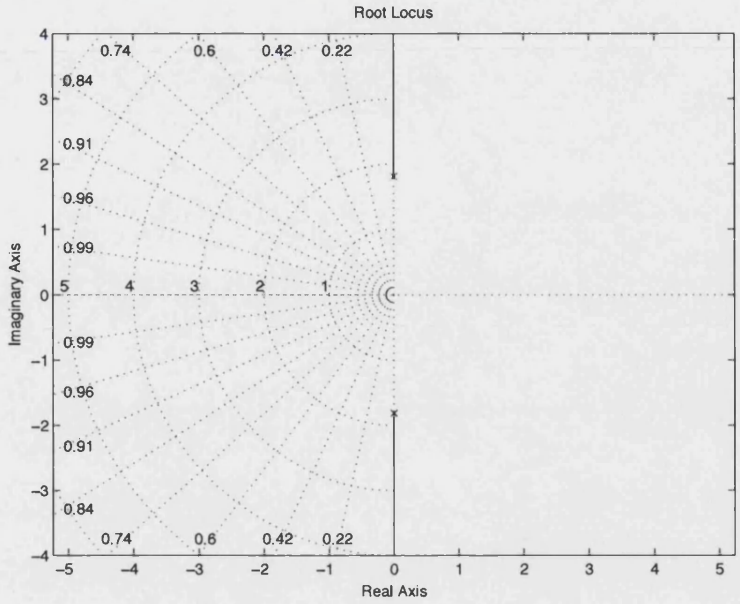

Figure 3.3: Root locus diagram for DTC system with no damping

will introduce damping, as will the hydraulic valve flow-pressure characteristics. As this was an analysis of the control system only, an external controller using derivative control was used to simulate this damping action.

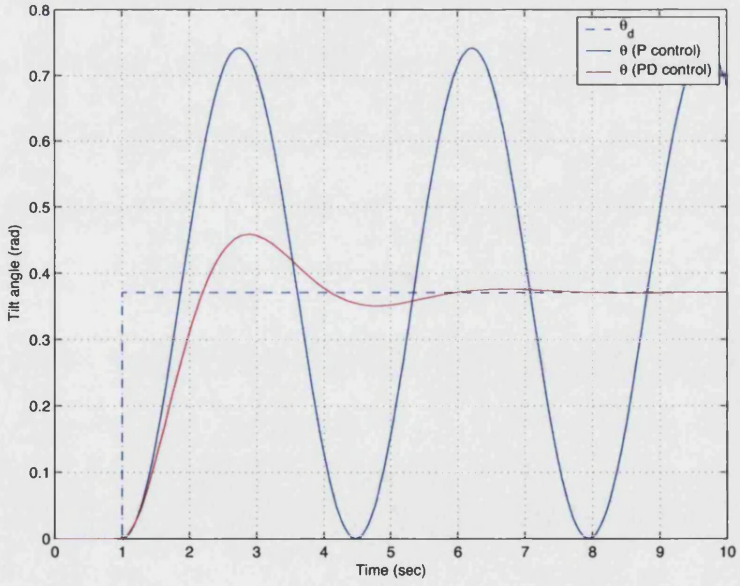

Figure 3.4: Comparison of response between proportional control and proportional plus derivative control

A proportional plus derivative control (PD) of actuator angle is used here to get a fast rise time and good damping. With the modification of the model with a

PD controller in place of the gain, G, (a proportional controller), the transfer function of the system becomes:

$$\frac{\theta}{\theta_d}(s) = \frac{k_d s + (k_p - mgh)}{(I_x + mh^2)s^2 + k_d s + (k_p - mgh)} \tag{3.11}$$

With $k_p = G = 1853$, introducing a scaled value for k_d damps the oscillation in the system, as shown by the red trace in figure 3.4. With this controller implemented, the DTC system can be simulated as a stable system. The root locus of this system with $k_p = 1$ and $k_d = 0.1$ is shown in figure 3.5. As can be seen, this is a stable system.

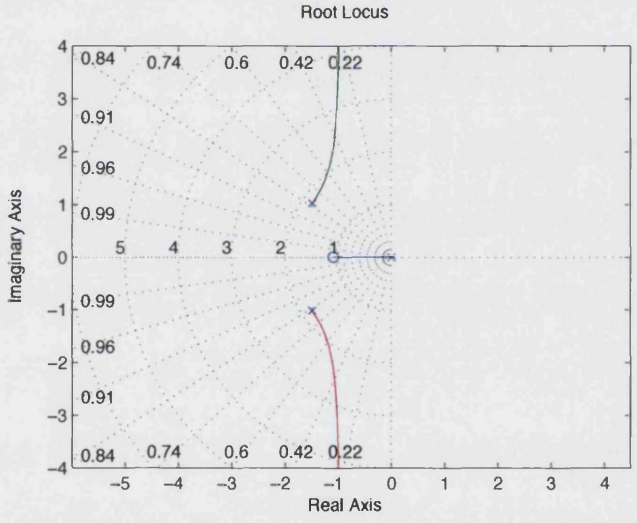

Figure 3.5: Root locus plot with PD control

3.2.3 Perceived Lateral Acceleration

When running the simulation, the real lateral acceleration experienced by the base can be calculated, since θ_d is a function of a_y, as shown in equation 3.5. The perceived lateral acceleration is that experienced 'laterally' inside the tilting cabin—this acceleration is that acting normally to the tilted cabin position—and this value can be calculated from examining the accelerations acting perpendicular to the inverted pendulum, shown in figure 3.1. The perceived lateral

acceleration at the centre of gravity position a_{per} can be shown to be:

$$a_{\text{per}} = a_y \cos\theta - g \sin\theta + h\ddot{\theta} \tag{3.12}$$

Linearised, as used in the model:

$$a_{\text{per}} = a_y - g\theta + h\ddot{\theta} \tag{3.13}$$

So, in an ideal system, in a steady-state turn, the last term is zero, and the lateral acceleration and gravity terms cancel each other out so no lateral acceleration is felt by the occupants in the tilting cabin. Note that if a_{per} can be measured at any point on the apparent vertical line connecting the tilt axis to the centre of gravity of the tilting body. If the accelerometer is between the tilt axis and the centre of gravity, the tilt acceleration term will be multiplied by a height less than h. In this analysis, the tilt acceleration term, $\ddot{\theta}$, is assumed to be measured at the centre of mass height, h.

3.2.4 Demand Signal Calculation

As mentioned in section 2.3.2, using an accelerometer on the non-tilting portion of the vehicle could provide an adequate signal with which to calculate the demand signal, but suffers when the road surface is not flat and is also susceptible to disturbances from noise.

Despite suffering the same limitations in terms of road camber, noise is less likely to significantly disturb a control signal determined from driver inputs. In this system, the measured driver inputs are the steer angle and the vehicle speed. On a flat dry road, assuming Ackermann steering principles that neglect tyre slip angles, these two signals are sufficient to determine the balanced tilt position for large radius corners. For these situations, the lateral acceleration, a_y is

$$a_y = \omega^2 R = \frac{V^2}{R} \tag{3.14}$$

where ω is the rotational velocity, V is the forward velocity and R is the corner radius.

A plan view of an Ackermann steering three-wheeled vehicle is shown in figure 3.6.

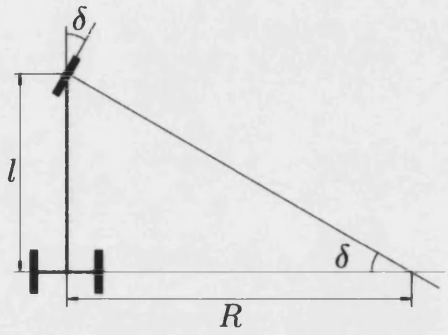

Figure 3.6: Plan view of three-wheeled vehicle

From figure 3.6, corner radius R is a function of steer angle, δ and wheelbase l:

$$\tan\delta = \frac{l}{R} \quad \rightarrow \quad R = \frac{l}{\tan\delta} \tag{3.15}$$

So, by combining equations 3.2, 3.14 and 3.15, the steady state tilt angle, which is the tilt demand angle, is a simple function of the measured driver inputs: steer angle and forward velocity.

$$\theta_{ss} = \theta_d = \tan^{-1}\left(\frac{V^2\tan\delta}{lg}\right) \tag{3.16}$$

Equation 3.16 is valid for the simple inverted pendulum representation of the vehicle, neglecting slip angles and assuming that the pivot point is at ground level. Taking the designed wheelbase length of 2.4 m, a control map can be constructed from this equation, one half of which is visualised in figure 3.7—the map is symmetrical about the 0° steer angle position. Note that the tilt angle is limited to ±45° from the vertical.

Note that limiting the tilt angle to ±45°, at high speeds, the range of acceptable steer angles at which the vehicle will be balanced is reduced considerably.

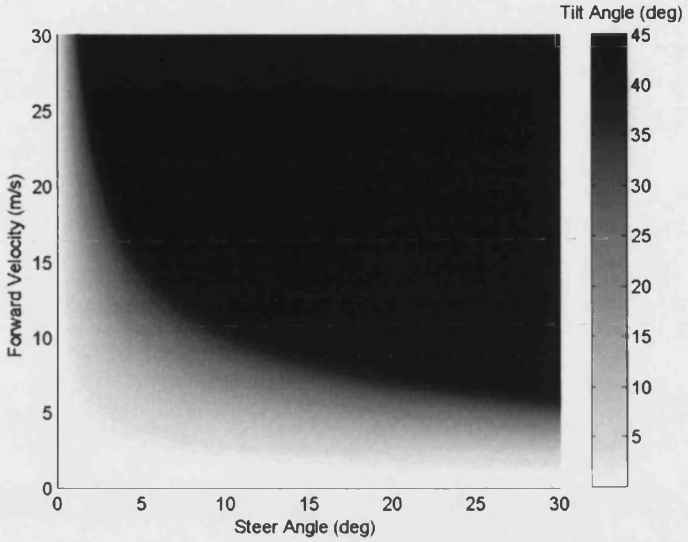

Figure 3.7: Lean angle demand control map for range of vehicle speeds and steer angles

For use in the model, equation 3.16 is linearised, resulting in equation 3.17.

$$\theta_d = \frac{V^2\delta}{lg} \tag{3.17}$$

3.2.5 Model Results

Using the above analysis, a model of the direct tilt control system was constructed in Matlab-Simulink in order to predict the behaviour of the system and determine initial gains for the controller.

The simulations were run with the vehicle travelling initially at 10 m/s, and two steering inputs were simulated: a step change from 0 degrees to 5 degrees to gain a full appreciation of the step response, and a sinusoidal input from -5 to $+5$ degrees. Equation 3.17 was followed to determine the corresponding θ_d for the inputs, which was used as the input to the controller. Table 3.1 lists the runs presented here.

(Note that the values of k_p and k_d are scaled in the simulation to incorporate G. When $k_p = 1$ and $k_d = 0.1$ in table 3.1, the gains in the simulation are

Run	k_p	k_d	δ	V	Input
1	1	0.2	5	10	Step
2	1	0.2	5	10	Sine
3	1.5	0.2	5	10	Step
4	1.5	0.2	5	10	Sine
5	2	0.2	5	10	Step
6	2	0.2	5	10	Sine
7	1	0.2	5	14	Step
8	2	0.2	5	14	Sine
9	1	0.2	5	14	Ramp
10	1.5	0.2	5	14	Ramp
11	2	0.2	5	14	Ramp
12	2.5	0.2	5	14	Ramp

Table 3.1: Description of simulation runs

$1 \times 1853 = 1853$ and $0.1 \times 1853 = 185.3$ respectively.)

Runs 1 and 2 are considered as a base reference case. Runs 3, 4, 5 and 6 show the influence of increasing the proportional gain, and runs 7 and 8 show the influence of increasing the speed to 14 m/s, therefore increasing the tilt angle demand. Runs 9–12 use a lightly smoothed ramp response to examine a more realistic response at higher speeds, with particular focus on the perceived lateral acceleration.

The gain chosen for the derivative component of the PD controller affects the performance of the simulation. Reduction of the k_d term increases the oscillation in the system, increasing the overshoot and settling time in a step response. An increase in the k_d term has the affect of damping the step response, which despite eliminating any overshoot, lengthens the time taken to reach the demand value. With the sine wave tilt demand, a high value of k_d causes the response to follow the demand closely. The value chosen for k_d strikes an appropriate balance for response and stability.

Figures 3.8 and 3.9 show the results for runs 1 and 2 respectively. The plots on the left in the figures is the tilt demand (θ_d) and tilt response (θ). The plots on the right are the real lateral acceleration at the base of the vehicle (a_y), and the perceived lateral acceleration at the centre of mass in the tilting cabin (a_{per}). Good response is shown for the step input, with little overshoot. Response for the sine wave however, is poor, with a significant lag between demand and response,

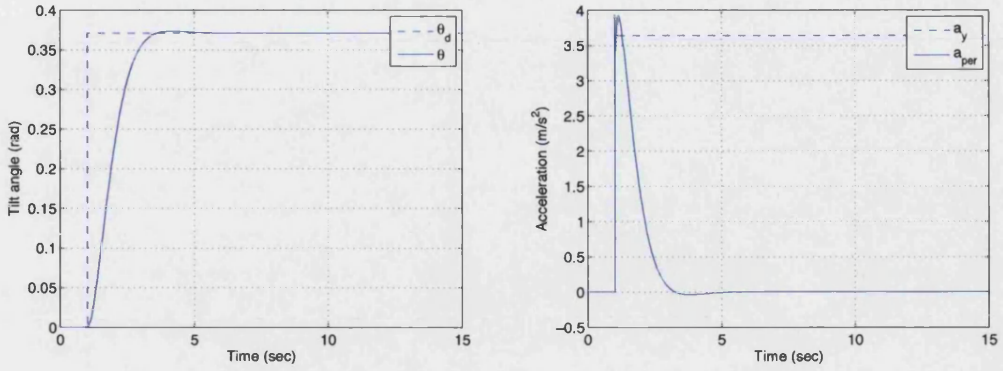

Figure 3.8: Simulation results for run 1

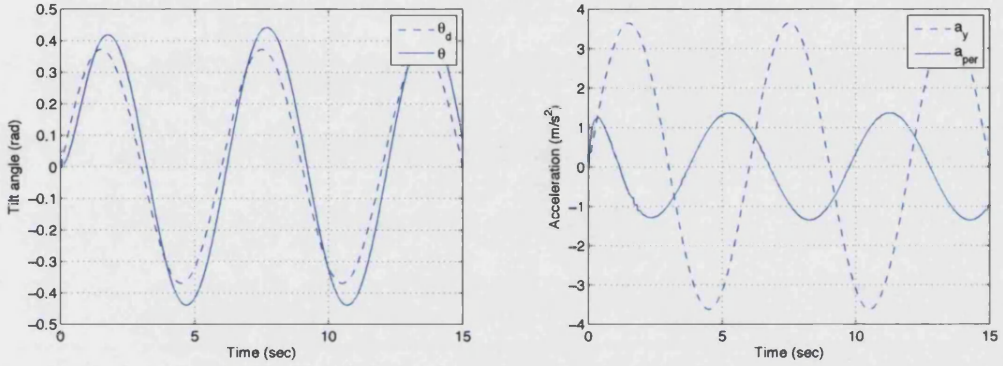

Figure 3.9: Simulation results for run 2

indicating an increase in proportional gain would be beneficial. Except for the sharp spike in perceived acceleration at the beginning of the step, owing to the domination of the tilt acceleration term in equation 3.13, the perceived lateral acceleration dies to zero for run 1, and is small for run 2; it occurs in run 2 due to the constant motion back and forth producing a constant tilt acceleration, and hence the $h\ddot{\theta}$ term in the equation for perceived lateral acceleration. The lag between the demand and response mean that the a_y and the $g\theta$ terms do not cancel, further increasing the perceived lateral acceleration.

The plots shown in figure 3.10 show the tilt response for runs 3 and 4. For these runs, the proportional gain is increased from $k_p = 1$ to $k_p = 1.5$, so the response is faster, and for the step response, shown on the left, there is an overshoot. With run 4, however, the response is closer to the demand. The acceleration plots of these runs are similar to those shown in figures 3.8 and 3.9, but the initial spike is slightly larger for the step response, associated with the higher gain value.

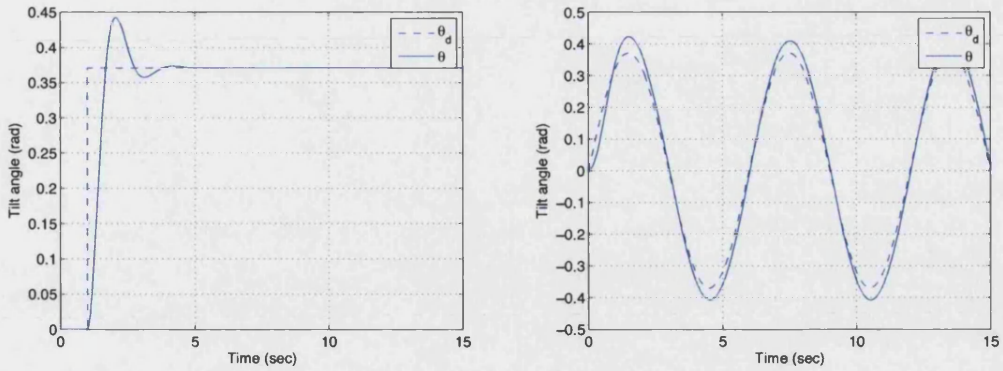

Figure 3.10: Simulation results for runs 3 and 4

For the sine wave, the reduced lag between response and demand result in lower values for the perceived lateral acceleration during the sinusoid. These plots are shown in figure 3.11.

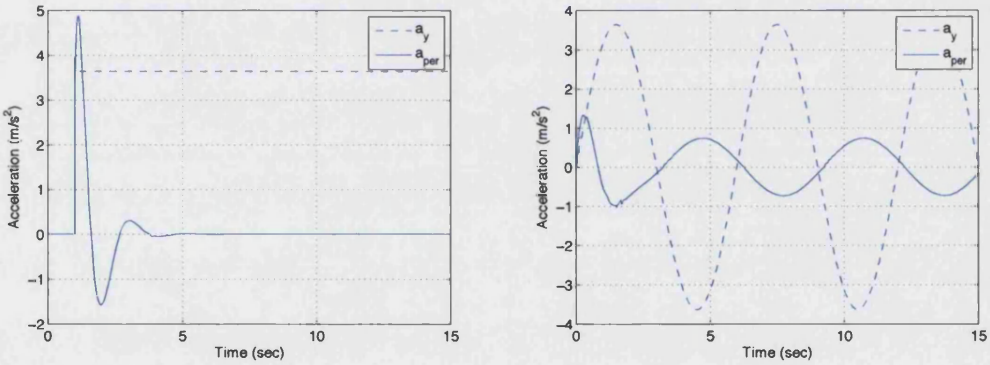

Figure 3.11: Perceived acceleration results for runs 3 and 4

Plots of tilt response for runs 5 and 6 are shown in figure 3.12. These results illustrate that the response is even faster with a proportional gain of two with the consequential increase in overshoot for the step response, but the very close tracking with the sine response.

The acceleration results for runs 5 and 6 are shown in figure 3.13. The same conclusions as those for runs 3 and 4 can be drawn for these results: the increase in gain increases the spike for the step response, but lowers the magnitude of the perceived lateral acceleration for the sine response.

In runs 1–6, the simulated speed of the vehicle is 10 m/s, so with a 5° turn, the tilt angle demand θ_d, from equation 3.17, is approximately 0.37 radians, or

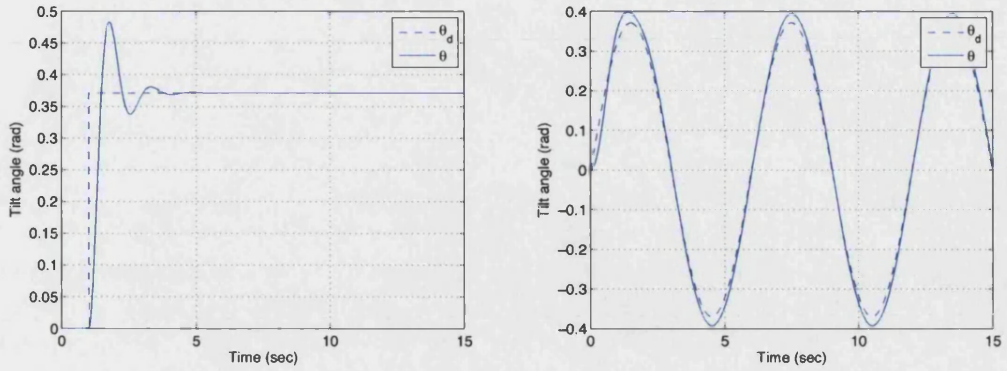

Figure 3.12: Simulation results for runs 5 and 6

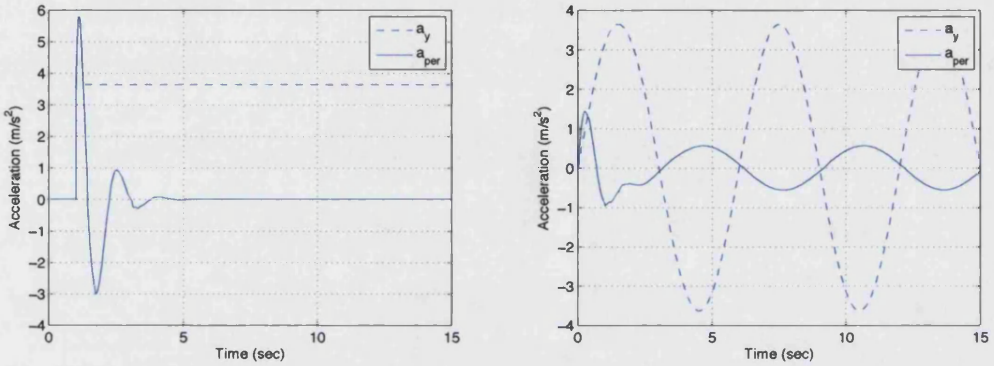

Figure 3.13: Perceived acceleration results for runs 5 and 6

21.2 degrees. Increasing the speed to 14 m/s, and maintaining the same steering demand has the effect of increasing the tilt demand angle to approximately 0.73 radians, or 41.6 degrees. Runs 7 and 8 use the same gains and inputs used in runs 1 and 6 respectively, but with this increased speed. The tilt response and acceleration plots are shown in figures 3.14 and 3.15.

As can be seen in the figures, despite the perceived lateral acceleration reducing to zero (in the case of the step response), or being very small (in the sinusoidal case), the maximum lateral acceleration experienced at the base is very high: 7.13 m/s^2, explaining the necessity to tilt to 41.6 degrees.

What is perhaps more significant with the results of runs 7 and 8 are the initial spikes in perceived lateral acceleration. It must be considered that a step response is unrealisable in real life, but due to the dominant term associated with tilt acceleration in equation 3.13, this perceived lateral acceleration can be very high.

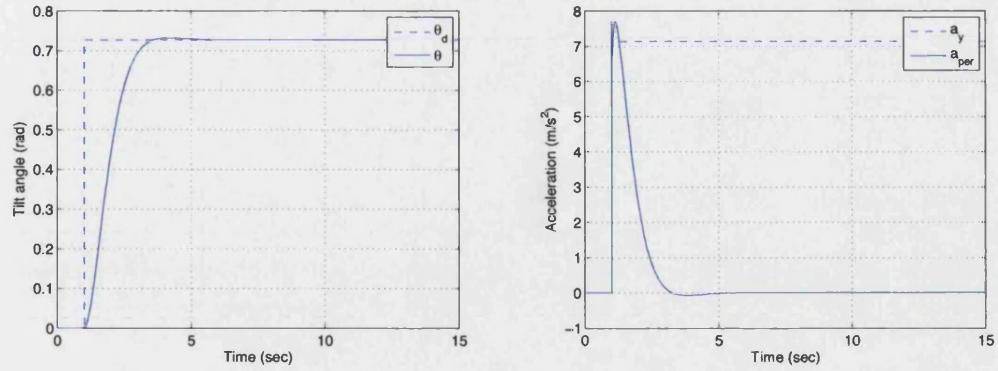

Figure 3.14: Simulation results for run 7

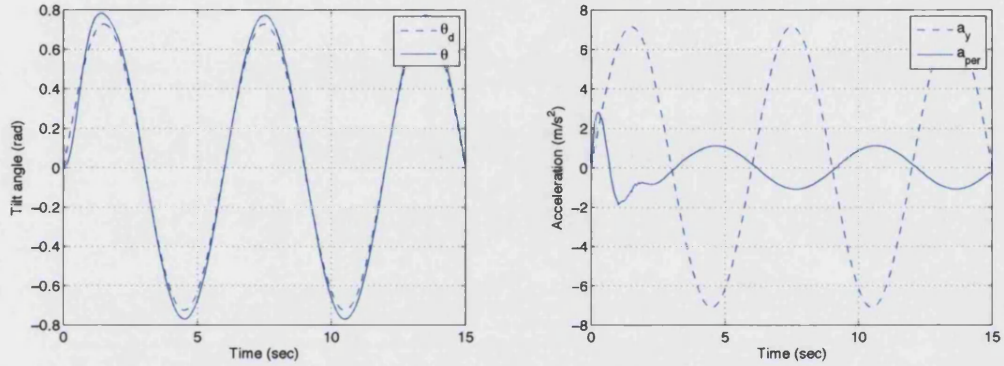

Figure 3.15: Simulation results for run 8

With more realistic ramp input, this peak is reduced. Runs 9, 10, 11 and 12 are ramp inputs where the tilt demand is the same for run 7, but the ramp to the target is over the period of half a second, as opposed to instantaneous. The runs vary with proportional gains ranging from 1 to 2.5. The acceleration results for these runs are shown in figure 3.16. As indicated in the figures, the magnitude of the accelerations is are smaller that those exhibited in run 7.

As expected, the spike in lateral acceleration at the beginning of the manoeuvre increases as the proportional gain is increased. This initial spike in lateral acceleration is important as it is associated with the moment necessary to tilt the vehicle, which has a limit.

The limiting case for the moment applied between the base and the tilting mass is if the mass of the vehicle (including the applied lateral force) is supported on one side of the vehicle's track. The calculations that produce equation 2.4 from

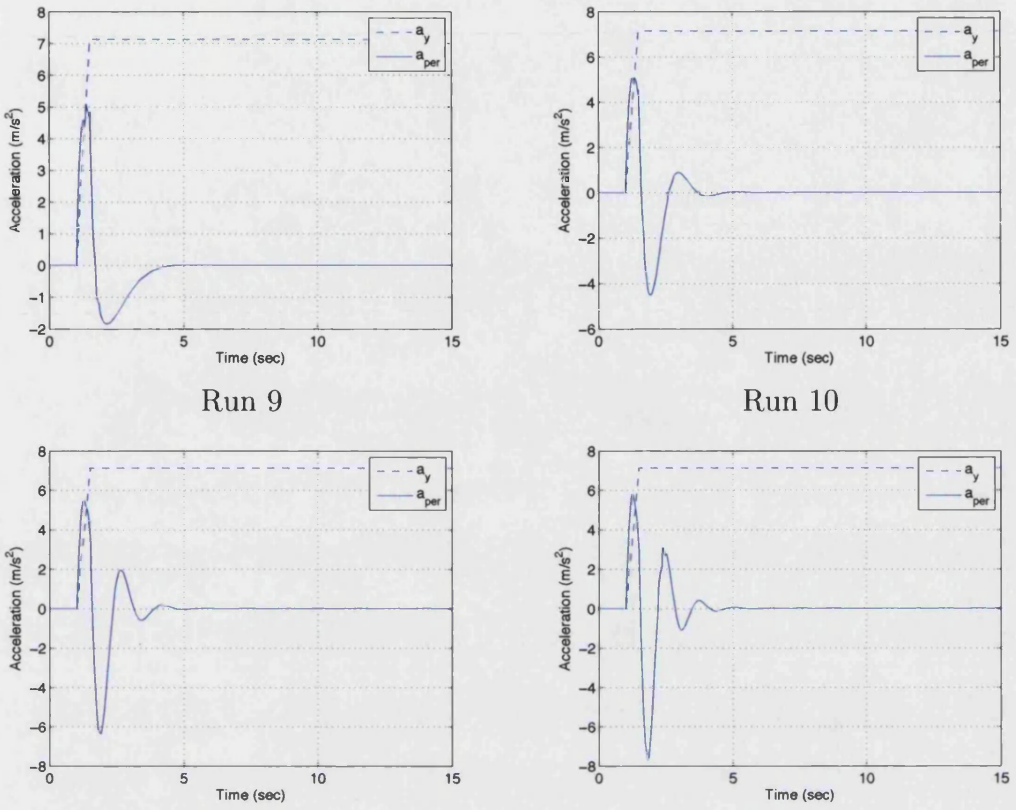

Run 9 Run 10

Run 11 Run 12

Figure 3.16: Simulation results for runs 9 and 10 (a_y and a_{per})

chapter 2 are similar, since it can be shown that the maximum moment that can be applied between the tilting body and the base is:

$$M_{\text{t,max}} = mg\frac{t}{2} \tag{3.18}$$

Hence, for a vehicle with a mass of 295 kg, and a wheel track of 1 m, $M_{\text{t,max}}$ is:

$$M_{\text{t,max}} = (295)(9.81)\frac{1}{2} = 1447\,\text{Nm} \tag{3.19}$$

The actual moment applied to tilt the vehicle can be extracted from equation 3.1 describing the dynamics of the inverted pendulum:

$$\begin{aligned} M_t &= (I_x + mh^2)\ddot{\theta} - mgh\sin\theta + ma_y h\cos\theta \\ &= mh(h\ddot{\theta} - g\sin\theta + a_y\cos\theta) + I_x\ddot{\theta} \end{aligned} \tag{3.20}$$

Combining equations 3.12 and 3.20 results in equation 3.21, where the moment applied, M_t is a function of perceived lateral acceleration and tilt acceleration.

$$M_t = mha_{\text{per}} + I_x\ddot{\theta} \tag{3.21}$$

So, from equations 3.18 and 3.21, it is evident that there is a limitation on the maximum tilt acceleration, and therefore large perceived lateral accelerations and large moment demands. An application of a torque greater than this maximum moment implies that the inner wheel of the base will lift.

Equation 3.21 is used to produce plots shown in figure 3.17, which illustrate the magnitude of the moments applied between the base and the tilting mass for simulation runs 9 and 12. For run 9, the peak moment applied is 973 Nm, but for run 12, the peak moment applied is 1687 Nm,

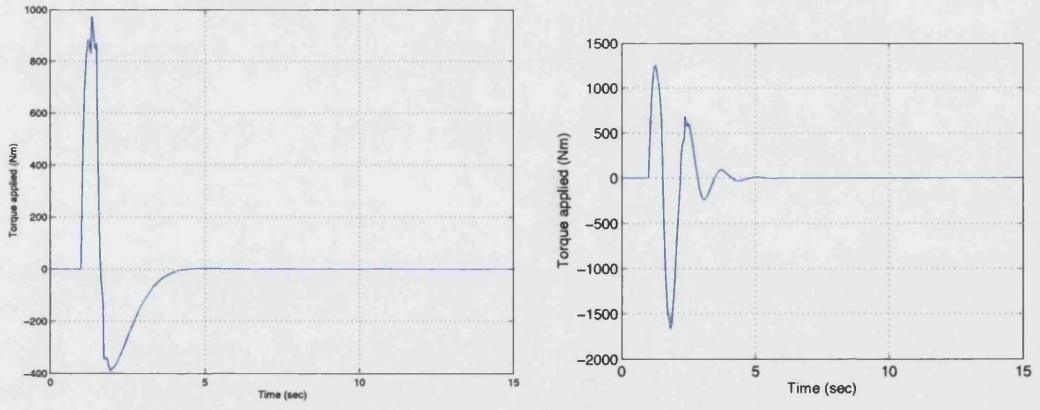

Run 9 Run 12

Figure 3.17: Simulation results for runs 9 and 12 (M_t)

The spikes in perceived lateral acceleration from runs 9 and 12 shown in figure 3.17 indicate that with a high enough gain necessary for quick response, tilt moment applied is greater than the moment limitation of the vehicle, indicating a possible rollover condition. In this simulation, their short duration and impulse-like form

may be insufficient to cause rollover, but tip the base of the vehicle. What is apparent, however, is that, with direct tilt control, there is a limit to the speed with which the steering can be applied. If the perceived lateral acceleration spike at the start of the turn is too great, the vehicle may roll over.

3.2.6 Remarks

This simulation demonstrates that adequate behaviour is obtained through the use of a direct tilt control system that takes driver input measurements to determine the tilt angle demand signal to balance the vehicle in turns. Selection of the appropriate proportional gain during implementation is important, as a low gain will result in a slow response, whereas a high gain results in a fast response, but also causes a large moment to be applied by the actuation system. This is important as while the vehicle may be able to meet the requirements in terms of steady state handling, acceptable performance in transient conditions may be limited due to this applied moment constraint. It is recommended that for implementation, the proportional gain in the controller should be set at 1, and gradually increased based on experimental assessments.

3.3 Controller Implementation

3.3.1 Control Algorithm

The first stage of the control algorithm was to use open loop control based on the steer angle and velocity. This gave a first guess at the demand tilt angle, but was based on Ackermann geometry, so was not an exact demand. While CLEVER has been optimised to follow Ackermann geometry when tilting, the use of Ackermann principles does not result in a true representation of the vehicle as tyre slip angles and road camber are not considered; this is discussed in more detail in [44].

Closed loop control develops upon this by initially calculating the demand using the steer angle and velocity, then using actuator position as a feedback signal. For

this first development stage, it was understood that this control method would not take into account road camber and one sided bumps. This is an area of further development; see section 7.5.

The control therefore functions as follows:

1. The initial lean angle demand was from the open loop controller, but this was improved from that presented in section 3.2 to account for non-linearities (vehicle geometry and tyres). This initial demand signal will be calculated using look up tables or in calculations conducted in real time.
2. From this demand angle signal, the hydraulic valve opening command was calculated.
3. The tilt angle position (measured via actuator extension) provided closed loop feedback correction.

The sensors mounted on the CLEVER vehicle measured the following: velocity, steer angle, lean angle (actuator length), yaw rate, and perceived lateral acceleration.

3.3.2 Hardware

The hardware for the tilt actuation system comprised a programmable electronic controller, custom made signal conditioner cards to condition input and output signals and a range of transducers with which to measure and monitor the driver inputs and vehicle behaviour.

Controller: Tern TD40

The controller implemented on the CLEVER Vehicle to control the tilting system is the TERN TD40, a C/C++ programmable micro-controller manufactured by TERN, Inc [60]. The controller uses a 40 MHz 16-bit AMD186 processor and all the required peripheral interfaces are contained in a single unit. The controller

was mounted in an aluminium case and includes a 16 button keypad and 16x2 character LCD display screen on the front, allowing an element of user interactivity. The controller was programmed so that the driver of CLEVER can monitor the control system, select and change parameters and manually control the tilting system.

The controller has the following specifications:

- 40 MHz 16-bit x86 compatible AMD186 CPU
- Power Consumption 190mA at 5V
- Power Input +8.5 V–+35 V using a switching regulator
- 512 KB battery backed SRAM
- 12-bit ADC and DAC, 0–4.095 V
- 35 I/O lines connected to screw terminals comprising 7 inputs, 14 outputs, and 14 hardware configurable inputs or outputs
- 3 16-bit programmable timers
- Real time clock
- Dimensions: 122 mm×87 mm×33 mm
- RS232 Serial interface port for computer connection

Further complete technical details can be found in [60].

All connections to the TD40 were made through the screw terminals and jumper connections beneath the keypad interface. Power was supplied to the controller through these screw terminals, and the supply may be unregulated, so a direct connection to a 12 V automotive based system was suitable. A regulator gives a 5 V supply to the external electronics.

The TD40 Controller is shown in figure 3.18.

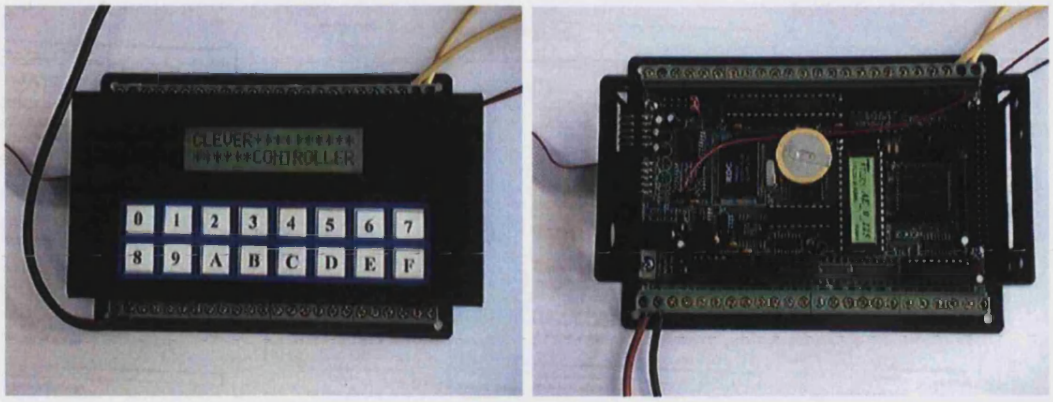

Figure 3.18: Photographs of the TD40 controller with and without the keypad interface

Transducers and Switches

For CLEVER the TD40 was configured to use 6 analogue input channels, AD0–AD5. These were connected to the transducers as shown in table 3.2. All channels used an input range of 0–5 V, which was converted in to a 12-bit integer (0–4095) within the controller. Signals were conditioned to give approximately 0–5V for the ranges listed.

Channel	Transducer	Range
AD0	Tilt Angle	−45 to +45 deg
AD1	Vehicle Speed	0–97.5 kph
AD2	Steer Angle	−30 to +30 deg
AD3	Lateral Acceleration	−5 to +5 g
AD4	Yaw Rate	−250 to +250 deg/s
AD5	Hydraulic Pressure	0–250 bar

Table 3.2: Transducers connected to controller analogue channels

Two digital input channels were used for a software mode switch and engine management system signal. A digital output channel was used to return a signal to the engine management system.

Two analogue output channels were used to send command signals to the hydraulics: the proportional directional control valve and the proportional relief valve employed as the unloading valve. Both of these outputs gave a voltage of 0–4.095 V. These signals were amplified to give −10 V to +10 V full scale for the hydraulic control valve, and 0–10 V for the proportional relief valve.

An emergency stop button was implemented that was not connected to the controller. When pressed, this button earthed the command signal supplied to the proportional directional hydraulic control valve, closing the valve.

Details about transducer placement are included in the rig design chapter, (chapter 5) under section 5.3.7.

Signal Conditioner

A separate signal conditioner prepared the analogue and digital input signals for conversion within the controller, and vice-versa for the outputs to the hydraulic valves and engine management system. The conditioner provided filters in order to reduce aliasing and supplied regulated power for the transducers. A frequency to voltage converter was also implemented to convert the frequency of pulses from the speed pickup transducer to a voltage for the analogue input channel AD1.

Output signals to the hydraulic valves were also prepared and amplified by the signal conditioner. A connector was installed so that all input and output signals were available for data-logging equipment. The schematic in figure 3.19 details the flow of signals to and from the signal conditioner and controller.

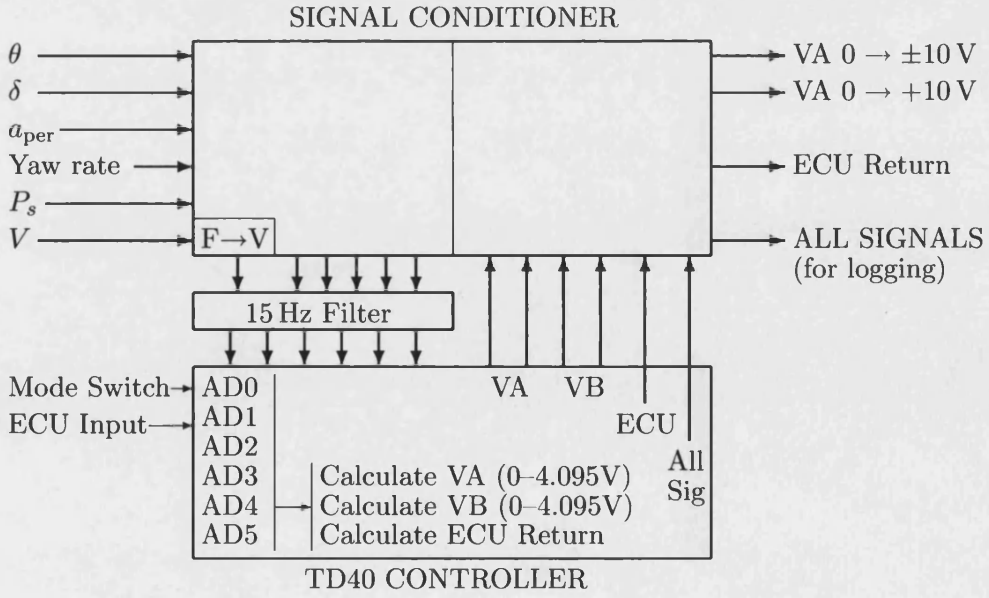

Figure 3.19: A schematic diagram of the signal conditioner and controller

Interaction with Engine ECU

As the hydraulic oil pump was driven by the engine there was a concern that the torque requirement from the hydraulic system (and hence the torque supplied by the engine to the pump) would adversely effect the performance of the engine, reducing the driveability of the vehicle in general, and possibly stalling the engine when idling. Because of this, an element of interactivity was necessary between the engine ECU and the tilt ECU. When the hydraulic system requires charging, a digital signal was sent to the engine ECU to check that enough surplus power was available. If so, the engine ECU returned a digital signal indicating this was the case, and the controller then operates the proportional relief valve through VB as necessary to load and unload the system. This was particularly important at idle speeds, as a bypass valve in the engine intake needed to be opened to provide the necessary power required to charge the system. More details can be found in chapter 4.

3.3.3 Software

Program Structure

As previously stated, the software in the controller was programmed in two stages. The first stage was the construction of the 'backbone' software, which initialises the controller; integrates the LCD display and keypad buttons with the program structure; sets up the different operating modes (manual, automatic, calibration, map select, software reset); reads transducer measurements from the signal conditioner; and writes output signals to the signal conditioner. The flow chart shown in figure 3.20 is the main software control loop.

The controller boots automatically when power is supplied. During the boot process, a series of screens are shown indicating the title and version number of the software loaded. The global variables for the various functions are also set during this process, and the ADC and DAC units are initialised.

In the next step, the loop timer starts; the loop time is regulated by one of the

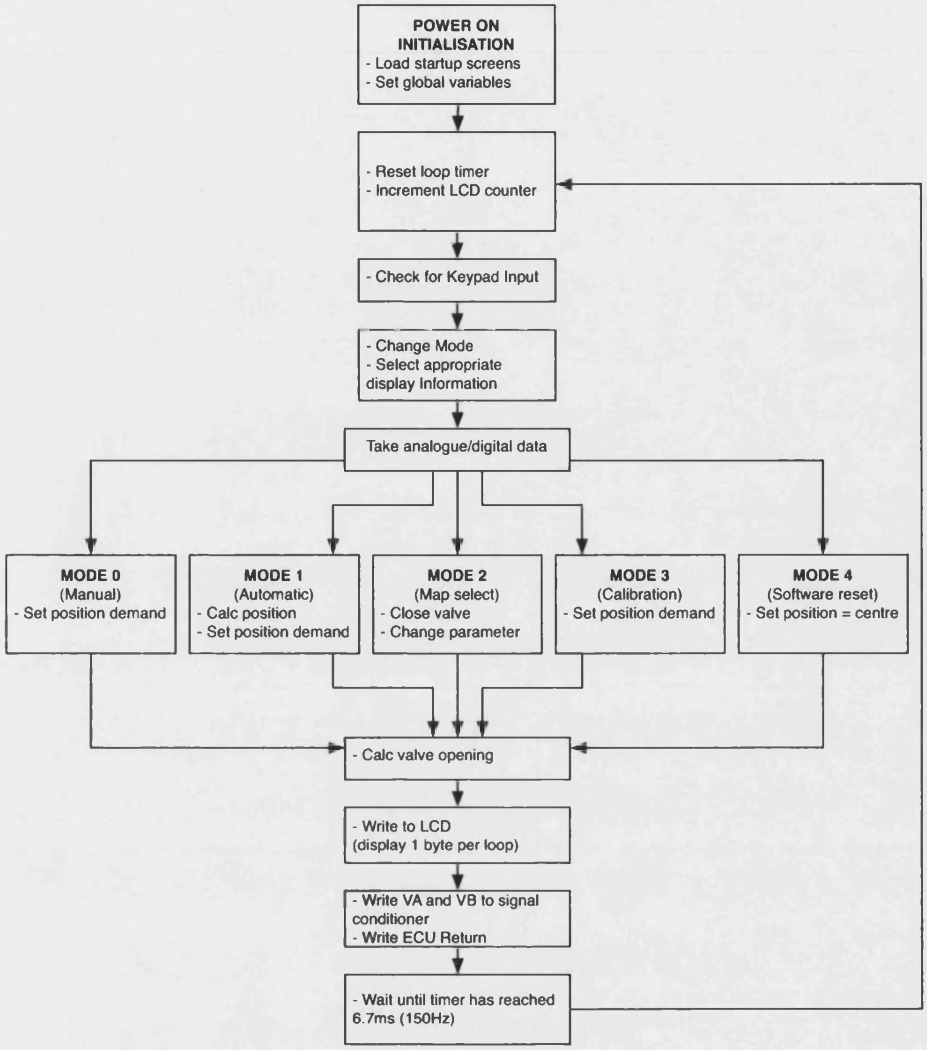

Figure 3.20: Flow diagram of main control loop

onboard timers which runs at 10 kHz, so by resetting the counter at the start of each loop, the controller pauses at the end of the loop waiting until the timer reaches 6.7 ms so that the loop execution time can be regulated to run at 150 Hz. All processes undertaken within the loop have to be completed within this 6.7 ms, and to check this is the case, it is possible to monitor the counter to see if the controller is still pausing at the end of each loop before resetting.

The keypad interface is scanned during every loop to check to see whether any key is being pressed. Depending on the mode and the key being pressed, the controller performs the function associated with the key, such as changing the metered channel, the parameter selection, the manual control of the tilting system, and the mode.

Sensor signals are read from the ADC in a sequential manner between the channels. It takes approximately 2.8 ms to read the 6 analogue channels, so a delay of 0.46 ms for each successive channel. For example, during one particular loop, the data taken from channel 2 will be from 0.46 ms later than the data taken from channel 1 during the same loop. The main control variables, speed and steer, are therefore positioned in adjacent channels to minimise any error occurring associated with this delay.

Digital data are then collected, checking for a digital signal from the engine ECU (to check that pump loading can be initiated) or the mode change switch. Initially, the mode change switch puts the controller in mode 4, an emergency stop mode that sets the position demand to centre and ignores any driver inputs.

Depending on the selected mode, the controller then conducts the necessary code to calculate the position demand and the valve output. These pieces of code are developed as the second stage of controller development.

Data are written to the screen in the next step, and in order to not slow down the loop, one character is written to the screen in each loop, with a counter recording which character is written and where.

The outputs of the control are then sent to the signal conditioning cards via the DAC to be amplified and sent to the valves. The digital signal for the ECU is also sent if necessary.

Program Function

The LCD display shows channel information and current operating mode details. In all modes, the meter and value display are shown. The meter is a block that moves left and right indicating from 0–100% the value of the transducer or VA or VB outputs. The value display shows the real calibrated value in modes 0–2, and in mode 3 shows the integer value that the controller is using for the calculations (i.e. 0–4095 bits). The channels being viewed are shown on the far left of the display, and can be changed using the meter and value change buttons. This is shown in figure 3.21.

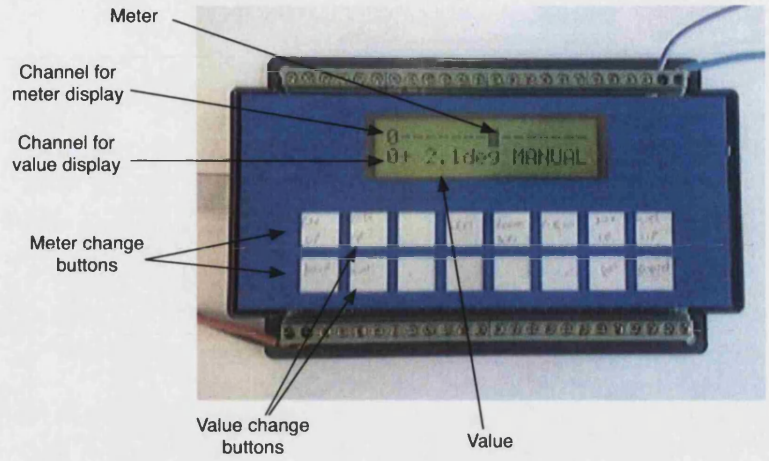

Figure 3.21: Description of LCD display

After booting, the controller defaults to mode 0, manual control mode. This modes allows monitoring of calibrated real values from the transducers on both the value display and the meter. The tilt angle of the vehicle is controlled manually, and the valve opening is limited to reduce the speed of response. The controls for mode one are shown in figure 3.22.

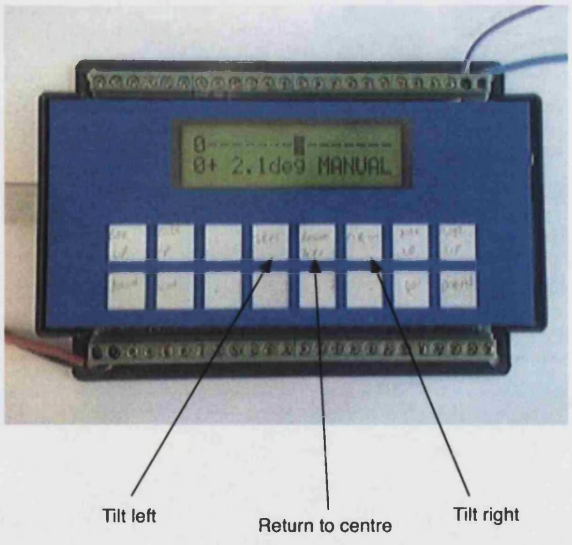

Figure 3.22: Mode 0: Manual Control

To change the mode, the user has to press the mode change buttons, on the right of the keypad. A mode change display is shown for the new mode. This is shown in figure 3.23.

Mode 1 is the normal operating mode for automatic tilt control. In this mode, the

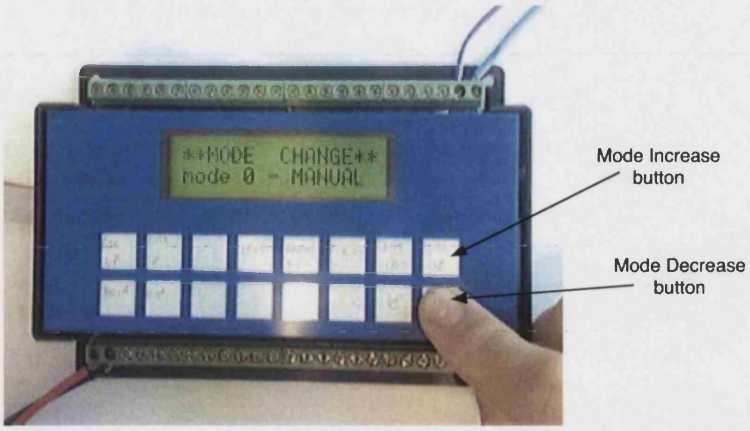

Figure 3.23: Mode Change Display

user can monitor the values and the meter, but shown at all times are the vehicle speed and selected map or parameter. The manual tilt buttons are disabled in this mode, as the tilt angle is calculated from the driver inputs. The LCD display for this mode is shown in figure 3.24.

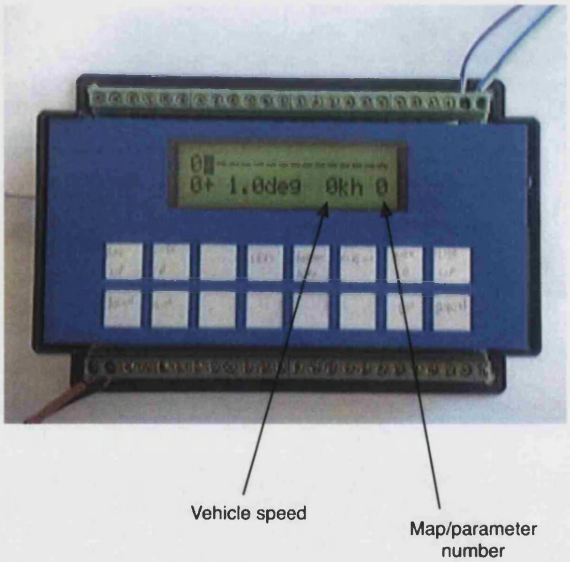

Figure 3.24: Mode 1: Normal Mode

Mode 2 is the map or parameter select mode. Here, variables can be stored under different map numbers, so that controller parameters can be changed without having to download different programs between runs. Examples of the variables that can be changed using this function are over-lean factors, filter frequencies, and controller gain values. In this mode, the valve position is closed, disabling any tilting motion, and the user selects the maps using the appropriate buttons

on the keypad interface. This is shown in figure 3.25.

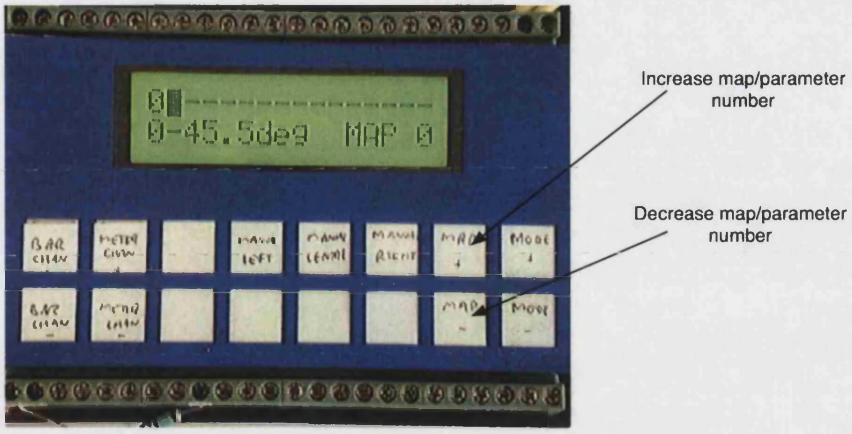

Figure 3.25: Mode 1: Map/Parameter Select

Mode 3 is identical to mode 0, manual control, except the values shown are the integer values used for calculations in the controller. This mode is used for diagnostics, to check the transducer functioning and for calibration purposes. Mode 3 is also used for specific testing conditions, where testing is conducted using an external input. For example, a modified mode 3 was used when conducting a frequency sweep of the tilting system to examine vibration modes of the chassis—valve input is not calculated in the controller, but by an external function generator, and is used as an input into the system.

Mode 4 is used as the 'emergency stop' mode, which was selected by pressing a switch in the cabin. This centres the demand tilt angle.

Tilt Demand Calculation

One important aspect to note about the TERN TD40 controller is that it does not possess a floating point processor, and as such, any floating point calculations are conducted in emulation, resulting in extremely slow execution times. Because of this, all calculations conducted within the unit use signed, unsigned and long integers. Unsigned integers are limited to 2^{16}, while long unsigned integers are limited to 2^{32}. Signed are 2^{15} and 2^{31}, as one bit is used for the sign. This limitation in the controller significantly increased the time and effort required to produce the controller code, as when an integer value is divided by another,

an integer results (i.e. $3/2 = 1$). The numbers following the decimal point are ignored.

As stated in section 3.3.1, the first step of the control algorithm was to calculate the tilt angle position demand from the measurement of velocity and steer angle. One method of obtaining the tilt angle demand would be to use a pre-prepared two-dimensional 'map' of the control algorithm, where the intersection of specific speed and steer angles would give a particular tilt angle demand. The advantages of such a method were simple implementation, very quick processing time and a selection of maps with different tilt gains could be produced and tested promptly. The disadvantages are the memory requirements in the controller to store the map data—the resolution required to produce an accurate map and to minimise errors using linear interpolation between points would result in a large map, and consequently high memory requirements. For example, a map comprising 64 specific steer angles and 64 specific speeds would result in a map comprising 4096 elements. Additionally, if one map was used for the complete steer and speed domain range of the vehicle, as presented in figure 3.7 in section 3.2.4, large areas of the map would be constrained by the mechanical tilting limit of the vehicle—high steer angles and high speeds will result in a tilt angle of greater than 45 degrees from the vertical position. Additionally, a matrix of 64 by 64, although providing adequate resolution at lower speeds, would not provide sufficient variation at higher speeds. This could lead to the controller demanding a tilt angle of -45 followed almost immediately by a demand of $+45$ for very small changes in steer angle, leading to an uncomfortable and possibly unstable vehicle. This problem could be alleviated by having separate maps for low, medium and high speeds that focus on the areas requiring a high resolution. The transitions between these maps would require careful consideration. An element of overlap with hysteresis would be necessary to avoid problems when operating around the transition of two maps with different resolutions.

The alternative to using a pre-prepared map for the first stage of the control algorithm would be to calculate the demand signal in real time within the controller. This has the disadvantage of using valuable processing time to calculate a value that could be otherwise pre-prepared and the processor has to conduct this calculation every time the control loop is run. The advantages, however, are the considerably reduced memory requirements, and no interpolation is required between discrete points—all possible combinations of steer angle and speed are

accounted for in one equation and the resolution of the result is limited by digital resolution of the signals ($0–2^{12} = 0–4095$).

The method chosen during the initial controller development stages was using a pre-prepared map, but it was quickly determined that the TD40 controller (see section 3.3.2) could not handle a map with a sufficiently fine resolution for the complete steer and speed domain. Separate maps for low, medium and higher speeds were considered, but faced the same memory constraints within the controller. Thus, the method of calculating the demand signal within the program was chosen.

To calculate the tilt angle demand, it was necessary to use equation 3.16 as a starting point:

$$\theta_d = \tan^{-1}\left(\frac{V^2 \tan\delta}{lg}\right)$$

The lack of a floating point unit meant that non-linear trigonometric functions, such as tangent, were not possible within the controller, so linear approximations were used. While small angle approximations were sufficient for the steer angle element of equation 3.16, since it is limited to $\pm 30°$, for the tilt angle, a linear approximation of tangent was determined that results in values closer to those produced by assuming $\tan\theta \approx \theta$. The linear approximation of tangent used is shown in figure 3.26.

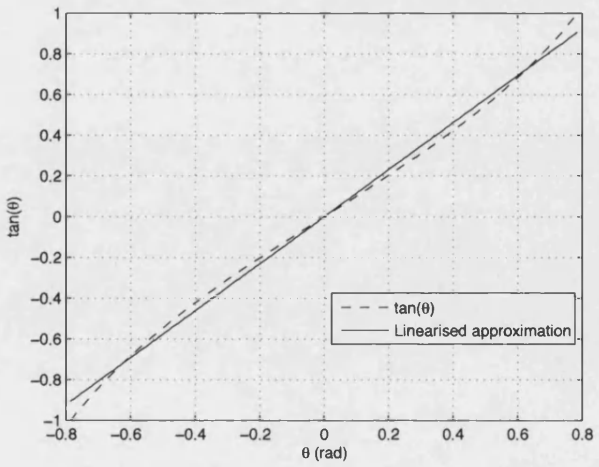

Figure 3.26: Linear approximation of tangent function

The equation for the linear approximation is shown in equation 3.22.

$$\tan(\theta) \approx 1.1545(\theta) \tag{3.22}$$

So equation 3.16 becomes equation 3.23:

$$\theta_d = 0.8662\left(\frac{V^2\delta}{lg}\right) \tag{3.23}$$

In addition to the calculations being limited to linear approximations of non-linear functions and the use of integer values, the transducer signals were scaled so that the minimum gave an integer reading of 0, and the maximum gave an integer reading of 4095. For example, the minimum tilt position, $-45°$, gave an integer reading of 0, while the maximum tilt position, $+45°$, gave an integer reading of 4095. This is shown in figure 3.27. The same was also true of steering ($\delta = -30° \rightarrow$ AD2 $= 0$ and $\delta = +30° \rightarrow$ AD2 $= 4095$). For equation 3.16 to be valid, these integer values had to be recentred around 0, such that AD0 $= 0$ when $\theta = 0°$.

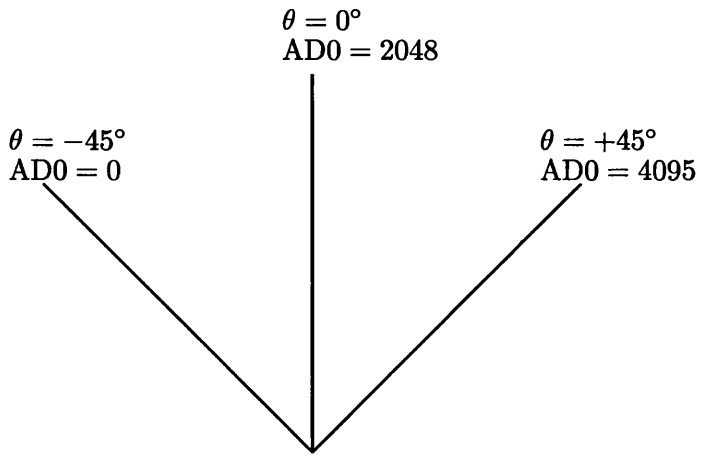

Figure 3.27: Relationship between real and integer values

Taking these issues into account, a flow chart for the position demand calculation was constructed. This is shown in figure 3.28.

The process is readily explained through an example. Following equation 3.23, we know that with a forward speed of 10 m/s and a 2° steer angle, the tilt angle should be approximately 7.35°.

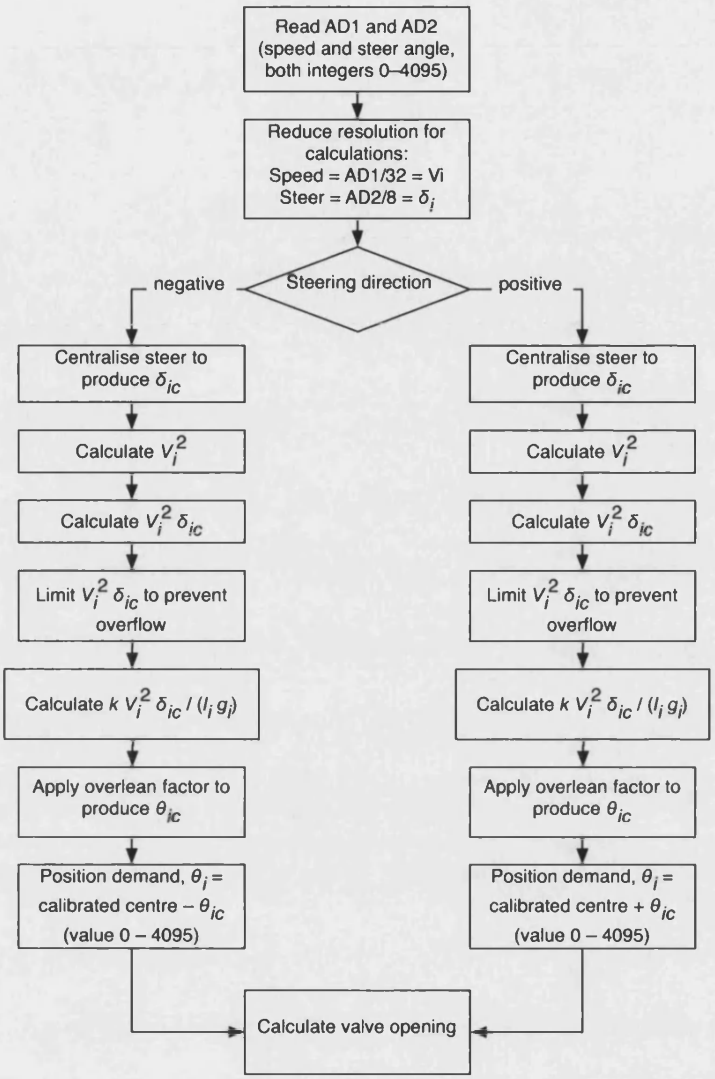

Figure 3.28: Flow chart for position demand calculation

The first step is to read the integer values of AD1 (speed) and AD2 (steer angle). A forward speed of 10 m/s relates to an integer speed of AD1 = 1512, and a 2° steer relates to a steer value of AD2 = 2184. Since these are two values in the range of 0–4095, multiplying the square of velocity by the steer angle could result in an integer value exceeding that capable in the 16-bit controller. So, the first stage was to reduce the resolution of the readings. The integer value for speed is divided by 32, resulting 128 discrete speeds. The integer steer value is divided by 8, resulting in 512 discrete steer positions. In this case, $V_i = 47$ and $\delta_i = 273$.

The next stage is to centralise the integer values around the real centre position. Since the steer input is positive (2179 is greater than the centre steering position

of 2048), we follow the right path in the flow diagram. Centralising the steer input involves subtracting $2048/8 = 256$ from the integer value we have, resulting in δ_{ic}. So in this example, $\delta_{ic} = 17$.

The next step is to calculate V_i^2, which with an integer value of 47, $V_i^2 = 2209$. This is multiplied by δ_{ic} producing the product: $V_i^2\delta_{ic} = 37553$.

As only integers can be dealt with, we reassign the wheelbase a value of 240 ($l_i = l \times 100$), and gravity is deemed to be 981 ($g_i = g \times 100$). For the calculation to be correct, an additional factor, k, has to be calculated to take into account the scaling that occurs by using integers. This factor is determined to be 2103. So the next step of the process is to multiply $V_i^2\delta_{ic}$ by the factor, k, and then divide by l_i and g_i. The calculation must be done in this order to reduce rounding errors occurring when dividing two integers by each other. However, before this can be done, to ensure that the integer value of $kV_i^2\delta_{ic}$ does not exceed the maximum value of a long integer in the controller, $V_i^2\delta_{ic}$ is limited to $2^{32}/k$. So now, we can find the centralised integer value of tilt angle, θ_{ic}:

$$\theta_{ic} = \frac{kV_i^2\delta_{ic}}{l_i g_i} = \frac{(2103)(2209)(17)}{(240)(981)} = 335$$

To find the position demand, this needs to be de-centralised to an integer value between 0 and 4095, so θ_{ic} is added to the centre position integer value of 2048, producing a θ_i of 2382. Converting this value back to a tilt angle in degrees, we result in a tilt value of 7.35°.

The step shown in the flow diagram, but not implemented in the demonstration above, is where an over-lean factor is applied. The purpose of this step is described in more detail in section 3.4.2.

Valve Input Command Signal Calculation

The next stage is to calculate the valve opening based on the position demand signal and the feedback position. A flow diagram of this process is shown in figure 3.29.

The first step is to subtract the real value from the demand value to produce the

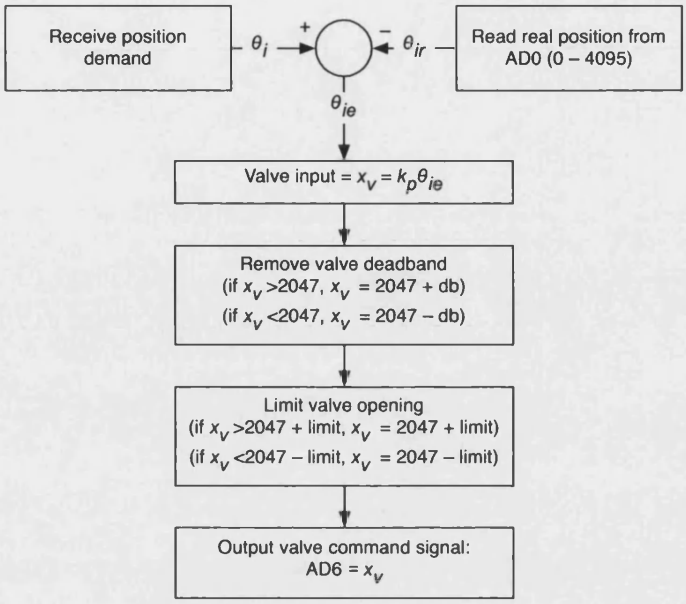

Figure 3.29: Flow chart for position control calculation

error signal. This value is then multiplied by a proportional gain to produce the valve opening. It must be considered that since the demand and error signals are both the full 0–4095 scale, the gain used here is half the proportional gain, if looking at centralised signals (as used in the simulation). The value of this gain was tuned during testing – the higher the gain, the faster the response, but this must be offset against both the amplification of noise in the system, and that a higher response increases the moment being applied by the hydraulics. As shown previously in section 3.2.5, there is a limit to the moment applied between the base and the tilting unit to maintain stability.

The valve chosen for the CLEVER vehicle was overlapped, and therefore had a dead band around the centre position to minimise any leakage while the valve was closed. As such, the first 15% of valve opening each side the valve spool is in this dead band. To remove this dead-band in the control code, the dead-band was compensated for in the control code by adding an integer value equivalent to a 15% opening to the command signal.

In order to limit the tilt speed, a cap was placed on the valve command signal. In the manual mode and calibration modes, the valve opening was limited to reduce the maximum speed of the tilting motion. In automatic mode, a limit was still imposed, but was set much higher.

3.4 Other Considerations

3.4.1 Calibration and Trim of Transducers

In the real vehicle, the transducer placement does not necessarily produce a linear relationship between integer value and actual position. For example, the central tilt position has an integer value of 2433, with a maximum of 4095 and a minimum of 65. This was partially due to inadequate manufacturing tolerances, whereby the tilt actuator mounting positions on the vehicle cabin were not at equal heights. As a result the vehicle can tilt further to the left than to the right. In addition, the tilt angle is being calculated from the actuator extension, and the relationship between actuator extension and tilt angle is not perfectly linear. Similarly, the relationship between steering angle and steering integer value is non-linear, with the central position being at 2016. The calibration and trim of the transducers was taken into account in the final code used in the controller.

3.4.2 Over-lean

In section 2.2.2, it was noted that when the tilt axis was inclined and above ground level, the balancing action is reduced, as the rotation about the projected ground level tilt axis was less than the actual rotation about the tilt axis. To compensate for this, a step in the position demand calculation allows for the implementation of 'over-lean', where the tilt angle demand can be increased (or indeed decreased) by a factor, to increase or decrease the balancing effect. The value of this factor was determined in subjective testing. Crucially, it does not effect the vehicle handling to a significant degree, as the tilt axis in CLEVER was optimised to give Ackermann steering when tilting—the additional cornering force generated by camber thrust at the front wheel was compensated by the rear wheels steering in the same direction as the front wheel [44]. The implementation of this over-lean factor is discussed in further detail in section 6.4.2.

3.5 Conclusions

The design of controller of the CLEVER vehicle tilting system was based on the idea of direct tilt control, where driver inputs and vehicle behaviour were used to calculate the demand tilt angle, and this value was used to calculate the necessary signal to tilt the vehicle to the correct angle.

A simple simulation model was developed of the tilting body of the vehicle, represented by an inverted pendulum. From the equation of motion, a transfer function was developed relating demand signal to output position and this was shown to be marginally stable. Implementing a PD controller stabilised the system by introducing the damping and giving a fast rise time.

Simulation results indicate adequate performance can be achieved, but highlights an issue when large perceived lateral accelerations are experienced. These perceived lateral acceleration spikes relate to large tilt moment demands, and analysis has shown that if these demands breach a specific limit, the stability of the vehicle may be compromised.

In order to implement direct tilt control in the development vehicle, a controller was acquired and integrated with the transducers and a signal conditioner to reliably measure the driver inputs and vehicle behaviour. The control software was developed in two stages: the first stage involved the coding of the main structure of the code, incorporating the user interface, reading input signals and writing to the output terminals. The second stage was the development of the code to determine the tilt angle demand and calculate the necessary valve command signal to tilt the vehicle.

Due to the lack of a floating point processor within the controller, considerable additional time and effort was required to process the signals and run the calculations necessary to determine the correct valve opening. Linearisations of simple functions had to be developed, and since integer values had to be used throughout, considerable checking had to occur to ensure that the variable values did not overflow. Despite these limitations, the controller program was developed based on the analysis and simulation work presented within this chapter.

Chapter 4

Actuation

4.1 Introduction

The CLEVER vehicle has an active direct tilt control system to calculate the required lean angle to stabilise the vehicle in corners. In order to implement this, the vehicle requires an energy efficient actuation system to provide the necessary torque between the non-tilting rear base unit and the tilting cabin.

Initial research conducted as part of the CLEVER project highlighted two main options in terms of actuation technology: electric and hydraulic. Owing to the high current requirements associated with high power electric motors with a low voltage automotive electrical system, the electric option was not feasible for the CLEVER vehicle. The chosen hydraulic actuation solution offered greater power density and flexibility of component placement and hence aided packaging within the rear frame of the vehicle.

The design and conceptual development of the hydraulic circuit to actuate the tilting system is discussed, identifying the various components necessary to meet the tilt actuation requirements of the CLEVER vehicle.

A linear model of the valve-actuator system is developed in order to assess the basic dynamics of the hydraulics, and this is followed by the construction of a fully

non-linear simulation of the complete hydraulic system including the pump, accumulator, and unloading system in addition to the valve and actuator components. This simulation was used to size and select appropriate hardware components for implementation of the hydraulic tilt actuation system on the development prototype.

4.2 Design of Hydraulic System

The CLEVER vehicle prototype has a main tilting structure and a separate rear module that remains upright with respect to the ground. The hydraulic system fits between these two structures providing the actuation necessary to rotate the tilting cabin relative to the stationary base. This mechanism can be considered as a position control system for an inverted pendulum, with the length of the pendulum being the distance between the tilt axis and the tilting cabin centre of mass. A schematic is shown in figure 4.1.

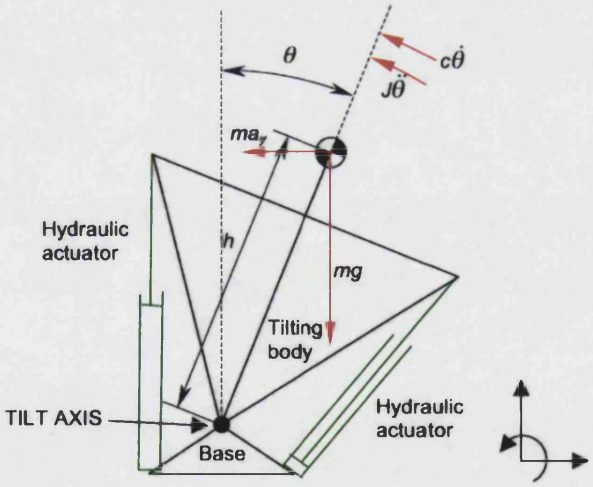

Figure 4.1: Representation of the system as position control of an inverted pendulum

The total torque the actuators have to provide is the sum of the torque due the pendulum mass, the torque due to the lateral acceleration on the mass, the torque required to accelerate the mass and overcome any damping and friction in the system, and the torque due to external forces on the mass, such as aerodynamic loading. Thus, assuming massless hydraulics, the torque required to tilt the

vehicle can be expressed as:

$$T = ma_y h\cos(\theta) - mgh\sin(\theta) + J\ddot{\theta} + c\dot{\theta} + T_{dist} \tag{4.1}$$

where J is the inertia of the tilting body, c is the damping of the tilting body, and T_{dist} is the torque loading due to external forces on the mass.

The 'worst case' dynamic requirement considered practically realistic was to tilt the body sinusoidally from the maximum left tilt position ($-45°$ from the central position) to the maximum right tilt position ($+45°$ from the central position) in 1.5 seconds (cycle frequency of 0.33 Hz). (This 'worst case' cycle does not include the large moment requirement at the start of a turn—once a slalom maneouvre is initiated, the large moment requirement can be neglected) The tilt angle, θ, as a function of time was therefore taken to be:

$$\theta(t) = \frac{\pi}{4}\sin\left(\frac{2\pi}{3}t\right) \tag{4.2}$$

For initial evaluation, a simple model of a stationary vehicle was used—no lateral forces are applied—and it was assumed that there is no damping in the tilt action. The torque, T, required to tilt the system is:

$$T = -mgh\sin(\theta) + mh^2\ddot{\theta} \tag{4.3}$$

Power, P, is calculated from torque:

$$P = T\dot{\theta} \tag{4.4}$$

With estimates suggesting m is 295 kg and h is 0.5 m, a plot of the sinusoidal variation in tilt angle, torque and power (equations 4.2, 4.3 and 4.4) is shown in figure 4.2. The maximum torque requirement is approximately 1.25 kNm, and the maximum power requirement is approximately 1 kW. To put this in perspective, the maximum engine output power is 12.5 kW so the tilt demand requires a significant proportion of engine power [61].

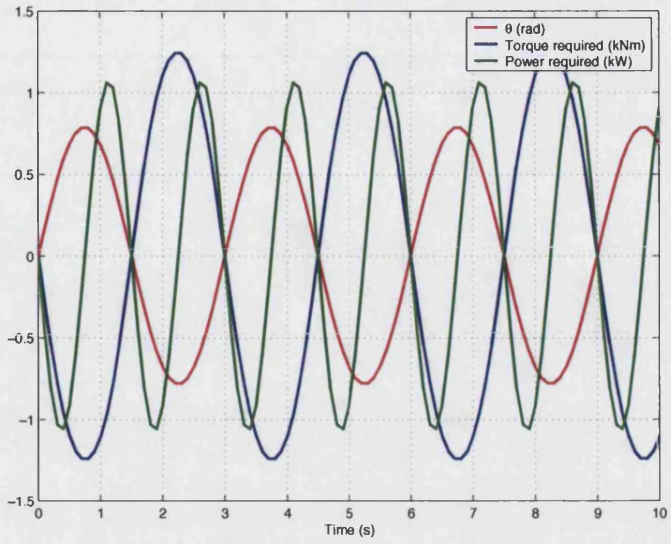

Figure 4.2: Tilt angle and torque requirement

4.3 Hydraulic Circuit

4.3.1 Proposed Design

The hydraulic circuit was designed to control the position of the tilting part of the vehicle with two single acting linear hydraulic actuators. When pressurised, these cylinders control the lean angle of the tilting cabin by rotating it with respect to the upright rear module. A proportional directional control valve with a closed centre position modulates the flow to the actuators and controls their position and locks the cylinders when no command is given. Figure 4.3 shows the hydraulic circuit.

Flow in the system is provided by a gear pump driven directly from the engine crankshaft, providing adequate flow for sinusoidal tilting from maximum to minimum tilt angle at 0.33 Hz. In order to unload the pump, augment the flow and provide flow in the event of pump or engine failure, an accumulator was incorporated in the circuit in conjunction with an unloading valve. When the desired system pressure is reached, the unloading valve opens, allowing flow generated by the pump to return to tank, decreasing the torque demand on the engine. When the accumulator has discharged and the pressure in the system falls below a minimum threshold value, the unloading valve closes, directing flow from the pump

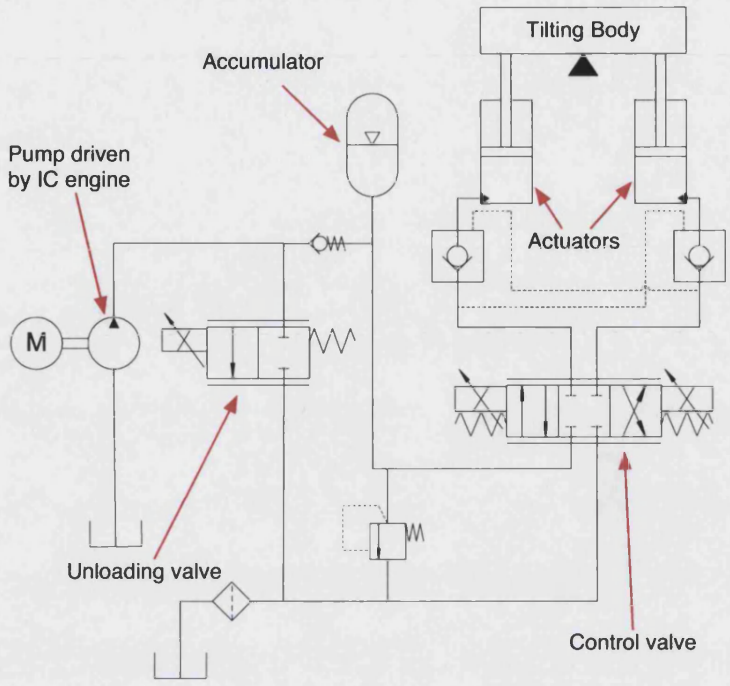

Figure 4.3: Proposed hydraulic circuit for tilting vehicle

back to the system to charge the accumulator until maximum system pressure is reached. Two pilot operated check valves mounted in a cross-port manifold are implemented between the actuators and the control valve so that the actuators are locked when the valve is closed, and any leakages across the ports in the valve does not affect the tilt angle. The bandwidth of these pilot operated check valves is sufficiently high enough not to affect the dynamic performance of the tilting system.

Actuators

The hydraulic actuators were positioned in the vehicle between the tilting body and the upright rear module. They are positioned to optimise the torque generation within the package design constraints. As a result of the system kinematics, an actuator stroke of 200 mm is required. Also due to tilting kinematics lever arm through which the tilting moment is generated varies with respect to tilt angle, as shown in figure 4.4. From the figure, it can be seen that the lever arm is greatest when a large moment is required—i.e. when the vehicle is tilted to the left, the left hand actuator is required to return the vehicle to the upright position. The

large moment requirement will be required between a tilt angle of $-45°$ and $0°$, which is also a region where the blue trace has the greatest magnitude.

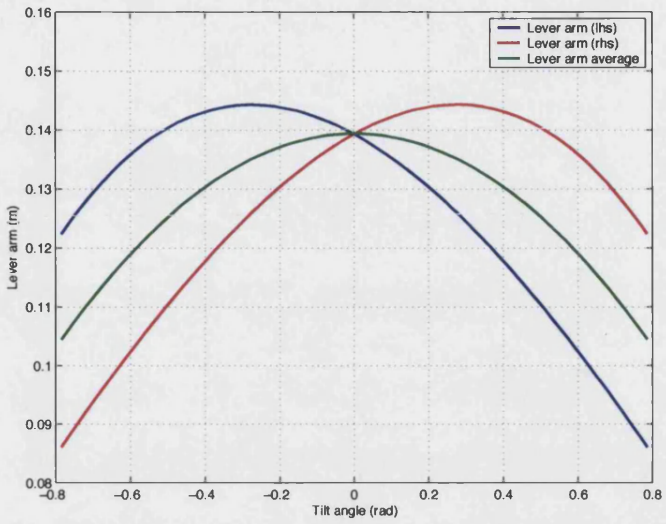

Figure 4.4: Actuator lever arm against tilt angle

The hydraulic actuators are single acting, being pressurised on the piston side only. For example, when the body tilts to the right to make a right hand turn (θ is positive), the left hand actuator provides the necessary force, extending and tilting the vehicle cabin with respect to the rear unit. The right hand actuator is retracted, sending flow through the valve and filter back to the reservoir.

The actuators were sized according to the force demand. The piston diameter was determined from the torque equation of a pressurised actuator:

$$T = P_s A_p b \quad \rightarrow \quad A_p = \frac{T}{P_s b} \quad \rightarrow \quad d_{\text{cyl}} = 2\sqrt{\frac{T}{\pi P_s b}} \tag{4.5}$$

where P_s is the system pressure, b is the lever arm, A_{act} is the piston area, and d_{cyl} is the piston diameter. The highest load on each actuator occurs when fully contracted, so from figure 4.4, b is 0.122 m. With the maximum torque requirement of 1.25 kNm occurring at the initial position with zero flow, and a system pressure of 160 bar, the piston diameter needed to be at least 28.5 mm. Commercial cylinders fulfilling this requirement have a piston diameter of 32 mm. Therefore, the maximum applied moment is 1.57 kNm with a system pressure of

160 bar. Approximately 0.16 litres of oil is required for one complete tilt from $-45°$ to $+45°$.

Control Valve

The chosen control valve for the system was a 4-port, 3-position proportional directional control valve with a closed centre. A proportional valve was necessary to achieve the system's dynamic requirements and continuous regulation during normal driving. The size of the valve was determined by the peak flow requirement. Assuming the same 0.33 Hz sinusoidal duty cycle shown in figure 4.2, the maximum piston speed, and therefore the peak flow requirement can be determined: this is calculated to be 10.1 l/min. The selected valve provided a nominal flow of 16 l/min at a pressure drop of 10 bar.

Pump

The pump choice was determined by considering the flow requirement and the internal combustion engine used to drive the pump. Analysis of the CVT transmission [62] suggested that when cruising, the engine will spend much of the time operating at around 5500 rpm. Engine idle speed was 1700 rpm, and maximum engine speed was limited to 8500 rpm [61]. The chosen pump would have to operate and function between these two extremes, while providing mean flow at the normal operating point. In order for a gear pump to operate at these engine speeds, the pump had to be driven through a reduction gear ratio to operate within its speed limitations.

The 0.33 Hz sinusoidal duty cycle was used to determine flow requirements. As the dimensions of the actuators were known, the mean flow requirement for the 'worst case' duty cycle was calculated to be 6.43 l/min. Commercial gear pumps operate between 750 rpm and 4000 rpm, so choosing a 3 cc/rev gear pump and matching that to 6.43 l/min results in a pump speed of 2150 rpm. In order to match this pump speed to an engine speed of 5500 rpm, the necessary gear ratio between the pump and the engine is 2.56:1. A V-belt pulley system was designed to drive the pump from the engine crank shaft (see section 5.2.6 for more details

of this drive system).

Accumulator

The accumulator was used within the system primarily for three purposes:

1. To provide the necessary flow during periods when the pump was unloaded.
2. To provide peak flow when the pump was loaded and harsh manoeuvres were being undertaken by the vehicle consequently requiring a high flow demand.
3. To provide emergency flow if the pump or engine failed.

Diaphragm accumulators were considered, owing to their lighter weight and reduced size compared to bladder accumulators. The higher pressure and flow capabilities of the latter were surplus to requirements for this application.

Sizing the accumulator not only involved examining the simulation results, but also had to take into account suggested duty cycle and design constraints. Larger accumulators would be able to provide flow for more tilt cycles, allowing the pump to be unloaded for longer periods of time. However, this benefit has to be balanced with the longer charging time required while the pump was loaded, charging the system, and integrating the increased weight and size of a larger accumulator within the vehicle design. A smaller accumulator reduces the number of tilting movements available while the pump is unloaded and increases the frequency of charging cycles, arguably impairing the drivability. However, smaller accumulators would be quicker to recharge, and integration within the vehicle would be easier owing to their lighter weight and smaller size. Following simulation results (see section 4.5), a 1.4 litre diaphragm accumulator was chosen for the development prototype.

Unloading valve

The engine used in the final CLEVER vehicle was a 230 cc 4-stroke internal combustion engine running on compressed natural gas (CNG) with a maximum power of 12.5 kW. The development prototype built for tilt system development used an unmodified 176 cc version of the same engine running on gasoline. Output power and engine speed range for this engine was comparable to that of the CNG engine. Because maximum power was 12.5 kW, it was beneficial to unload the pump when the system was pressurised, and hence reduce the power demand on the engine. To accomplish this, an unloading valve was integrated into the circuit.

When the system starts, the valve is initially closed, sending flow from the pump through a check valve, charging the system. When the maximum system pressure is reached, the valve opens allowing flow from the pump to return to tank, unloading the pump and reducing the torque load on the engine. As the vehicle tilts, the pressure within the system is reduced until it reaches a lower threshold pressure, at which point the valve closes again, enabling the pump to recharge the system.

One challenge with this design of the hydraulic circuit was the transition between loading and unloading the system and the effect of this load change on the drivability of the vehicle. With a standard two-position valve, it was suggested that the loading could be quite harsh. By using a proportional or soft-start [58] valve, it would possible to smooth the transition when loading the pump. When unloading, there is little point in gradually opening the valve, since the throttling through this valve would simply waste energy. A proportional valve would also require careful control, including pressure measurement to predict when the system will need charging, and hence start to close the valve. A proportional unloading valve was tested in simulation (see section 4.5).

4.4 Linearised Model

A linearised model of the hydraulic system was developed to conduct initial analysis of the dynamic behaviour of the valve-actuator system, including the influences of individual parameters on the position control. For the model to be suitable for dynamic analysis, it was necessary to include the effects of fluid and mechanical compliance in the system. It was assumed that the supply pressure, P_s, was constant irrespective of the flow rate demand. As such, the unloading valve and accumulator are not included in this model. The simulation is confined to a valve-actuator model.

4.4.1 Valve

Using small perturbation analysis, the linearised equation for a valve is:

$$q = C_x x_v + C_p p \tag{4.6}$$

where C_x and C_p are the flow gain and the flow-pressure gain evaluated around the operating position. The flow through the valve is a function of the valve spool position, x, and the pressure drop across the opening, p. As the valve employed in CLEVER is a 4-port 3-position valve, equivalent equations (4.7 and 4.8) can be generated for the flow into one actuator (chamber one) and the flow exiting the other actuator (chamber two). As CLEVER tilts in both directions, it is appropriate to linearise the valve equations about the null position—the valve operates approximately equal amounts of time on either side of the null position.

$$q_1 = C_{x1} x_v + C_{p1} p_1 \tag{4.7}$$

$$q_2 = C_{x2} x_v + C_{p2} p_2 \tag{4.8}$$

The values of C_{x1}, C_{x2}, C_{p1} and C_{p2} are partial derivatives of the characteristic valve orifice equation: equation 4.9 for the flow into chamber one and equation 4.10 for the flow out of chamber two:

$$Q_1 = C_e X \sqrt{P_s - P_1} \tag{4.9}$$

$$Q_2 = C_e X \sqrt{P_2} \tag{4.10}$$

It is assumed that X is positive: for any valve opening, fluid entering the P port of the valve flows to the A port (actuator one), and fluid entering the B port of the valve flows to tank via the T port.

The values of C_{x1}, C_{x2}, C_{p1} and C_{p2} are therefore:

$$\begin{aligned} C_{x1} &= \frac{\partial Q_1}{\partial X} = C_e\sqrt{P_s - P_1} \\ C_{x2} &= \frac{\partial Q_2}{\partial X} = C_e\sqrt{P_2} \\ C_{p1} &= \frac{\partial Q_1}{\partial P_1} = \frac{-C_e X}{2\sqrt{P_s - P_1}} \\ C_{p2} &= \frac{\partial Q_2}{\partial P_2} = \frac{C_e X}{2\sqrt{P_2}} \end{aligned}$$

The valve coefficient, C_e, is calculated from valve characteristics: specifically the nominal flow at a specified pressure drop with 100% valve opening. The values of q_{nom} and ΔP_{nom} are listed in the valve catalogue [63], and the calculation required is equation 4.11:

$$q_{\text{nom}} = C_e\sqrt{\frac{\Delta P_{\text{nom}}}{2}} \quad \rightarrow \quad C_e = \frac{q_{\text{nom}}}{\sqrt{\frac{\Delta P_{\text{nom}}}{2}}} \tag{4.11}$$

Plugging in the values for q_{nom} and ΔP_{nom} of 16 l/min for a pressure drop of 10 bar [63]:

$$C_e = 3.771 \times 10^{-7} \qquad \left[\frac{\text{m}^4}{\text{s}\sqrt{\text{N}}}\right]$$

This value of C_e is based on normalised valve opening: $X = 0$ being closed and $X = 1$ being fully open.

4.4.2 Actuators

In order to develop a suitable simulation model for the actuators, two aspects must be considered: the flow-pressure relationship and the force-acceleration relationships. The proposed circuit for CLEVER is to employ two single acting actuators. For this reason, each actuator is dealt with separately.

Flow-Pressure Relationship

Considering firstly the flow relationship, the flow into actuator one, Q_1, is composed of flow due to compliance of the fluid and flow due to the displacement of the actuator piston. This is illustrated in figure 4.5 and represented by equation 4.12.

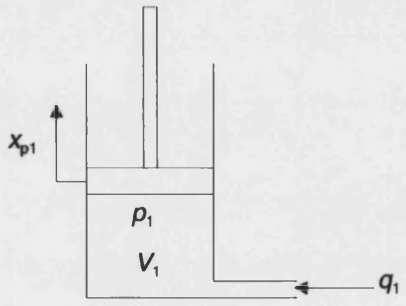

Figure 4.5: Flow relationship: Actuator 1

$$q_1 = Q_{compl} + Q_{displ} \tag{4.12}$$

where

$$Q_{displ} = A_p \frac{\mathrm{d}x_{p1}}{\mathrm{d}t}$$

An expression for Q_{compl} is developed from equations governing the compliance of the hydraulic fluid. We know that the bulk modulus is the volumetric stress over the volumetric strain:

$$\beta_e = -\frac{V_1 \mathrm{d}P_1}{\mathrm{d}V_{compl}}$$

with $\mathrm{d}V_{compl}$ being the change in volume of the mass of fluid in actuator one due to compressibility of the fluid. Rearranging we get:

$$\mathrm{d}V_{compl} = -\frac{V_1}{\beta_e}\mathrm{d}P_1$$

The flow due to the compliance of the fluid is the rate of change in volume:

$$\begin{aligned} Q_{compl} &= -\frac{\mathrm{d}V_{compl}}{\mathrm{d}t} \\ &= \frac{V_1}{\beta_e}\frac{\mathrm{d}P_1}{\mathrm{d}t} \\ &= \frac{V_1}{\beta_e} sP_1 \end{aligned}$$

Therefore, the flow into chamber 1 is:

$$q_1 = Q_{compl} + Q_{displ} = A_p s x_{p1} + \frac{V_1}{\beta_e} s p_1 \tag{4.13}$$

The other actuator is shown in figure 4.6.

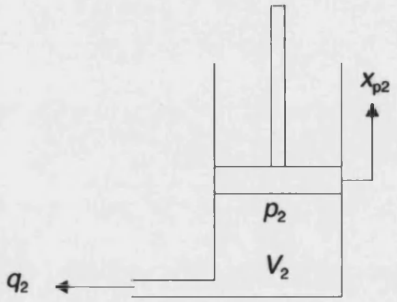

Figure 4.6: Flow relationship: Actuator 2

The flow leaving the cylinder, q_2, is defined as positive. Following the same process, a comparable equation can be derived for q_2:

$$q_2 = -A_p \frac{\mathrm{d}x_{p2}}{\mathrm{d}t} - \frac{V_2}{\beta_e} \frac{\mathrm{d}P_2}{\mathrm{d}t} = -A_p s x_{p2} - \frac{V_2}{\beta_e} s p_2 \tag{4.14}$$

Note, that the flow due to displacement is negative (as actuator 2 extends (i.e. $\dot{x}_{p2}$ is positive), flow is entering the chamber). The flow due to compliance is also negative as the fluid compliance within the actuator reduced the flow leaving the actuator.

By combining equation 4.7 with equation 4.13 and equation 4.8 with equation 4.14, equations expressing p_1 and p_2 can be found (equations 4.15 and 4.16 re-

spectively:

$$\begin{aligned} C_{x1}x_v + C_{p1}p_1 &= A_p s x_{p1} + \frac{V_1}{\beta_e} s p_1 \\ p_1 &= \frac{C_{x1}x_v - A_p s x_{p1}}{\frac{V_1}{\beta_e}s - C_{p1}} \end{aligned} \tag{4.15}$$

and

$$\begin{aligned} C_{x2}x_v + C_{p2}p_2 &= -A_p s x_{p2} - \frac{V_2}{\beta_e} s p_2 \\ p_2 &= \frac{C_{x2}x_v + A_p s x_{p1}}{-\frac{V_2}{\beta_e}s - C_{p2}} \end{aligned} \tag{4.16}$$

Force-Acceleration Relationship

To complete the block diagram of the actuators, the force-acceleration (FA) relationship needs to be considered. As both actuators act upon the tilting cabin of the vehicle, the forces to overcome are the rotational inertia of the tilting cabin about the tilt axis, $J\ddot{\theta}$, and the forces due to friction $B_p\dot{\theta}$. The schematic in figure 4.7 shows the moments being applied.

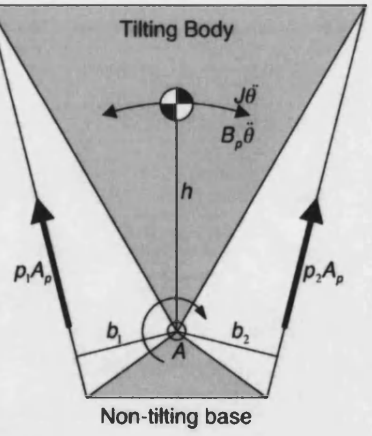

Figure 4.7: Schematic showing actuator forces and moments on tilting cabin

The values b_1 and b_2 are the lever arms, perpendicular to the force direction of the actuators. The variation of lever arm is shown in figure 4.4.

Examining the moments about the tilt axis, A:

$$\sum F_A = J\ddot{\theta} = p_1 A_p b_1 - p_2 A_p b_2 - B_p\dot{\theta}$$

Therefore:

$$\begin{aligned} A_p(p_1b_1 - p_2b_2) &= J\ddot{\theta} - B_p\dot{\theta} \\ A_p(p_1b_1 - p_2b_2) &= (Js^2 - B_ps)\theta \\ \theta &= \frac{A_p(p_1b_1 - p_2b_2)}{Js^2 - B_ps} \end{aligned} \tag{4.17}$$

where J is the inertia of the tilting body about the tilt axis ($I_x + mh^2$), and B_p is associated with the friction in the tilting motion.

To incorporate this into the system, a relationship between the tilt angle, θ, and the actuator extension is necessary, as actuator extension forms part of equations 4.15 and 4.16. As each actuator is analysed individually, the relationship between actuator extension and tilt angle can be stated to be:

$$\begin{aligned} x_{p1} &= k_{\theta 1}\theta \\ x_{p2} &= k_{\theta 2}\theta \end{aligned} \tag{4.18}$$

4.4.3 Valve Actuator System

From the analysis above, a block diagram relating the tilt angle, θ, with the input x_v can be constructed. This is shown in figure 4.8.

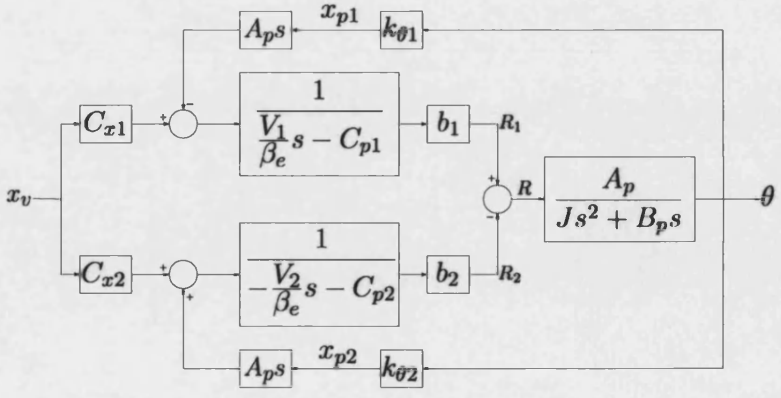

Figure 4.8: Block diagram of complete system

The terms R_1, R_2, and R are terms to aid understanding the following manipulation in order to obtain the transfer function relating x_v with θ.

From the block diagram shown in figure 4.8, we can determine the equations for R_1 and R_2:

$$\begin{aligned} R_1 &= p_1 b_1 = \frac{-A_p k_{\theta 1} \theta b_1 s + x_v C_{x1} b_1}{\frac{V_1}{\beta_e} s - C_{p1}} \\ R_2 &= p_2 b_2 = \frac{A_p k_{\theta 2} \theta b_2 s + x_v C_{x2} b_2}{-\frac{V_2}{\beta_e} s - C_{p2}} \end{aligned}$$

The reference term $R = R_1 - R_2$, therefore:

$$R = p_1 b_1 - p_2 b_2 = \frac{-A_p k_{\theta 1} \theta b_1 s + x_v C_{x1} b_1}{\frac{V_1}{\beta_e} s - C_{p1}} - \frac{A_p k_{\theta 2} \theta b_2 s + x_v C_{x2} b_2}{-\frac{V_2}{\beta_e} s - C_{p2}} \tag{4.19}$$

From 4.19, the output of the system is:

$$\theta = \left[\frac{-A_p k_{\theta 1} \theta b_1 s + x_v C_{x1} b_1}{\frac{V_1}{\beta_e} s - C_{p1}} + \frac{A_p k_{\theta 2} \theta b_2 s + x_v C_{x2} b_2}{\frac{V_2}{\beta_e} s + C_{p2}} \right] \frac{A_p}{J s^2 + B_p s} \tag{4.20}$$

At this point, it is appropriate to analyse the relationship between actuator extension and tilt angle, as if this relationship is linear, simplifications can be made greatly facilitating the goal of isolating the terms containing θ and hence obtaining a single transfer function relating x_v with θ. Figure 4.9 is a plot of the right and left hand actuator extension (as viewed from the rear), versus tilt angle. As can be seen, the design positions of the actuators do not give perfectly linear relationships, but they can be approximated to be linear with little error. The approximation indicated in the plot is the ideal relationship, with full tilt to the right equating to full extension of actuator one ($x_{p1} = 0.1\,\text{m}$) and full retraction of actuator two ($x_{p2} = -0.1\,\text{m}$); for the central tilt position, $x_{p1} = x_{p2} = 0\text{m}$. The coefficient of determination (the R-square value) for these approximations compared to the actual values is 0.935, indicating close correlation to the real system.

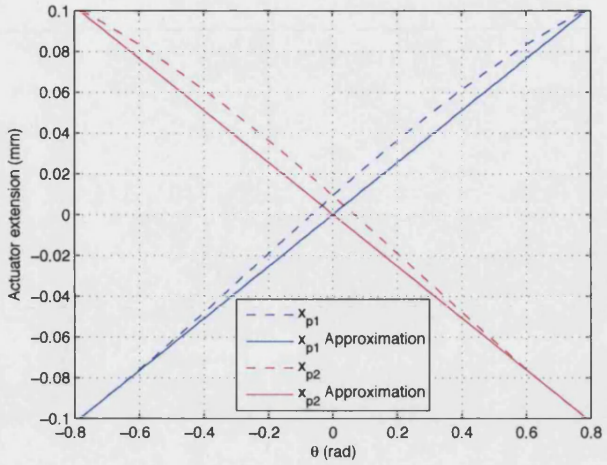

Figure 4.9: Actuator extension versus tilt angle

The equations of these approximations are:

$$\begin{aligned} x_{p1} &= \frac{0.4}{\pi}\theta \\ x_{p2} &= \frac{-0.4}{\pi}\theta \end{aligned}$$

Setting $k_\theta = \frac{0.4}{\pi}$ results in:

$$\begin{aligned} x_{p1} &= k_{\theta 1}\theta = k_\theta\theta \\ x_{p2} &= k_{\theta 2}\theta = -k_\theta\theta \end{aligned}$$

Therefore:

$$k_{\theta 1} = -k_{\theta 2} = k_\theta \tag{4.21}$$

Therefore, from equation 4.21:

$$x_{p1} = -x_{p2}$$

As a consequence:

$$\begin{aligned} \dot{x}_{p1} &= -\dot{x}_{p2} \\ &\text{and thus} \\ Q_1 &= Q_2 \end{aligned}$$

Since the flows are equivalent, using equations 4.9 and 4.10, the pressure drop across one side of the valve is equal to the pressure drop on the other side. Thus:

$$P_s - P_1 = P_2 \tag{4.22}$$

This simplifies the model, as the system can now be represented as a system with equal area actuators with equal flow characteristics for both actuators. There is now a relationship between the flow and flow-pressure gains as follows:

$$C_{x1} = C_{x2} = C_x = C_e\sqrt{P_2} \tag{4.23}$$

$$-C_{p1} = C_{p2} = C_p = \frac{C_e X}{2\sqrt{P_2}} \tag{4.24}$$

To determine values for C_x and C_p, appropriate values of $P_s - P_1$ (and thus P_2) and X need to be found. The method of obtaining these values is covered in section 4.4.4.

So, equations 4.7 and 4.8 become equations 4.25 and 4.26:

$$q_1 = C_x x_v - C_p p_1 \tag{4.25}$$

$$q_2 = C_x x_v + C_p p_2 \tag{4.26}$$

As we are linearising about the cabin in the central tilting position, we can also say that:

$$V_1 = V_2 = V \tag{4.27}$$

$$b_1 = b_2 = b \tag{4.28}$$

So combining equations 4.21, 4.25, 4.26, 4.27 and 4.28 with the equation for θ, 4.20:

$$\begin{aligned}\theta &= \left[\frac{-A_p k_\theta \theta b s + x_v C_x b}{\frac{V}{\beta_e}s + C_p} + \frac{-A_p k_\theta \theta b s + x_v C_x b}{\frac{V}{\beta_e}s + C_p}\right]\frac{A_p}{Js^2 + B_p s} \\ &= \frac{2A_p x_v C_x b - 2A_p^2 k_\theta \theta b s}{\left(\frac{V}{\beta_e}s + C_p\right)(Js^2 + B_p s)} \\ &= \frac{2A_p x_v C_x b - 2A_p^2 k_\theta \theta b s}{\frac{JV}{\beta_e}s^3 + C_p J s^2 + \frac{VB_p}{\beta_e}s^2 + B_p C_p s}\end{aligned} \tag{4.29}$$

Rearranging, to put all the terms containing θ on one side leads to:

$$\begin{aligned}\theta\left[\frac{JV}{\beta_e}s^3 + C_p J s^2 + \frac{VB_p}{\beta_e}s^2 + B_p C_p s\right] + 2A_p^2 k_\theta \theta b s &= 2A_p x_v C_x b \\ \theta\left[\frac{JV}{\beta_e}s^3 + \left(C_p J + \frac{VB_p}{\beta_e}\right)s^2 + (B_p C_p + 2A_p^2 k_\theta b)s\right] &= 2A_p x_v C_x b\end{aligned}$$

This leads to a transfer function relating θ to x_v:

$$\frac{\theta}{x_v} = \frac{2A_p C_x b}{\frac{JV}{\beta_e}s^3 + \left(C_p J + \frac{VB_p}{\beta_e}\right)s^2 + (B_p C_p + 2A_p^2 k_\theta b)s}$$

Dividing the numerator and denominator by $2A_p^2$ results in:

$$\frac{\theta}{x_v} = \frac{\frac{C_x b}{A_p}}{\frac{JV}{2\beta_e A_p^2}s^3 + \left(\frac{C_p J}{2A_p^2} + \frac{VB_p}{2\beta_e A_p^2}\right)s^2 + \left(\frac{B_p C_p}{2A_p^2} + k_\theta b\right)s} \tag{4.30}$$

We know from equation 4.21 that:

$$x_{p1} = k_\theta \theta \quad \rightarrow \quad \theta = \frac{x_{p1}}{k_\theta}$$

Substituting the above for θ results in a transfer function relating x_{pl} with x_v:

$$\frac{x_{pl}}{x_v} = \frac{\frac{C_x}{A_p} k_\theta b}{\frac{JV}{2\beta_e A_p^2} s^3 + \left(\frac{C_p J}{2A_p^2} + \frac{VB_p}{2\beta_e A_p^2}\right) s^2 + \left(\frac{B_p C_p}{2A_p^2} + k_\theta b\right) s} \tag{4.31}$$

It is acceptable to assume that the term $\frac{C_p B_p}{2A_p^2}$ is negligibly small [64]. Dividing the top and bottom by the term $k_\theta b$ results in a transfer function in the form:

$$\frac{x_{pl}}{x_v} = \frac{\frac{C_x}{A_p}}{s\left(\frac{s^2}{\omega_n^2} + \frac{2\zeta s}{\omega_n} + 1\right)} \tag{4.32}$$

where

$$\omega_n = \sqrt{\frac{2\beta_e A_p^2 b k_\theta}{JV}} \tag{4.33}$$

and

$$\zeta = \frac{C_p}{2A_p}\sqrt{\frac{\beta_e J}{2V b k_\theta}} + \frac{B_p}{2A_p}\sqrt{\frac{V}{2\beta_e J b k_\theta}} \tag{4.34}$$

The term ω_n is the natural frequency of the tilting system, and ζ is the damping ratio.

4.4.4 Determining Operating Conditions

In order to model and conduct analysis of the hydraulics accurately, the operating conditions must be determined in order to calculate the values of the various terms in the transfer function shown in equation 4.32.

One method of determining the operating conditions of the hydraulics is to plot the operating domain on the flow-pressure diagram. The equation of motion of

the inverted pendulum is shown in equation 4.35.

$$T = P_m A_p b = m a_y h \cos\theta - mgh \sin\theta + (I_x + mh^2)\ddot{\theta} \tag{4.35}$$

When linearised, equation 3.2 from chapter 3, shows that in the steady state

$$a_y = g\theta \tag{4.36}$$

Combining equation 4.36 with a linearised equation 4.35 results in equation 4.37:

$$P_m A_p b = (I_x + mh^2)\ddot{\theta} \tag{4.37}$$

Actuator dynamics also tell us that

$$Q = A_p \dot{x}_{p1} \tag{4.38}$$

By recalling equation 4.2:

$$\theta(t) = \frac{\pi}{4} \sin\left(\frac{2\pi}{3}t\right)$$

The relationship between the tilt angle, θ, and the actuator extension is assumed to be linear (see figure 4.9), with a tilt angle of 45° being equivalent to actuator one extension of 0.1 metres. As discussed above, equation 4.21 relates actuator extension to tilt angle. Manipulated, equation 4.21 becomes:

$$\theta = 2.5\pi x_{p1}$$

Hence equations 4.37 and 4.2 become equations 4.39 and 4.40 respectively:

$$P_m A_p b = 2.5\pi(I_x + mh^2)\ddot{x}_{p1} \tag{4.39}$$

$$x_{p1}(t) = x_o \sin(\omega t) \tag{4.40}$$

where $x_o = 0.1$ and $\omega = 2\pi/3$, representing the assumed 'worst case' tilting scenario. By differentiating 4.40, $\dot{x}_p$ and $\ddot{x}_p$ can be found:

$$\dot{x}_{p1}(t) = x_o \omega \cos(\omega t) \tag{4.41}$$

$$\ddot{x}_{p1}(t) = -x_o \omega^2 \sin(\omega t) \tag{4.42}$$

Subsituting equation 4.41 into equation 4.38 and 4.42 into 4.39 and rearranging to isolate the trigonometric functions results in:

$$\sin\omega t = \frac{-P_m A_p b}{2.5\pi(I_x + mh^2)x_o\omega^2} \tag{4.43}$$

$$\cos\omega t = \frac{Q}{x_o\omega A_p} \tag{4.44}$$

Trigonometry defines that:

$$\sin^2 x + \cos^2 x = 1$$

so

$$\left(\frac{-P_m A_p b}{2.5\pi(I_x + mh^2)x_o\omega^2}\right)^2 + \left(\frac{Q}{x_o\omega A_p}\right)^2 = 1 \tag{4.45}$$

which is the equation of an ellipse centred at the origin of a pressure-flow diagram. This ellipse, the upper right quarter of which is shown on the left in figure 4.10, represents the boundary of the operating conditions of the tilting system.

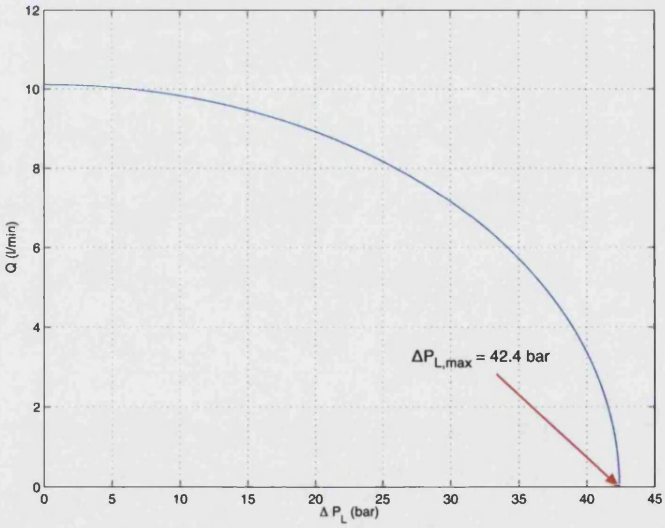

Figure 4.10: Ellipse representing operating condition boundary on pressure-flow diagram

The valve characteristics from the valve catalogue [63] of the chosen valve are shown in figure 4.11. The value ΔP in the figure 4.11 is the pressure loss on one side of the valve—either from P to A or B to T (or indeed from P to B or A to

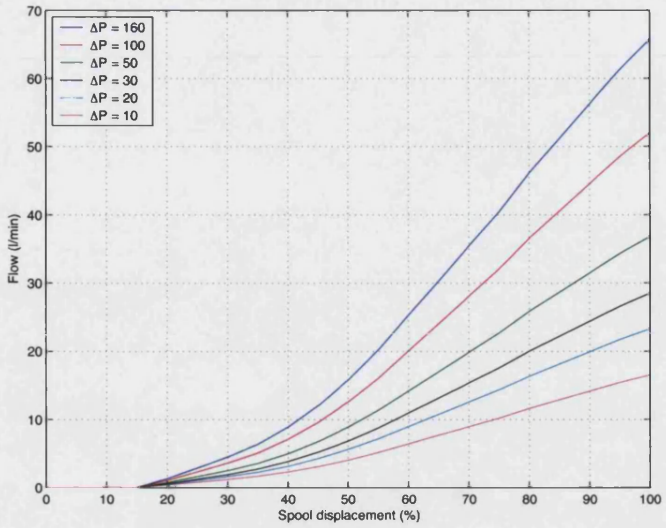

Figure 4.11: Valve characteristics for proposed valve [63]

T). Thus we know that:

$$\Delta P = P_s - P_1 \tag{4.46}$$

From equation 4.22, for an equal area actuator:

$$P_s - P_1 = P_2 \qquad \text{and} \qquad P_m = P_1 - P_2$$

Thus

$$P_m = 2P_1 - P_s \tag{4.47}$$

By combining equations 4.46 and 4.47, we find that:

$$P_m = P_1 - \Delta P \tag{4.48}$$

Using equation 4.48, the valve characteristics can be plotted on the same axes as the boundary condition shown in figure 4.10. Figure 4.12(a) shows these valve characteristics and the boundary ellipse. The maximum valve opening is between $x_v = 45\%$ an $x_v = 50\%$. Zooming in on a small area, figure 4.12(b), it is determined that the maximum valve opening, whose curve is tangent to this boundary condition, is $x_v = 48.5\%$.

It would be unreasonable to take the ΔP and x_v value for the point at which the valve opening curve touches the boundary ellipse, as this represents an extreme condition when the vehicle is tilting in its 'worst case' scenario. From the analysis

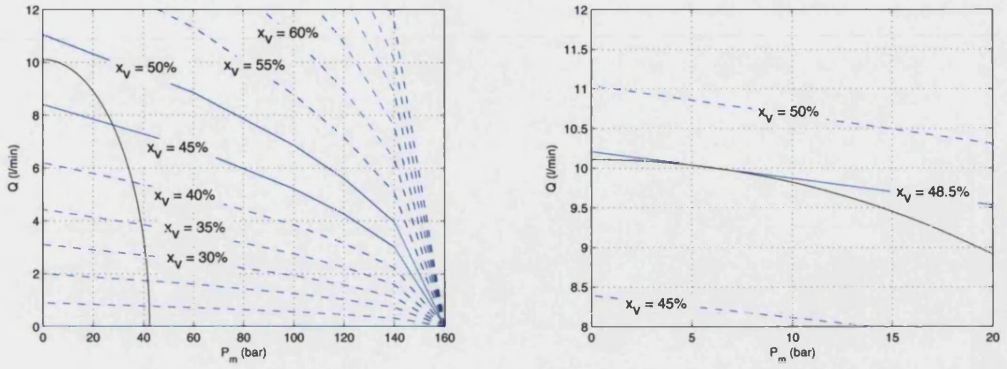

(a) (b)

Figure 4.12: Valve characteristics on flow pressure diagram

above, the maximum valve opening is 48.5%, and from the boundary ellipse, the maximum value of the load pressure, P_m, is 42.4 bar. In the 'worst case' scenario of the tilting system tilting from maximum left tilt to maximum right tilt at 0.33 Hz, it can be assumed that the valve opening varies sinusoidally, as does the load pressure. By plotting the absolute value of these sinusoidal signals, figures 4.13(a) and 4.13(b), the mean values, as shown in the figures, are suggested as reasonable estimates of the operating conditions, with which to determine the flow and flow-pressure coefficients for the valve, C_x and C_p respectively.

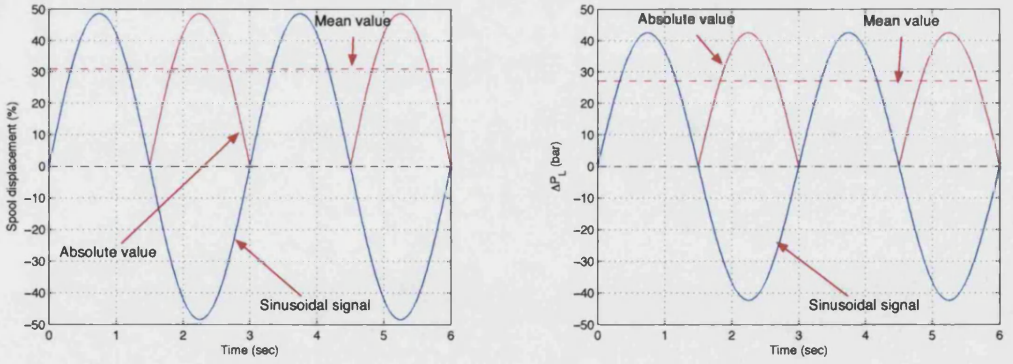

(a) (b)

Figure 4.13: Plots to determine mean values of x_v and P_m

These mean values are calculated to be:

$$x_v = 30.8\% \qquad \text{and} \qquad P_m = 26.95\,\text{bar}$$

Because the system is being modelled assuming equal area actuators, the following is true:

$$\begin{aligned} P_1 &= \frac{P_s}{2} + \frac{P_m}{2} \\ P_2 &= \frac{P_s}{2} - \frac{P_m}{2} \end{aligned} \tag{4.49}$$

where P_s is the supply pressure, and P_m is the load pressure, $P_1 - P_2$.

From equation 4.49, with a supply pressure of 160 bar:

$$P_2 = \frac{160}{2} - \frac{26.95}{2} = 66.525\,\text{bar}$$

By substituting this values into equations 4.23 and 4.24, the coefficients C_x and C_p are:

$$C_x = 9.726 \times 10^{-4} \qquad \text{and} \qquad C_p = 2.252 \times 10^{-11}$$

Total Volume

The volume of one side of the valve-actuator system is made up of the volume of one actuator and the volume of the hose connecting the actuator to the valve. Since the dimensions of the proposed actuators and hoses are known, the total volume is shown to be:

$$V = \frac{d_{\text{cyl}}^2 \pi}{4} x_{p,\text{mid}} + \frac{d_{\text{hose}}^2 \pi}{4} l_{\text{hose}} \tag{4.50}$$

Effective Bulk Modulus

The bulk modulus of the proposed hydraulic fluid is approximately 18000 bar. Since flexible hoses are used between the valve and the actuators, the bulk modulus value is reduced by a factor to take into account the wall elasticity of the hoses. Reference [65] shows that the effective bulk modulus, β_e, is approximately one quarter of the oil bulk modulus, β, when flexible hosing is used. The effective hydraulic stiffness of the valve actuator system, $\frac{A^2\beta}{V}$, was calculated by consider-

ing the volume of oil trapped in the actuators together with the fluid in the more compliant flexible hoses.

Tilting System Damping

Damping in the tilting system is defined by the term B_p. The main source of damping within the system is the viscous damping in the actuators, which is proportional to actuator velocity. Thus, knowing that $\dot{x}_{p1} = k_\theta \dot{\theta}$:

$$\begin{aligned} \text{Damping in actuator} &= C\dot{x}_{p1} \\ \text{Damping with respect to tilting system} &= Ck_\theta\dot{\theta} \\ \therefore B_p &= Ck_\theta \end{aligned}$$

where C is the term for viscous damping within the actuator. A typical value for C is 2000 Ns/m, leading to a value of B_p of 254.6 Ns/rad.

Values of Constants

Table 4.1 shows the values of the parameters used in the model.

4.4.5 Linear Model Results and Analysis

With the operating conditions determined, and the values of constants calculated, equations 4.33 and 4.34 can be used to calculate the natural frequency and damping ratio respectively.

Recalling equation 4.33:

$$\omega_n = \sqrt{\frac{2\beta_e A_p^2 b k_\theta}{JV}} = \sqrt{\frac{2(4500)(8.0425 \times 10^{-4})^2(0.127)(0.4)}{(1.0022 \times 10^{-4})(123.75)(\pi)}} = 0.0871 \text{ rad/sec}$$

Symbol	Description	Value	
C_e	Valve coefficient	3.771×10^{-7}	
P_s	Supply pressure	160	bar
C_x	Flow gain	9.726×10^{-4}	
C_p	Flow pressure gain	2.252×10^{-11}	
A_p	Area of actuator piston	8.0425×10^{-4}	m^2
V	Volume of one side of system	1.0022×10^{-4}	m^3
β	Oil bulk modulus of fluid	18000	bar
β_e	Effective bulk modulus of fluid	4500	bar
M_t	Mass of piston and rod	2429.8	kg
C	Viscous damping of piston	2000	Ns/m
B_p	Damping in tilting system	$0.4/\pi$	Ns/rad
b	Average lever arm	0.127	m
k_θ	Gain relating actuator extension to tilt angle	0.127	m/rad
m	Mass of tilting cabin	295	kg
h	Height of tilting cabin centre of mass	0.5	m
J	Inertia of tilting cabin $(I_x + mh^2)$	123.75	kg m^2

Table 4.1: Numerical data used in the linear hydraulic simulation model

Similarly, recalling equation 4.34:

$$\begin{aligned}
\zeta &= \frac{C_p}{2A_p}\sqrt{\frac{\beta_e J}{2Vbk_\theta}} + \frac{B_p}{2A_p}\sqrt{\frac{V}{2\beta_e J b k_\theta}} \\
&= \frac{2.252 \times 10^{-11}}{2(8.0425 \times 10^{-4})}\sqrt{\frac{(4500)(123.75)(\pi)}{2(1.0022 \times 10^{-4})(0.127)(0.4)}} \\
&\quad + \frac{254.6}{2(8.0425 \times 10^{-4})}\sqrt{\frac{(1.0022 \times 10^{-4})(\pi)}{2(4500)(123.75)(0.127)(0.4)}} \\
&= 11.8135
\end{aligned}$$

4.4.6 Frequency Response

A frequency response of the open loop transfer function shown in equation 4.32 can be obtained by replacing the Laplace operator, s, with $j\omega$:

$$\frac{\frac{C_x}{A_p}}{s\left(\frac{s^2}{\omega_n^2} + \frac{2\zeta s}{\omega_n} + 1\right)} \rightarrow \frac{\frac{C_x}{A_p}}{j\omega\left(\frac{-\omega^2}{\omega_n^2} + \frac{2\zeta j\omega}{\omega_n} + 1\right)} \tag{4.51}$$

Rearranging:

$$\frac{\frac{C_x}{A_p}}{j\omega\left[\left(1-\frac{\omega^2}{\omega_n^2}\right)+\frac{2\zeta\omega}{\omega_n}j\right]} \tag{4.52}$$

The amplitude ratio, AR, and phase angle, ϕ are defined as:

$$\begin{aligned} AR &= \frac{1}{\sqrt{\Re^2+\Im^2}} \\ \phi &= -\tan^{-1}\left(\frac{\Im}{\Re}\right) \end{aligned}$$

So for the linear model analysis:

$$AR = \frac{C_x/A}{\omega\sqrt{\left(1-\frac{\omega^2}{\omega_n^2}\right)^2+\left(\frac{2\zeta\omega}{\omega_n}\right)^2}} \tag{4.53}$$

$$\phi = -\tan^{-1}\left(\frac{\frac{2\zeta\omega}{\omega_n}}{1-\frac{\omega^2}{\omega_n^2}}\right) - 90° \tag{4.54}$$

Converting equation 4.53 to the a log modulus, R:

$$R = 20\log(C_x/A) - 20\log\omega - 20\log\sqrt{\left(1-\frac{\omega^2}{\omega_n^2}\right)^2+\left(\frac{2\zeta\omega}{\omega_n}\right)^2} \tag{4.55}$$

From equations 4.55 and 4.54 and the determined numerical data, a Bode plot of the transfer function (equation 4.32) is shown in figure 4.14.

As can be seen, the system is heavily damped, indicated by no resonant peak in the magnitude plot. Due to this high damping coefficient in the system, operating at or near the natural frequency does not result in an oscillatory or unstable system without the control gain being unreasonably high.

At the natural frequency, ω_n, there is little deviation from the asymptotic straight

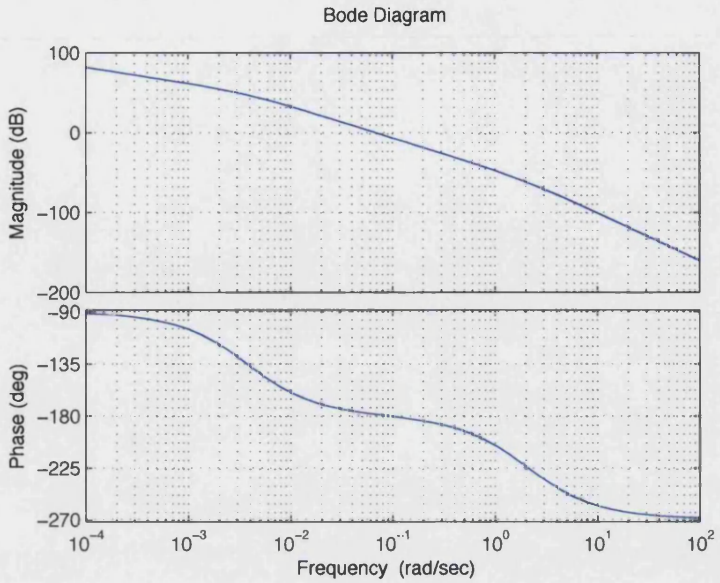

Figure 4.14: Bode plot for linear hydraulics model

line approximation. When $\omega = \omega_n$, from equations 4.55 and 4.54:

$$\begin{aligned} AR &= \frac{C_x}{2\zeta\omega_n A_p} = 0.5875 \\ \phi &= -180^\circ \end{aligned} \tag{4.56}$$

System stability of the open loop control can be determined by examining the Bode diagram. For the system to be stable, the amplitude ratio must be less than 0 db when $\phi = -180^\circ$ and ϕ must be greater than -180° when $R = 0$ dB. From the Bode plot, the gain margin is 4.62 dB, which satisfies the first criterion, and the phase margin is approximately 1.3°, which satisfies the second criterion, thus the system is stable. It must be noted, however, that it is desirable that the gain margin is greater than 6 dB ($AR \leq 0.5$) and a phase margin of at least 30° [66]. Despite exhibiting stable behaviour, these results place some doubt in the specific operating point chosen for this analysis.

4.4.7 Closed Loop Position Control

The block diagram of the actuation system with closed loop position feedback is shown in figure 4.15. The term K_A is the amplifier gain, K_v is the valve gain,

and K_T is the position transducer gain.

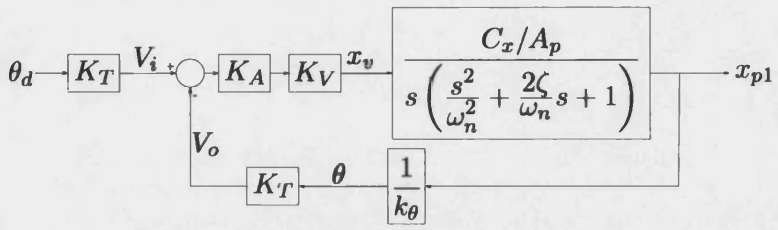

Figure 4.15: Block diagram of closed loop system

Contracting the block diagram results in that shown in figure 4.16:

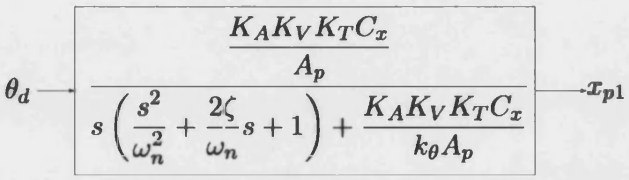

Figure 4.16: Block diagram of closed loop system (contracted)

It is appropriate here to remove the higher order terms of s to approximate ths system as a first order transfer function. The block diagram for this is shown in figure 4.17: where

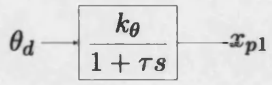

Figure 4.17: Block diagram of closed loop system (contracted)

$$\tau = \frac{A_p k_\theta}{K_A K_V K_T C_x}$$

From equation 4.56, the stability criterion as discussed above requires that:

$$\frac{C_x K_A K_V K_T}{2\zeta\omega_n A_p k_\theta} \leq 0.5$$

Therefore, $\tau \geq 0.97\,\mathrm{s}$.

4.4.8 Remarks

While these results illustrate the promise of a valve-actuator system employed as the tilt system, it does not represent the full system including the accumulator and unloading system (and the consequence of variable pressure), nor the pump with its associated load on the crank shaft of the engine. While linearising using the small perturbation technique is useful to determine the stability by examining the frequency response of the open loop system, its use is limited in the accurate analysis of a variety of system scenarios—the system is operating around a very specific point. This specific operating point chosen leads to a very large damping ratio, and gain and phase margins that are below acceptable levels. In addition, the analysis also presents a relatively high time constant when approximating the closed loop hydraulic actuation system as a first order lag. These limitations support the development of a non-linear dynamic model of the complete system using a specific hydraulic blockset that takes into account the non-linear nature of many of the components.

4.5 Non-linear Dynamic Model

4.5.1 MatLab-Simulink environment

A non-linear dynamic model representing the hydraulic system of CLEVER was developed in Matlab-Simulink using a third party hydraulic blockset developed by ExpertControl GmbH [67]. The motivation for the development of this model was to accurately evaluate the proposed hydraulic circuit, and in doing so, size and select appropriate hardware components for the development prototype. A detailed description of the initial model development is reported in [68]. The organisation of the blocks follows the organisation of a real hydraulic system. A block diagram of the complete model is shown in figure 4.18.

This model differs from the linear model in that it represents a non-linear representation of the hydraulics, and includes an assessment of the system behaviour with the application of the expected non-linear forces on the actuation system.

4.5.2 Assumptions/Simplifications

The following assumptions and simplifications were made in order to implement a representative hydraulic system in the model.

- As with the linear model, the relationship between actuator extension and tilt angle is assumed to be linear, hence two single acting actuators were represented as one double acting double rod cylinder with the annulus area the same as the single acting piston area.
- A specific unloading valve was not available in the model, therefore it was represented as a two-port, two-position valve with a relay used to open and close the valve based on system pressure.
- For the initial simulations, the unloading valve is modelled as a direct control valve (not a proportional valve).

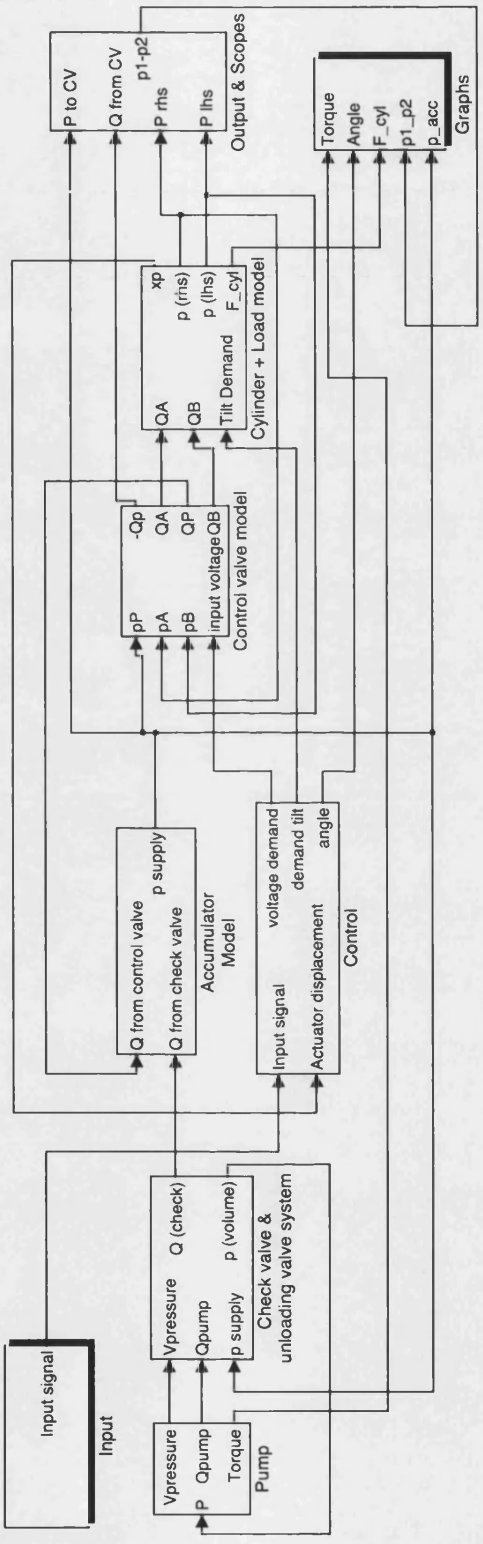

Figure 4.18: Hydraulic simulation block diagram

- The IC engine was assumed to be running at a constant speed of 5500 rpm throughout the simulations, thereby supplying flow at a constant rate.
- The numerical data values used in the simulation are listed in table 4.2 below.

Item	Symbol	Value	Units
Mass of tilting body	m	295	kg
Distance from tilting axis to CoM	h	0.5	m
Diameter of actuators	d	32	mm
Stroke of cylinders	l	0.2	m
Accumulator pre-charge pressure	–	80	bar
Lean angle limits	θ	+45 to −45	degrees
Effective bulk modulus	β_e	4500	bar
Inertia of tilting cabin	J	123.75	kg m^2

Table 4.2: Numerical data used in the hydraulic simulation model

Cylinder Force Calculation

Since the simulation of the hydraulic system reported here is in isolation of a vehicle model, the force the hydraulic system has to overcome needs to be calculated from the input demand signal and the system outputs. Recalling equation 4.1, the torque required to tilt the vehicle is:

$$T = ma_y h\cos(\theta) - mgh\sin(\theta) + J\ddot{\theta} + c\dot{\theta} + T_{dist}$$

where J is the inertia of the tilting body ($mh^2 + I_x$). T_{dist} is initially taken to be zero. The torque applied by each hydraulic actuator in the system is:

$$T = F_a b \tag{4.57}$$

where b is the lever arm and F_a is the force provided by each hydraulic actuator. From the geometry of the tilt mechanism, the lever arms for the actuators vary with respect to tilt angle, as shown in figure 4.4.

When the body is tilting to the right, the left hand cylinder provides the necessary force and vice versa. While approximations of each curve could be used, the average of the two curves adequately represents the real lever arm. This average

curve, as shown in figure 4.4, can be represented by the following quadratic equation:

$$b = -0.057\theta^2 + 0.139 \tag{4.58}$$

When the vehicle is tilted in the balanced position, the only forces governing θ are the lateral centripetal reaction force, ma_y, and the gravitational force, mg; both $\dot{\theta}$ and $\ddot{\theta}$ are zero. Since the aim of the tilting system is to balance the vehicle, the tilt angle in this situation can be considered as the demand angle, θ_d. So, from figure 4.1:

$$\tan\theta_d = \frac{a_y}{g} \tag{4.59}$$

This assumes Ackermann steering on a flat road [35] with no tyre, suspension, or road camber effects included, and the tilt axis is at ground level. In this situation, the centripetal reaction force is dependent on a specific steer input at a certain vehicle speed. Because these two values are used to calculate the demand tilt angle, centripetal reaction force is a function of tilt demand:

$$ma_y = mg\tan\theta_d \tag{4.60}$$

Because one of the main outputs from the hydraulic model is actuator extension, it was necessary to have an equation relating actuator extension to tilt angle to include in the cylinder force calculation. The relationship between actuator extension and tilt angle can be approximated as a straight line:

$$x_p = \frac{0.4}{\pi}\theta \quad \rightarrow \quad \theta = 7.85x_p \tag{4.61}$$

where x_p is the actuator extension; $x_p = 0\,\text{mm}$ when $\theta = 0\,\text{rad}$, and $x_p = 100\,\text{mm}$ when $\theta = 0.785\,\text{rad}$ (45°). The combination of equations 4.1, 4.57, 4.58, 4.60 and 4.61 results in equation 4.62. Each actuator has to provide this force:

$$F_a = \frac{mgh\tan\theta_d\cos(7.85x_p) - mgh\sin(7.85x_p) + 7.85mh^2\ddot{x}_p + 7.85c\dot{x}_p + T_{dist}}{-3.49x_p^2 + 0.139} \tag{4.62}$$

4.5.3 Model Development

Pump

The pump of the system was modelled using the Variable Displacement Pump block from the blockset, with the displacement fixed as a constant throughout the simulation. The input ports for the block are: pressures at the pressure connection and suction ports of the pump, pressure at the leakage connection, pump speed, and swash plate angle. Outputs from the pump were flows from the pressure and suction connections, flow to the leakage connection, torque load, and fluid volumes on the pressure and suction connections. The pump block is shown in figure 4.19.

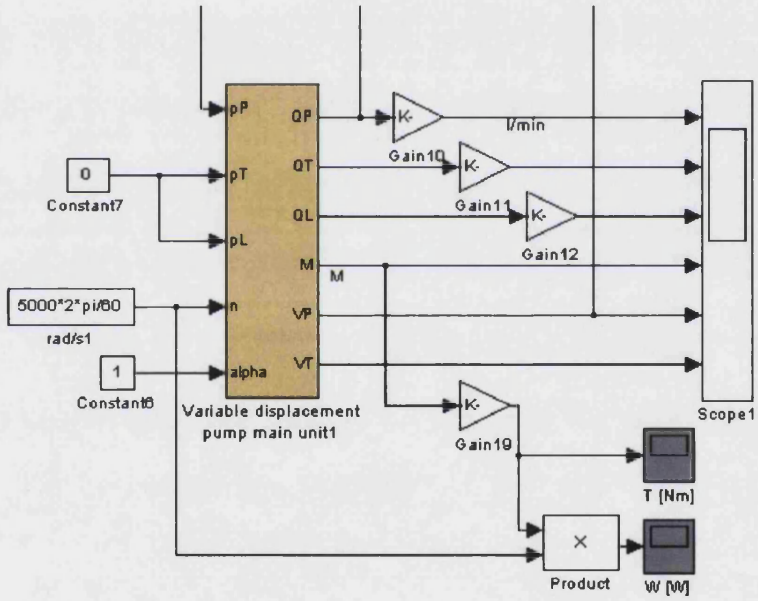

Figure 4.19: Simulink blocks representing the pump

The various parameters such as pump displacement, volumetric efficiency and internal leakage were taken from the pump catalogue [69]. The power take off from the internal combustion engine was calculated by multiplying the torque requirement (an output from this block) by the rotational velocity.

Unloading and Check Valves

The unloading valve was modelled as a pilot operated check valve with a relay controlling the pilot pressure to simulate the real unloading valve. This relay opened the valve at the maximum pressure threshold (sending flow generated from the pump back to the reservoir), then closed when a lower pressure threshold was reached, recharging the system. The check valve block permits flow when the input pressure is higher than the opening pressure. The significant output from these valve blocks are flow through the valve—flow back to tank from the unloading valve, and flow to the system side from the check valve. The blocks used to model these valves are shown in figure 4.20. Both valves require pressure

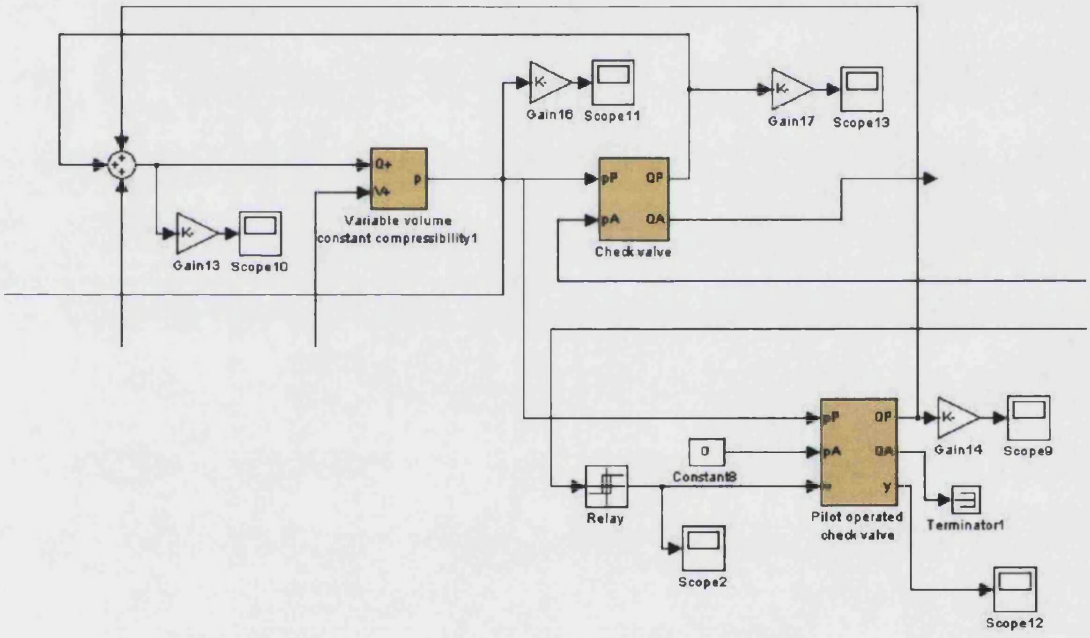

Figure 4.20: The unloading and check valves modelled in Simulink

as an input, so the flow outputs from the pump block were processed by 'volume' blocks, which integrates the flow to compute the pressure. Information about oil compressibility is included in this volume block.

Accumulator

Flow from the check valve then passes through the block representing the accumulator. This block takes flow as an input, with pressure as an output. The accumulator block computes the pressure build-up in the accumulator by compression of the gas pre-charge on the basis of the thermodynamics of real gases and while taking the compression of the fluid in the accumulator and the connected devices into account.

Control Valve

The four port, three-position control valve is a dynamic second order model of a hydraulic proportional valve. The parameters of the valve were taken from the valve catalogue [63]. Inputs to the valve are the pressures for the different ports (P from the accumulator block, T from the reservoir, and A and B from the actuator model, discussed below), with outputs being flows for the four ports. The blocks used for the control valve is shown in figure 4.21.

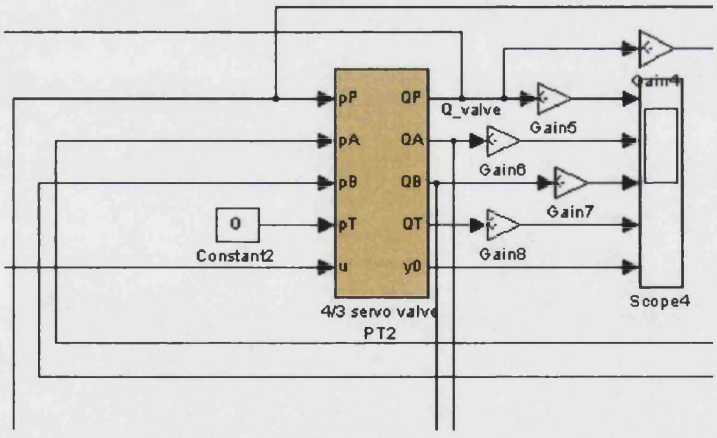

Figure 4.21: Simulink blocks representing the 4/3 control valve

Actuators and Load

As stated above, the two single acting actuators were represented by a double acting, double rod actuator with a piston annulus area equivalent to the single acting actuators. Inputs into the block are the pressures from the control valve, (pressure into each chamber) and the load force, calculated using equation 4.62 derived above. The outputs are the flows for the ports, the position, speed and acceleration of the piston, and the volumes of the chambers. The flows from the control valve are converted to pressures using 'volume' blocks, which integrates the flow to obtain pressure. Similarly, the same method is used for the output flows from the actuator block, to convert them to pressures as required by the control valve. The blocks representing the actuators and load are shown in figure 4.22.

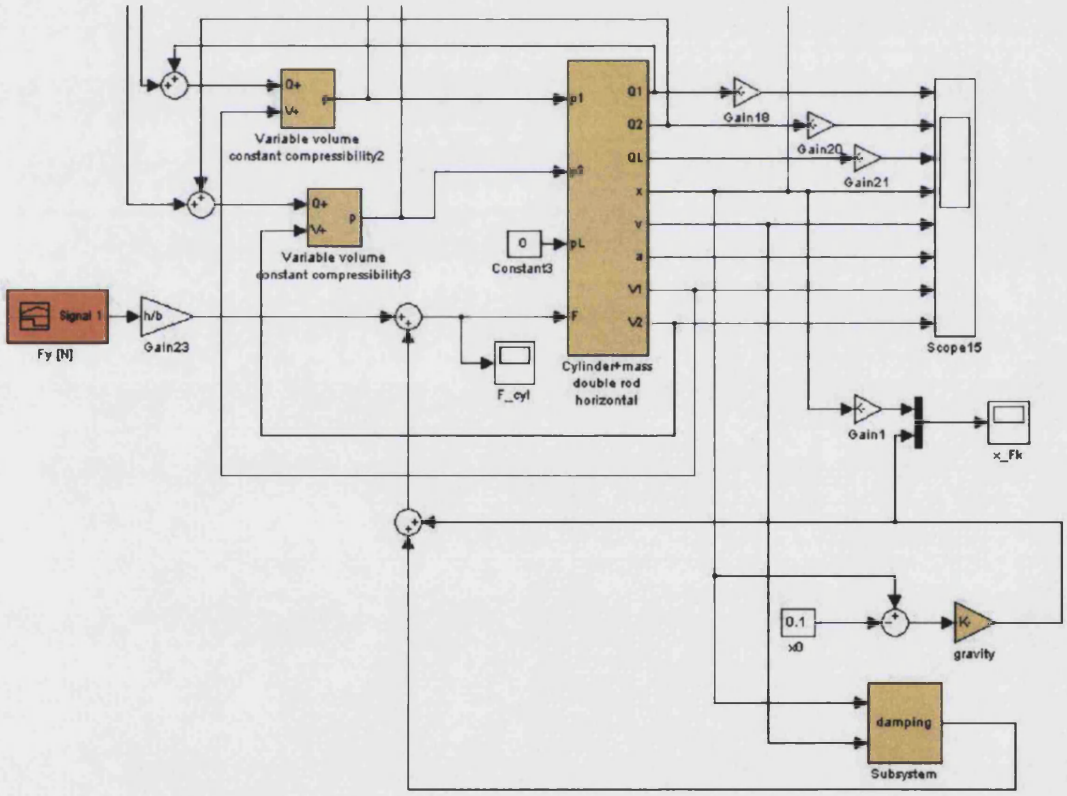

Figure 4.22: Simulink blocks representing the actuators and load

The position, speed and acceleration outputs are converted to rotational tilt position using equation 4.61 above.

Control system

The control system is modelled by subtracting the output tilt position from the demand signal, creating an error signal. The control valve input is simply a function of this error based on the analysis from Chapter 3.

4.5.4 Results

Harsh Ramp Input

This situation is unlikely to occur in normal driving. It was used to test the response of the system to sudden harsh inputs, especially the central ramp that has a tilt requirement of -45 to $+45$ degrees in 1 second (this is beyond the performance required by the system). The simulation results of demand and real tilt angle, torque load on the internal combustion engine crankshaft, force in the cylinders, and system pressure are shown in figure 4.23. These results show that

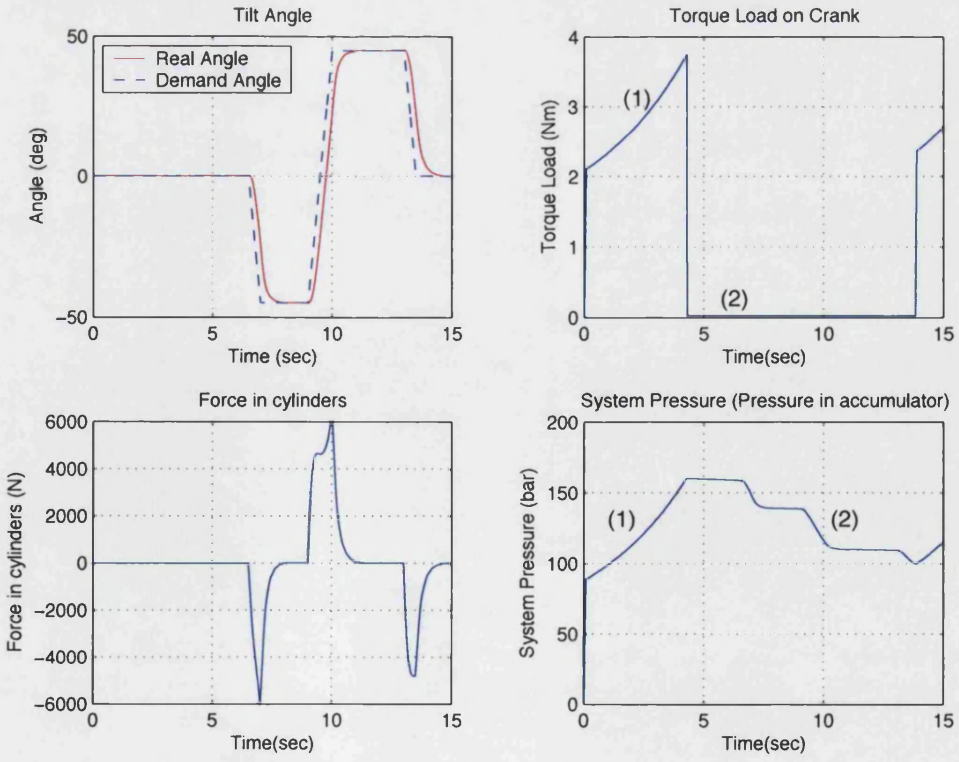

Figure 4.23: Simulation results for harsh ramp input

the response of the hydraulic system closely matches the demand signal. During the ramp inputs, based on these simulation results, the response lags the demand by approximately 0.25 seconds. After the initial startup (1)—pressurising the system by charging the accumulator—the pump unloads and the manoeuvre is almost completed using only the flow from the accumulator (2). As can be seen, when the pump is unloaded, it is taking almost no torque from the engine (2). When the pump is loaded, the maximum torque requirement is approximately 3.7 Nm. With the engine speed running at 5500 rpm, this torque requirement can be accommodated and a charging cycle takes just over 3 seconds. The maximum power required at this engine speed is approximately 2 kW.

Slalom

This input signal represents a slalom manoeuvre from the straight-ahead position. The tilting frequency is 0.25 Hz (i.e. full tilt from $-45°$ to $+45°$ in 2 seconds). It would be possible to replicate this manoeuvre in the prototype vehicle. The simulation results are shown in figure 4.24.

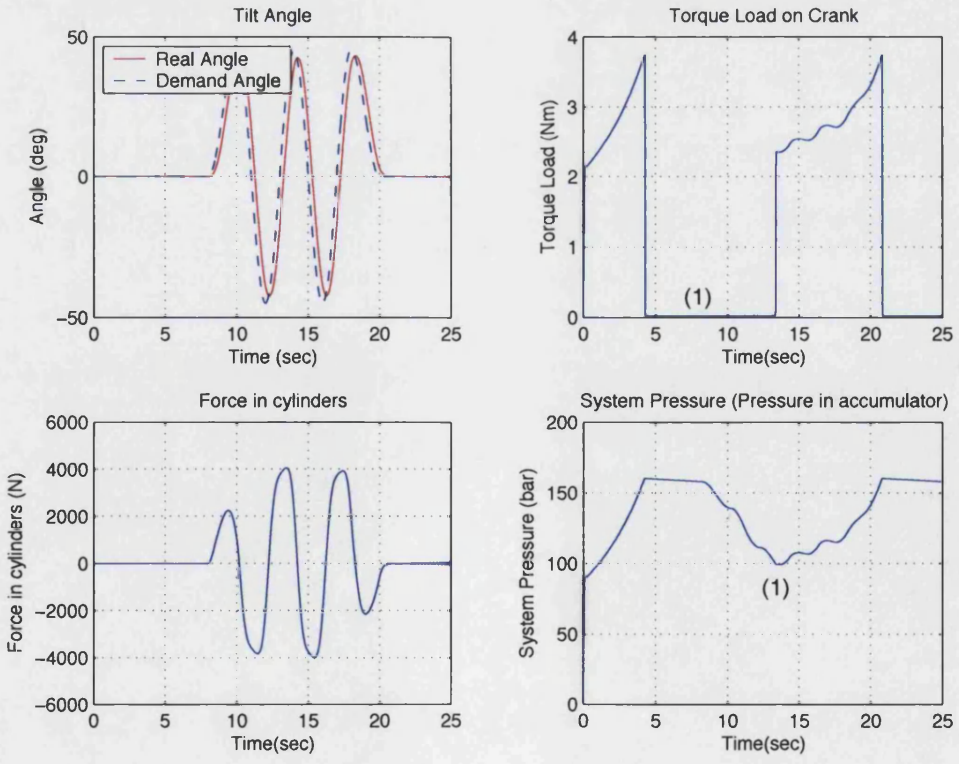

Figure 4.24: Simulation results for slalom (0.25 Hz)

Again, the system shows acceptable behaviour, with the accumulator providing flow for approximately half of the manoeuvre (1).

Harsh Slalom

This input signal represents the worst case possible with the CLEVER vehicle. The tilting frequency is 0.33 Hz (i.e. full tilt in 1.5 seconds). The simulation results are shown in figure 4.25.

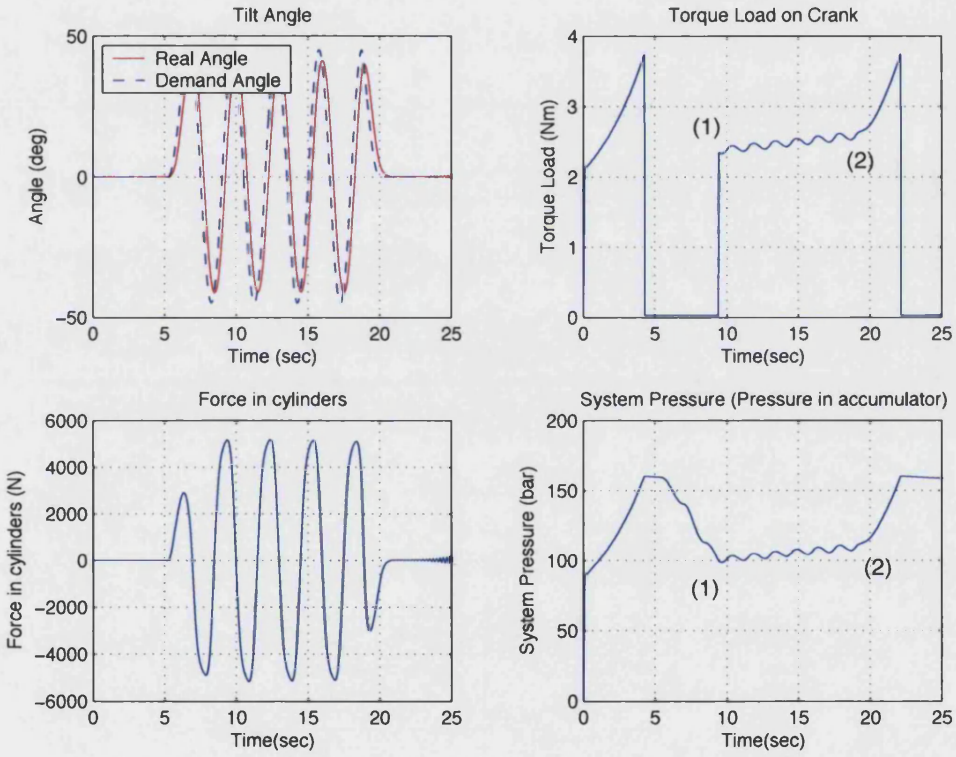

Figure 4.25: Simulation results for harsh slalom (0.33 Hz)

As can be seen, when the pump is charging the system, it can provide the mean flow, with the accumulator supplementing the flow to provide the peak requirements (1). The system cannot recharge until this harsh manoeuvre is completed, as signified in the rise in system pressure at 20 seconds (2).

Disturbance Force

The hydraulic tilt system has to take into account disturbances on the tilting body such as wind forces. To test this, a side wind force was added to the forces applied in the cylinder associated with the tilting force. The side wind force, F_w, was defined as:

$$F_w = \frac{1}{2}\rho C_d A_{\text{side}} V^2 \tag{4.63}$$

where ρ is the air density (taken as 1.226 kg/m^3), C_d is the drag coefficient, A_{side} is the projected area facing the wind, and V is the velocity of the wind. Taking, for example, a wind speed of 110 kph, a C_d value of 1.3, and an area estimation of 2.5 m^2, F_w is 1563 N. The C_d value used in this calculation is particularly pessimistic. The correct value for the side of the CLEVER vehicle is unknown, so a value of 1.0 was taken as the worst case. See table 4.3 for typical C_d values for certain objects.

	Drag coefficient, C_d
Conventional cars (frontal)	0.3–0.4
Rough sphere ($Re = 10^6$)	0.4
Square flat plate 90° to flow	1.17
Articulated lorry	0.6–0.9
Wire cables 90° to flow	1.0–1.3

Table 4.3: Typical drag coefficients [70]

Taking a wind force of 1600 N acting at the centre of mass (0.5 m above the tilt axis), this translates to a disturbance torque around the tilt axis of 800 Nm. This is introduced as a step input (simulating a gust of wind) between 7 and 11 seconds during the harsh slalom tilting manoeuvre (see section 4.5.4). The results for the simulation are shown in figure 4.26.

Examination of the simulation results shows the effect of the aerodynamic side force. However, comparing the tilt angle plot with the previous result with no disturbance (figure 4.25), there is little difference in behaviour. Closer analysis of the results shows that the amplitude of the tilting motion is reduced by less than 3.5° with this force. This angle is negligible compared to the additional system tilt angle due to suspension and tyre compliance when the vehicle is subjected to a side force of this magnitude. At wind speeds above 130 kph, this reduction would be greater; however, it is likely that the CLEVER vehicle would be blown over, irrespective of the tilt angle.

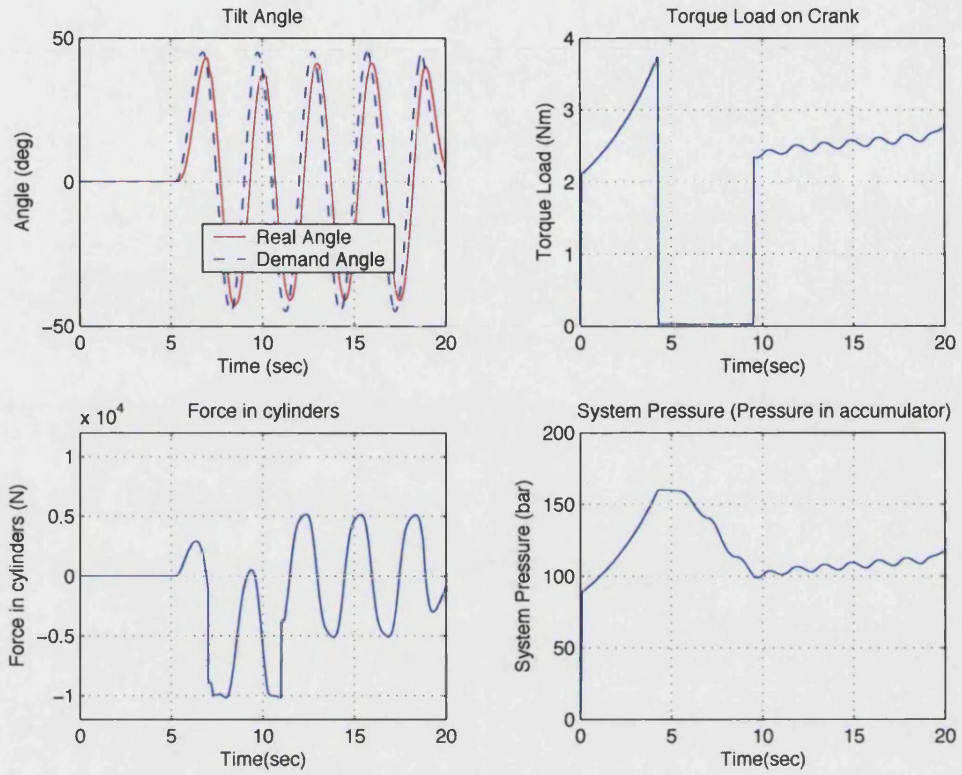

Figure 4.26: Simulation results for harsh slalom with side force introduced

Unloading valve

As can be seen in previous results, the torque loading on the engine is quite sudden, and the effect on the drivability of the vehicle is currently unknown. In an effort to smooth the transition between the loaded and unloaded state, a two-port, two-position proportional valve was substituted for the unloading valve in the model. By implementing a first order lag between the relay switch and the valve control voltage, the control signal is 'smoothed', gradually closing the valve, and loading the engine. Although shown in simulation, repeating this smoothing action when unloading the engine is not beneficial, since energy would be wasted throttling the flow back to tank. Figure 4.27 below illustrates the difference between a standard valve (as used in previous simulations) and the first order lag controlled proportional valve.

Although this method has the effect of smoothing the transition, the actual loading time is extended with the proportional valve. It must also be noted that the time constant, τ, of the first order lag requires careful tuning, since if it is too

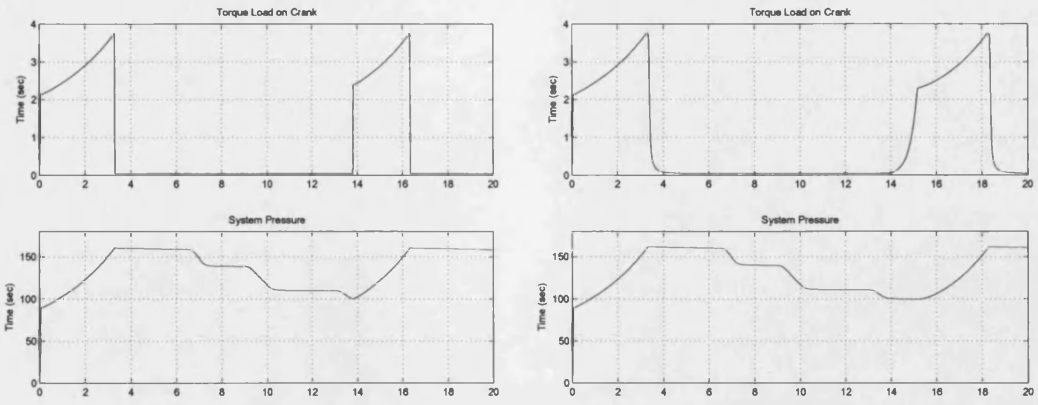

$\tau = 0\,\mathrm{s}$ $\tau = 0.6\,\mathrm{s}$

Figure 4.27: The effect of adding a first order lag in the unloading valve control

great, the system pressure would drop too low before the pump comes fully back online to recharge the system. This affects the overall response of the tilt system.

4.5.5 Final Components Selection

Based on the satisfactory results of the simulation, the final components and system parameters were chosen and are identified below.

Actuators: Two single acting linear actuators with a piston diameter of 32 mm, stroke of 200 mm, allowing full tilt from -45 to $+45$ degrees [71].

Pump: A 3 cc/rev gear pump, driven by a belt drive connected to the crankshaft of the IC engine. The gear ratio is 2.56:1 meaning an engine speed of 5500 rpm translates to pump providing mean flow for a 0.33 Hz tilting manoeuvre: -45 to $+45$ degrees in 1.5 seconds [69].

Accumulator: A 1.4 litre accumulator provides the best compromise between required system performance and packaging constraints [72].

Relief valve, control valve, unloading valve: These valves are standard 'off the shelf' components selected from recognised hydraulic component manufacturers. They have been sized to support the necessary flow requirements [73].

Unloading valve settings: The unloading valve is set to close (send flow from the pump to charge the system) at 100 bar system pressure, and to re-open (unload the pump) when the system pressure reaches 160 bar [72].

4.6 Concluding Remarks

A hydraulic system was identified as the best solution for tilt actuation for the CLEVER vehicle prototype. A hydraulic circuit system was designed and specific components were proposed.

To establish the dynamic characteristics of the hydraulic system, a linearised valve-actuator model was developed that represented the transfer function between valve spool position and actuator extension. Acceptable results were presented from this model, although limitations associated with the small perturbation technique arise, leading to a low natural frequency and high damping ratio, and gain and phase margins below acceptable levels for stability.

In order to evaluate the expected system performance, and to select and size components, a fully non-linear model of the complete system was constructed. This model aimed to simulate the behaviour of the hydraulic system in the prototype vehicle. A series of input demands were used and the resulting behaviour was assessed, looking specifically at the system response, the torque load on the engine, the force in the cylinders, and the resulting system pressure. Acceptable performance was achieved for all input demands using the final component specifications identified in section 4.5.5.

Chapter 5

Vehicle Design and Construction

5.1 Introduction

The vehicle design and construction process was performed as part of the CLEVER Project. The University of Bath's role in the vehicle design was the establishment of the overall vehicle concept and wheel arrangement (as explained in chapter 1) and the design and development of the vehicle chassis and chassis systems, including the tilt system. The first step of this was a review of the state of the art of appropriate vehicle technologies. A range of chassis systems were investigated and the following options were selected as being suitable for the CLEVER vehicle:

- Tilting system and vehicle arrangement: A 1F1T comprising two discrete modules—a tilting front cabin that tilts with the front wheel and a rear traction module that remains upright with respect to the ground. This was chosen as it provides the best flexibility concerning packaging and eases steering integration.
- Steering and front suspension: A hub-centre steering system was chosen owing to packaging and styling requirements.
- Rear suspension: Independent single sided swingarms were chosen, with an adjustable anti-roll bar between the two arms providing a degree of dependence. This arrangement offered the best solution taking into account

the packaging of the chosen engine and transmission system.

- Suspension components: standard motorcycle derived integrated 'mono-shock' adjustable components were chosen.
- Wheels and Tyres: Cast magnesium alloy motorcycle-based wheels were selected. These provided good crash protection characteristcs. The cambering front tyre was a standard motorcycle design, while the rear tyres were designed for the unique implementation on CLEVER where they remain upright with respect to the road.
- Braking system: a linked front-rear system using a common master cylinder was used.
- Transmission: the integrated CVT tranmission that accompanies the chosen engine was used. A belt driven final drive system including a differential was designed in conjunction with the rear frame.

Other project partners covered the other aspects of the vehicle such as frame design and construction, CNG fuel systems, conversion of existing engine to run on CNG, safety systems and styling.

5.2 Design Work

The design of the chassis systems involved detailed design and the production of manufacturing drawings for vehicle chassis parts. Components, such as suspension springs and dampers and the steering gearbox, were standard 'off-the-shelf' components and were selected according to performance characteristics derived from design calculations. Design calculations and finite element methods were used to support the designs. Section 5.2 gives an overview of the design work undertaken to develop the CLEVER prototype vehicles, and hence the development prototype for the tilting system.

5.2.1 Front Suspension and Steering

Since the front suspension and steering system are exposed elements of the vehicle, much of the overall design work was constrained by styling. Styling dictated that the basic front-end design is a hub-centre system, similar to that used by the motorcycle manufacturer, Bimota, in their Tesi 1D and Tesi 2D motorcycle [74]. The front wheel axle remains perpendicular to the vehicle direction, while the steering pivot is contained within the hub. The complete assembled front end, as mounted on the show vehicle, is shown in figure 5.1.

Figure 5.1: Assembled front end of show vehicle, overall and detail of axle/hub

The front end detail design was broken down into four distinct component groups: front suspension design; the wheel hub and axle; the swing arm and rake control system, and the steering system.

Front Suspension Design

The front wheel of the vehicle is suspended using a leading swingarm mounted to the main vehicle frame. The swingarm is made up of four milled components welded together: two leading arms and two crossmembers. The suspension unit is mounted between the upper cross member and the main frame. The combined shock absorber and spring unit is fully adjustable for compression and rebound damping, spring rate, pre-load and mounted length. Figure 5.2 shows the front suspension design.

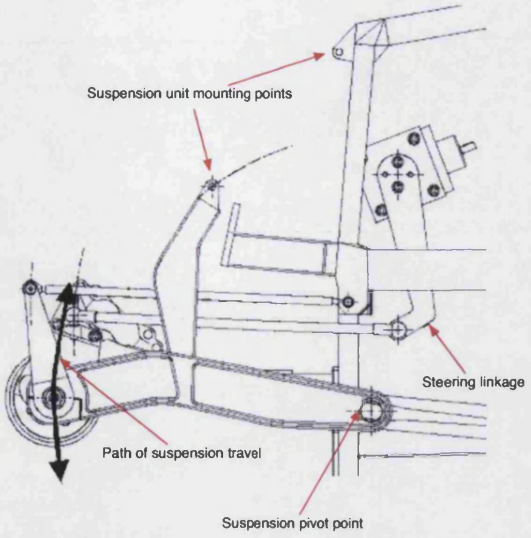

Figure 5.2: Front suspension design

Wheel hub and axle

The front wheel hub, as illustrated in figure 5.3, comprises two hub faces, one housing the steering pin located on the front axle, that are bolted together around the front wheel hub. The wheel rotates on two large sets of sealed single row ball bearings, sized and selected to take the lateral and radial forces expected at the front wheel. The hubs are designed to carry two brake calipers for the front wheel, and the steering rod bracket is located on the left hand side hub face.

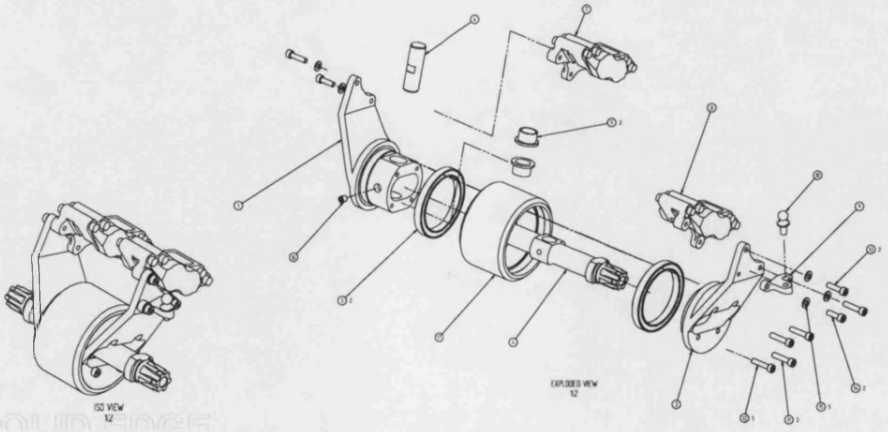

Figure 5.3: Front wheel hub and axle, isometric assembly and exploded view

Swing arm and rake control system

The exterior design of the swingarm was dictated by the vehicle's styling, but it was necessary to conduct the detail design of the swing arm mounting points and the clamping of the axle. For the swing arm mounting points, a plain bearing is pressed into the swing arm and a pin is pressed through this bearing. This pin in held in place by an interference fit with a hole in the main frame. Exploded and section views of the swing arm mount are shown in figure 5.4.

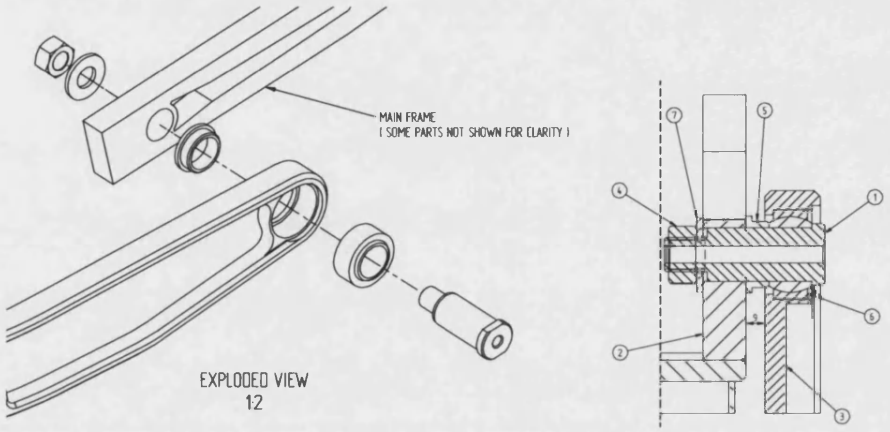

Figure 5.4: Exploded and section views of the front swing arm mount

The swing arm clamps around two single row ball bearing sets placed on each end of the axle. This allows rotation of the axle relative to the swingarm, necessary to maintain a constant rake angle irrespective of suspension movement. The ends of the axle have splines, to which the rake control arms are mounted. Two rake control rods connect the top of these rake control arms with the main frame, forming a parallelogram with the swingarm. This rake control system maintains rake in the event of bumps, and minimises the decrease in rake angle under braking—as the weight transfers to the front under braking, the rake angle decreases solely due to vehicle dive. The axle clamp is shown in exploded and section views in figure 5.5.

Steering System

The steering column design was the responsibility of another project partner, however the system connecting the column with the front wheel was part of the

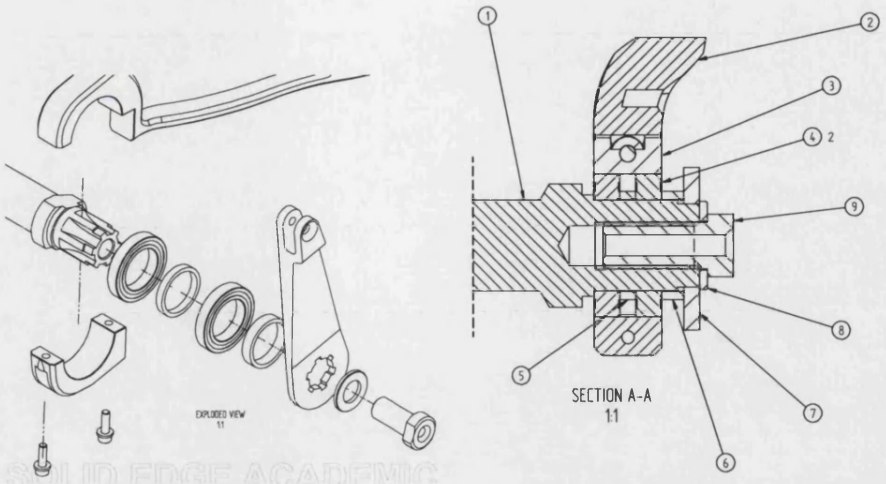

Figure 5.5: Axle clamp detail design, exploded and section views

work covered here. The system comprises a steering gearbox, which drives a drop arm for and aft. A steering rod is connected using a ball and socket joint to the bottom of this drop arm, with the other end connected to a bracket on the left hand side hub face. As the steering wheel rotates, this drop arm moves fore and aft, rotating the hub right and left, about the steering axis (within the hub). The steering system was designed to be as stiff as possible so that there was minimal play between the steering wheel and the front wheel. A CATIA CAD image of the steering system is shown in figure 5.6

Figure 5.6: CAD image of steering system

5.2.2 Tilt Joint and Rear Subframe

The tilt joint connects the front and rear halves of the chassis, and therefore the joint and supporting structure see high shear loads and bending moments. A section through the tilt pin (figure 5.7) shows that the pin has a larger diameter at the joint itself. The pin rotates in plain bronze bearings, which also provide an axial thrust face. Control of the axial thrust is achieved by shimming a conical collar; the correct clearance is important to maintain because it prevents the joint from binding as the pin bends under normal loads. Care was taken to ensure a minimum of tilt friction as this would make the behaviour of the active tilt system more difficult to predict and hence control.

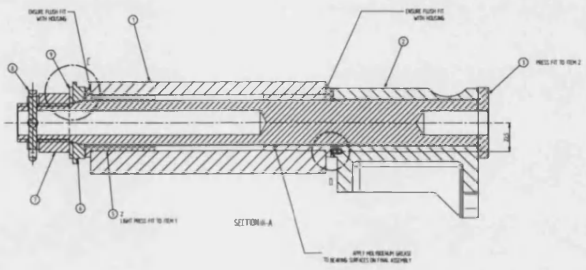

Figure 5.7: Section view of tilt joint

The structure supporting the tilt joint is fabricated from a number of milled aluminium parts welded together. The structure also needs to be stiff to prevent excessive bending and stress. Exploded and assembled views of the tilt joint frame are shown in figure 5.8.

5.2.3 Actuator Positioning

The hydraulic actuators are mounted to the tilt joint frame. The positions of the upper and lower actuator mounts were chosen to maximise the moment arm within the packaging constraints. The actuators function in a plane perpendicular to the tilt axis. Figure 5.9 shows the actuator positions and figure 4.4 in chapter 4 shows the relationship between the moment arm and the tilt angle.

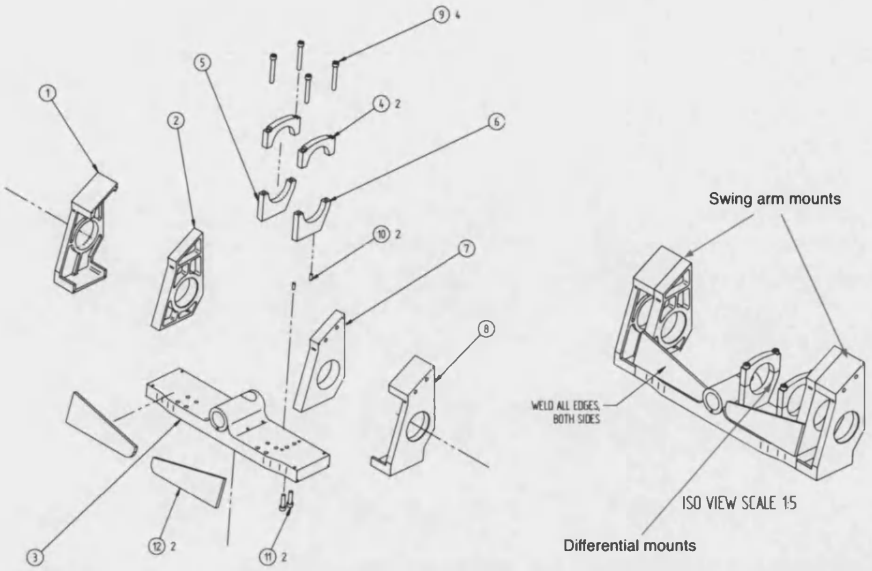

Figure 5.8: Exploded and assembled views of the tilt joint frame

5.2.4 Rear Suspension

The rear suspension of CLEVER comprises two trailing swing arms, with a stabiliser bar to suppress roll and give a solid platform against which the hydraulic system can operate. The rear suspension geometry was selected to give an almost linear relationship between wheel vertical movement and suspension compression. Like the unit used for the front suspension, the combined shock absorber and spring units are fully adjustable for compression and rebound damping, spring rate, pre-load and mounted length. Adjusting the cross section characteristics of the stabiliser bar is used to alter the roll stiffness of the rear unit.

The suspension arms attach to the tilt joint frame by use of a pivot that also contains the drive axis. As the suspension pivot point and the drive pulleys are coaxial, there is no change in final drive belt tension as the suspension articulates. The rear axles are mounted inside an eccentric adjustor that allows the drivebelts to be tensioned when installed. Figure 5.10 shows the rear suspension geometry and an exploded view of the stabiliser bar mounting viewed from the underside.

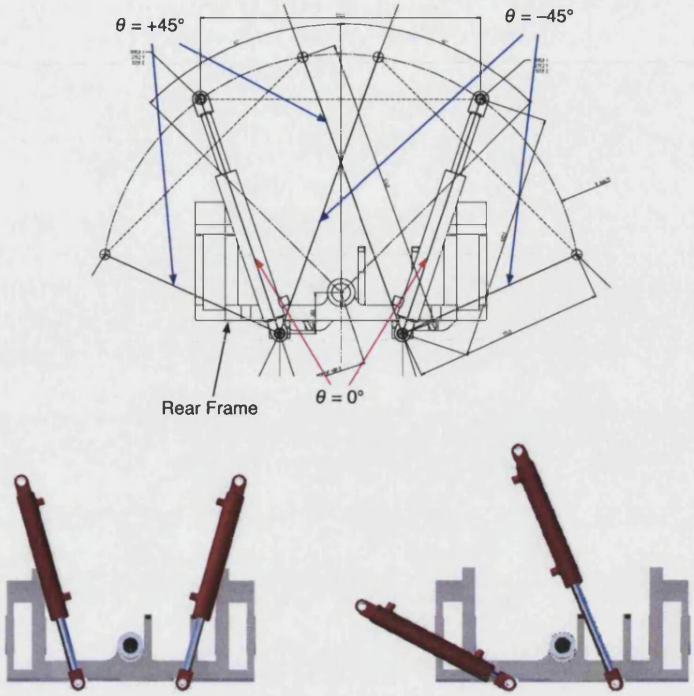

Figure 5.9: Actuator positioning to maximise torque generation

5.2.5 Transmission and Final Drive System

The transmission and final drive system was adapted from that used on the BMW C1 motorcycle. As CLEVER has two rear wheels, it was necessary to split the drive from the output of the CVT transmission via a differential. Driveshafts and toothed belt drives were used. Chains were excluded as a possibility, despite their slightly higher efficiency over toothed belts, as they require higher maintenance and regular lubrication. The assembled transmission is shown in figure 5.11

Final Drive

The optimum final drive ratio was calculated using an empirical model of the CLEVER transmission [75]. A pulley is mounted on the output shaft of the CVT, driving a differential with a tooth profile on the case. This differential sends power along two driveshafts, each with a pulley on the end, which in turn drive the pulleys attached to the rear wheel axles. All pulleys use an HTD profile with preferred tooth geometry as outlined in ISO13050 [76]. The belts used are high performance toothed timing belts. The belts were selected from standard

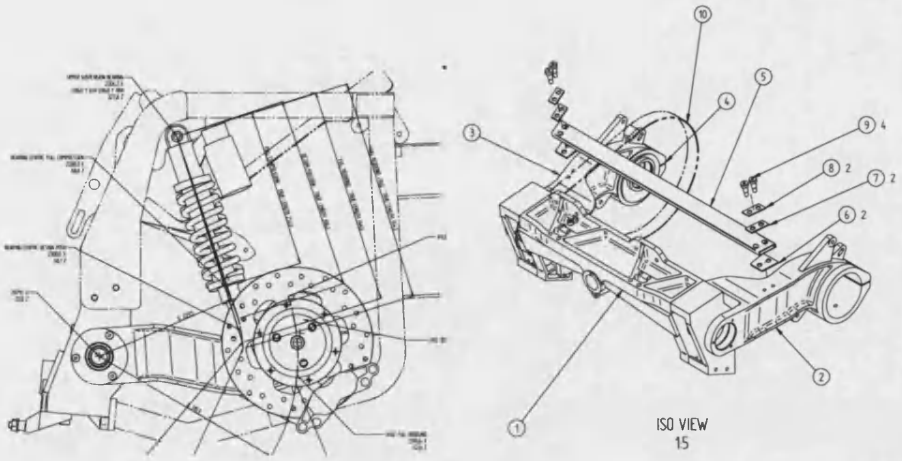

Figure 5.10: Rear suspension geometry and roll bar design

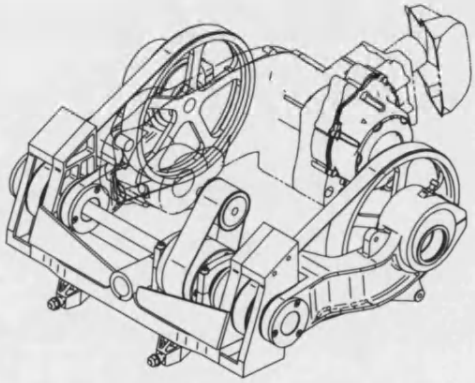

Figure 5.11: Transmission assembly

catalogue components to ensure maximum strength using a continuously wound belt. The size of the pulleys and belt therefore dictated the centre distances and eccentric adjustor geometry. Power requirements were calculated using the engine torque results (from reference tests [61]) and appropriate belt widths were chosen.

Differential and Driveshafts

Whilst having a desireable size, differentials used in ride on lawnmowers were not designed to transmit the torque loads expected from the CLEVER engine. For this reason, a differential was designed specifically for this application. The differential used the standard bevel gear arrangement, and this unique design also increased flexibility with connection to the other final drive components.

The outer case of the gearbox had a tooth profile so that it could be driven by the output belt from the gearbox. An exploded view of the differential is shown in figure 5.12.

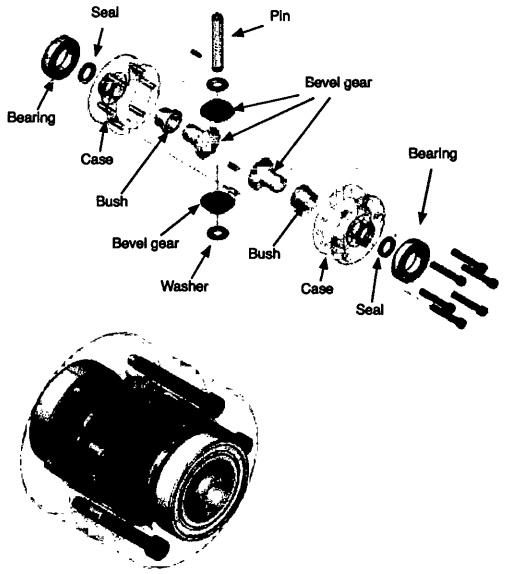

Figure 5.12: Exploded view and assembly of the CLEVER differential

Driveshafts were designed to be slotted into the CLEVER differential from outside the vehicle and form the final part of the transmission assembly. Estimated maximum stresses in all the driveline components were calculated using standard equations [77] and geometry and materials were selected appropriately.

CVT Output Modification

In order to drive the CLEVER differential in the correct direction, the drive from the CVT was taken from the intermediate shaft in the original final drive reduction gearbox (situated at the output end of the CVT case). This also allowed the transmission to be well positioned within the rear frame. A new CVT output shaft replaced the original intermediary shaft, and the transmission cases were modified accordingly, including the installation of roller bearings sized to take the radial loads applied by the belt drive—the previous intermediate shaft ran on plain bearings. The result of the modification with the new output shaft and pulley is shown in figure 5.13.

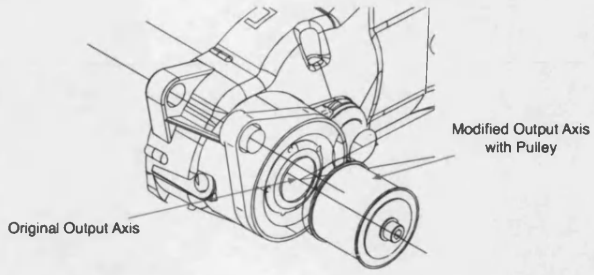

Figure 5.13: Modification to CVT output

5.2.6 Pump Drive

The elements of the hydraulic system used for the actuation system are standard 'off-the-shelf' components. Since flexible hoses are used to connect individual components together, the components were positioned in the rear frame where space permitted (section 5.3.6 covers this in more detail). The pump however, was to be driven by the engine. A V-belt drive system driven by the crank shaft was selected as the best solution for this. The working rotational velocity of the pump had to be matched to the working range of the engine, so an appropriate ratio was selected. The operational speed range of the selected pump [69] was 750 to 4000 revolutions per minute (see section 4.3.1).

The smaller drive pulley used on the crank shaft had to be supported by its own bearings, and an Oldham coupling between the crank shaft and the pulley shaft had to be designed, such that no radial loads were transmitted between the crank shaft and the pulley shaft. The bearings are mounted in a plate that is bolted to the transmission case of the engine. The exploded view of this assembly is shown in figure 5.14.

The pulley used to drive the pump was supported by its own bearings, since the plain bearings in the pump were not designed to support the radial loads associated with a belt drive. The pump also needed to be located on the rear frame in a suitable position, so the bearings are located in a bracket that supports the pump. An adjustment mechanism is included to enable tensioning of the pulley. Figure 5.15 shows the exploded view of this assembly.

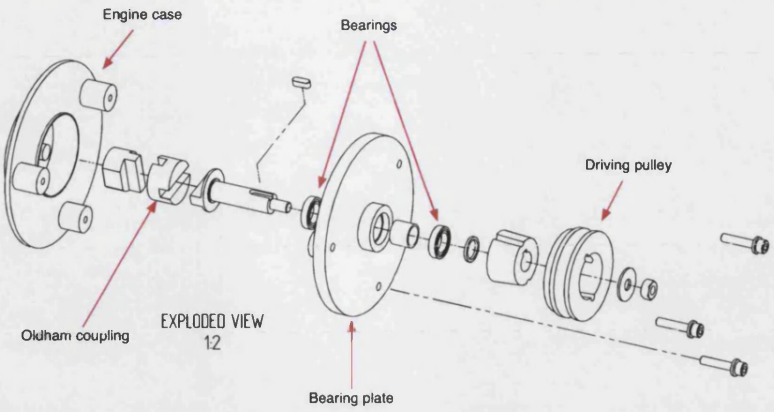

Figure 5.14: Crankshaft coupling for pump drive

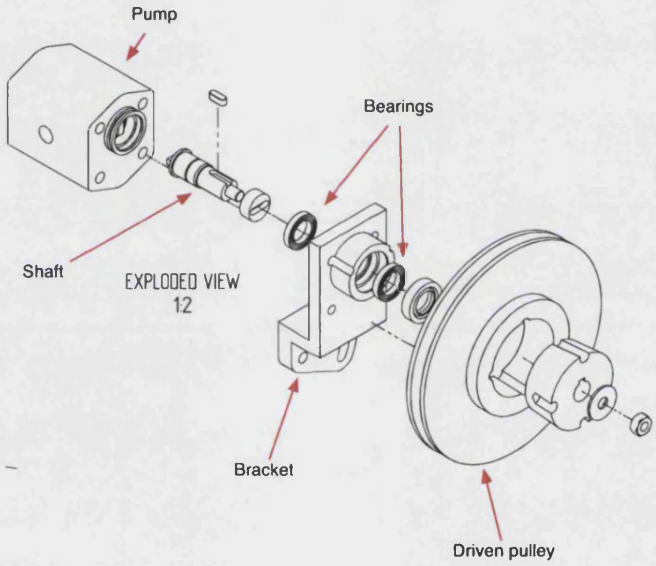

Figure 5.15: Pump bracket for pump drive

5.3 Construction

5.3.1 Component Manufacture

Chassis components were manufactured by external suppliers to the University of Bath. Five vehicle sets were required for the prototypes. Manufacture was performed using CNC multi-axis milling and turning machines, with CAD information provided in solid models, with supporting manufacturing drawings to give tolerances and finishing information. Transmission components (toothed pulleys,

the differential assembly and the output shaft for the CVT) were machined by a specialist gear manufacturer. Additional smaller machining and assembly work was performed at the University of Bath. Photographs shown in figure 5.16 shows some images of the front swingarm components after machining. Components in the background of the photographs are parts of the tilt joint frame.

Figure 5.16: Part manufacture

5.3.2 Chassis Subassemblies

Following the manufacture of the chassis components, the rear tilt joint frame was assembled. This involved inserting bushes, mounting the final drive components (differential, driveshafts, pulleys and belts), and mounting the swingarms, including the rear axles and eccentric adjusters. The front wheelhub was also assembled. Figure 5.17 show photographs of the rear and front sub-assemblies before integration to form the complete vehicle frame.

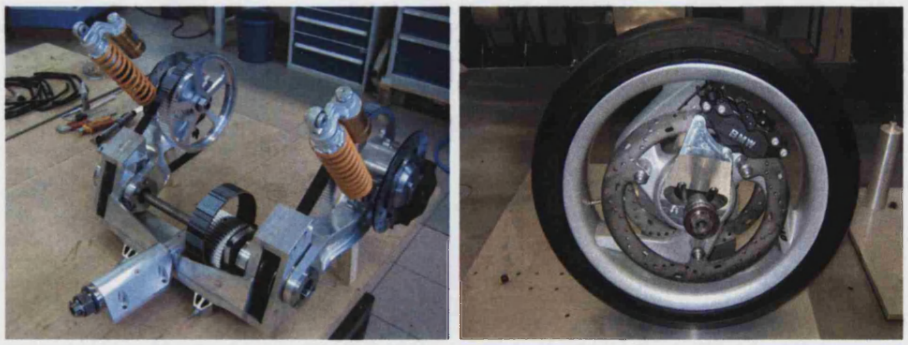

Figure 5.17: Tilt joint frame assembly and front wheel assembly

5.3.3 Vehicle Frame

The main cabin and upper rear frame of the vehicle was fabricated by ARC LKR in Ranshofen, Austria. LKR is one of the project partners whose specialities include lightweight metal components. The main vehicle frame comprises extruded sections, shaped using CNC bending machines, welded to aluminium nodes that are machined from solid. The first cabin frame is shown in figure 5.18. Also shown in the photograph is the lower body panel mounted to the frame.

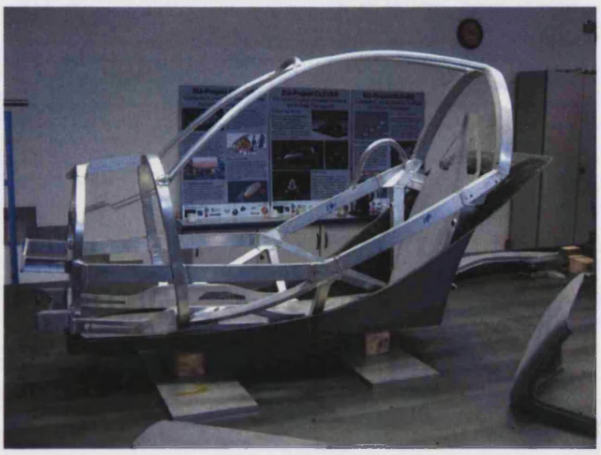

Figure 5.18: The assembled cabin frame, with lower body panel shown

The upper part of the rear frame was constructed from extruded sections and sheet metal parts welded together. This frame is bolted to the tilt joint frame sub-assembly (figure 5.17) to form the complete rear frame.

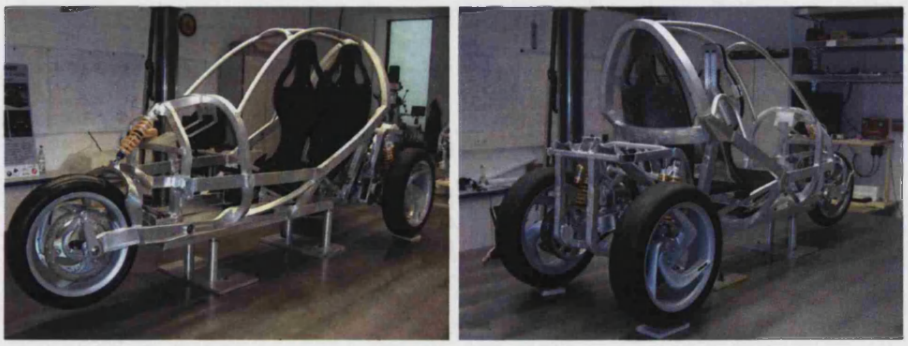

Figure 5.19: Complete vehicle frame

With the tilt joint frame and the front swingarm assemblies bolted to the main vehicle cabin, the complete vehicle frame is complete. Figure 5.19 shows photographs of the complete vehicle frame.

5.3.4 Installation of Components from Donor Vehicle

Engine, Transmission and Ancillary Systems

Since the engine and transmission of CLEVER is based on that used in the BMW C1, a BMW C1 was used as a donor vehicle for the CLEVER rolling chassis prototype. The engine and transmission were removed and dismantled so that the transmission case could be modified (see section 5.2.5). Once this modification had been made, the engine and transmission unit was reassembled and installed in the rear frame of CLEVER.

In addition to the engine and transmission, the engine ancilliary systems including the cooling, fuel, and intake systems from the donor vehicle were also installed in the rear frame. Owing to the different installation configuration in the CLEVER vehicle, the fuel tank was replaced with a custom tank with a separate fuel pump, and the intake chamber was replaced with a small conical filter, as space constraints prevented the use of the original air box. The throttle was connected via a cable to an accelerator pedal installed in the cabin.

The exhaust system used on the CLEVER vehicle was adapted from that used on the BMW C1 to fit within the design envelope of the vehicle's rear frame. This exhaust system was installed on the development vehicle.

Two photographs of the rear frame with the engine and ancillary systems installed in the vehicle is shown in figure 5.20.

Electrical System

In order to run the engine, the vehicle electrical system was also removed from the donor vehicle and installed on CLEVER. The engine management system was carried over unmodified and as such the switches and warning lights normally mounted on the handlebars or the dashboard of the C1 were replaced by switches and lights mounted behind the steering wheel of CLEVER (see section 5.3.7). Additionally, failsafe switches of the C1 that allow the engine to run (such as the stand and seatbelt switches) were installed, but disabled. The fuse and relay box

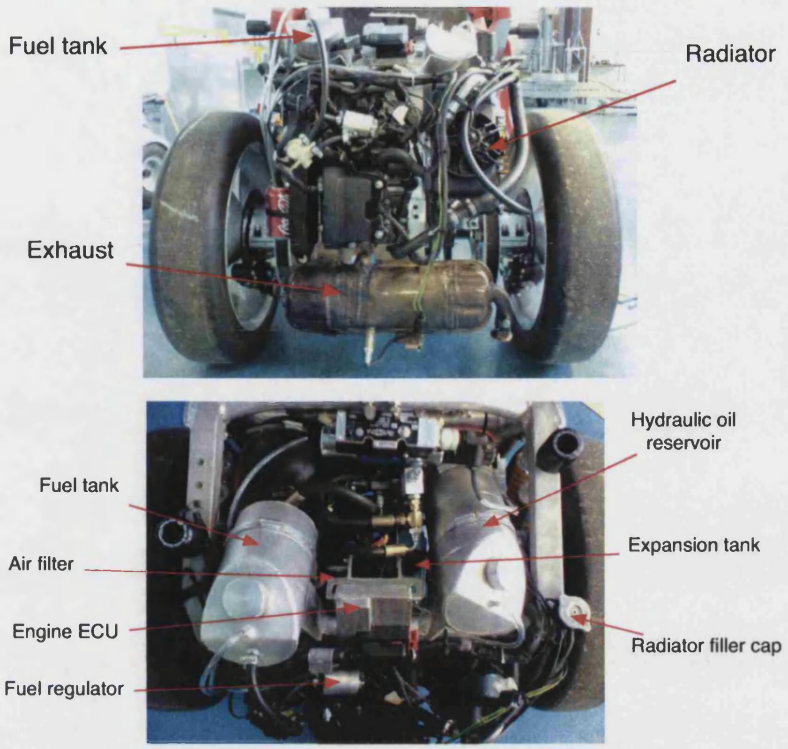

Figure 5.20: Engine installed in the rear frame

was also carried over unchanged from the BMW C1.

5.3.5 Braking System

The braking system was designed specifically for CLEVER. Two 320 mm diameter brake discs were mounted to the front wheel, and one 240 mm diameter disc on each rear wheel. Each disc uses a four piston caliper. The system required flexible and solid hoses to be manufactured and fitted to transmit the brake pressure from the master cylinder (mounted at the pedal) to all the calipers. A proportioning valve was implemented to balance the front and rear braking force. A schematic diagram of the braking system is shown in figure 5.21.

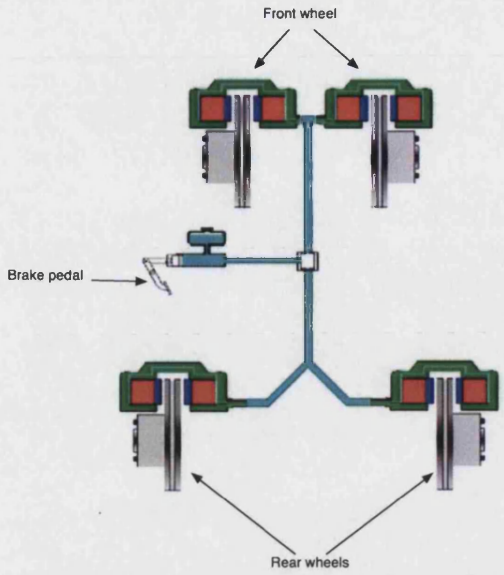

Figure 5.21: Schematic diagram of braking system [78]

5.3.6 Installation of Hydraulic Components

The pump drive system was assembled following the design (section 5.2.6). The pump bracket and the pump were mounted on the right hand side of the rear frame, with the crank shaft coupling mounted on the transmission cover, as designed. Figure 5.22 shows the pump drive system installed in the vehicle.

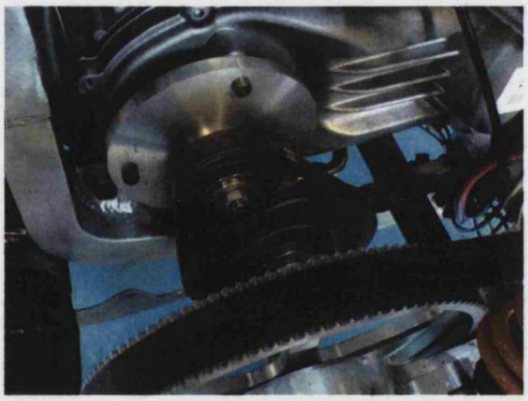

Figure 5.22: Pump drive system installed in the rear frame

A custom made hydraulic reservoir with a volume of approximately three litres was installed on top of the rear frame in one of the chutes designed for the exchangeable gas cylinders not used in this development prototype. The reservoir was specifically designed to reduce the possibility of any air entrained in the

system recirculating: the return port is tangential to the cylindrical shape of the reservoir to induce swirl, and a mesh is integrated to promote the release of bubbles. The other chute was used as a stable location for the accumulator. The hydraulic reservoir is the tank on the right hand side in figure 5.23, and the accumulator is below the fuel tank on the left hand side.

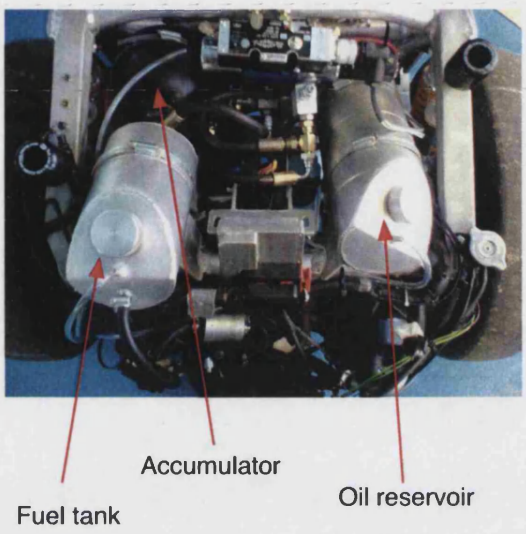

Figure 5.23: Fuel tank, oil reservoir and accumulator placement

A mechanical unloading valve (as opposed to a proportional relief valve originally proposed in the hydraulic chapter) was used to charge the accumulator and this was located on lower left hand side of the rear frame, behind the swing arm. (It was felt that the priority was to ensure that the hydarulics were functioning appropriately before focusing on refining the driveability of the vehicle.) These hydraulic components were connected together with custom made flexible hosing.

The control valve, cross-port check valves and the pressure relief valve were assembled together using rigid connectors and were mounted centrally on the rear frame to facilitate the installation of flexible hoses between the check valves and the actuators and accommodate the relative movement between the front and rear frames. These valves are shown in figure 5.24.

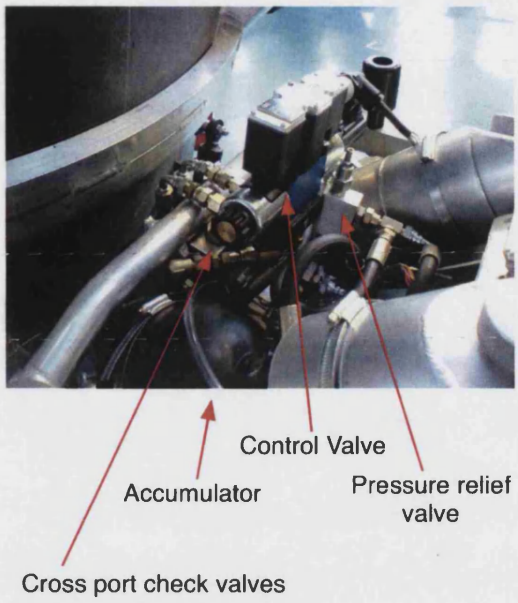

Figure 5.24: Location of control, cross-port check and pressure relief valves

5.3.7 Tilt Electronics and Controller Installation

To control the hydraulic system, the controller and signal conditioner box were installed behind the steering wheel, so that the driver of the vehicle could view the display and operate the buttons on the controller. To the left of the controller are the switches and warning lights associated with the engine operation (replicated from the BMW C1 donor vehicle). The CLEVER 'dashboard' is shown in figures 5.25.

Figure 5.25: Dashboard on the development prototype

Two additional batteries were used in conjunction with the main vehicle battery. This was to give a consistent 12 V supply for testing, and to give 24 V required to drive the hydraulic control valve. The second battery is not charged from

the engine generator, so must be charged externally between tests. Two voltage meters on the right of the controller indicate the total voltage available to the control valve.

Transducer Placement

Transducers for the tilt control system were installed on the vehicle. The tilt angle transducer was a 200 mm stroke potentiometer fixed to the side of the left hand side actuator. This gave a 0–5 V signal to the controller, supplying the position feedback signal. The steer transducers was also a potentiometer (with a 100 mm stroke) connected between the frame and the steering drop arm. Figure 5.26 shows the location of the tilt and steer transducers.

Tilt Steer

Figure 5.26: Tilt and steer transducers

The selected speed sensor was an inductive pick-up sensor, originally to be mounted to pick up the teeth cut in to the outer case of the differential. Following mounting difficulties in this location, this speed sensor was relocated next to one of the drive pulleys attached to the rear wheels axles. Initial testing conducted as part of stage one (see section 6.2) indicated that the frequency response of the inductive pick up was inadeqate, so this sensor was replaced with an optical pick up with a faster response. Further testing, as part of stage three (see section 6.4), revealed that this location was not a robust solution, since loss of grip of one of the driven wheels could give a false reading to the control system, compromising stability. For this reason, the optical sensor was relocated to the front wheel hub. These locations are shown in figure 5.27.

A tooth profile was cut onto the outer edge of one of the front brake discs, and

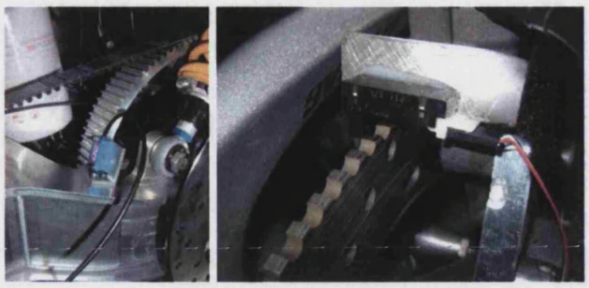

Figure 5.27: Speed sensor locations: rear swing arm and front wheel hub

the optical pickup was placed over the disc. As the teeth on the brake disc pass through the sensor, the light beam is broken, sending a pulse to the frequency to voltage (F–V) converter in the signal conditioning box. The controller reads the analogue voltage output from the F–V converter and calculates the speed. Initial tests with the speed pickup indicated that ambient light was interfering with the sensor, so a shroud was mounted around the sensor to overcome this issue.

The accelerometer used to measure the perceived lateral acceleration was mounted on the base of the tilting cabin and the yaw rate sensor was mounted underneath the tilt joint frame on the non-tilting rear portion of the vehicle. The pressure sensor was connected to the output of the unloading valve to measure the pressure in the supply line to the valve (and therefore, the accumulator pressure).

5.3.8 Safety equipment

Additional safety features were fitted to the CLEVER development prototype to prevent harm to the occupant during development of the controller. A window mesh was used to keep the occupant's arms in the vehicle in the case of vehicle rollover. A 4-point harness was used to completely prevent the occupant from falling out, and nylon blocks were fitted to the vehicle frame to prevent significant frame damage in the case of rollover. A single-use plumbed-in gas extinguisher was also installed on the vehicle in case of fire. Four nozzles were pointed at the rear frame and two nozzles at the electrical equipment beneath the rear seat. The photograph in figure 5.28 shows some of these safety features.

Figure 5.28: Safety features of the development vehicle

5.4 Commissioning of the Prototype

Before testing could commence, the development prototype underwent a commissioning process. The following tasks were performed:

- Filling and bleeding the brake system
- Initialising the fuel system
- Starting the engine and running until the cooling fan switched on and off

The hydraulic system was filled with oil and a low power external pump was connected to the system. A flushing plate was mounted in place of the control valve and the low power pump was switched on to flush the system of any debris from the assembly process. The flush plate was then removed and replaced with the control valve, in order to start initial testing.

5.5 The Completed Development Prototype

Figures 5.29 and 5.30 show the completed development vehicle used for testing the tilting system and providing experimental vehicle dynamics measurements. Specifications of the development prototype are detailed in table 5.1.

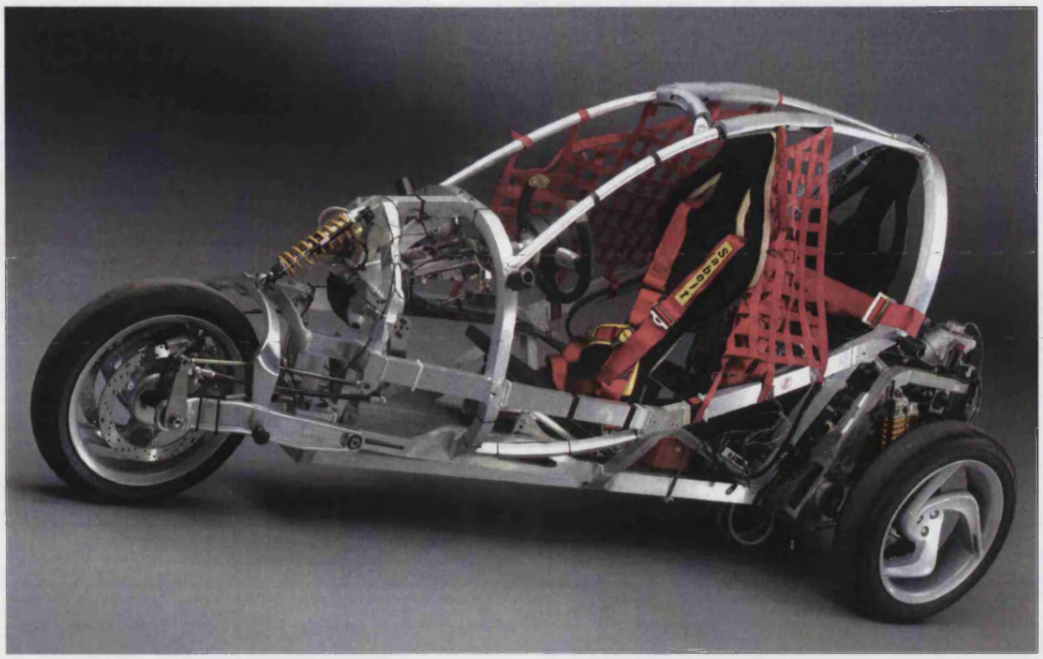

Figure 5.29: Development prototype vehicle

Figure 5.30: Complete development vehicle on display at final project meeting

5.6 Assembly of the Trim Vehicle

The University of Bath was also involved in the construction of four additional prototype vehicles as part of the CLEVER Project. Three prototypes were used

Engine	176 cc Single Cylinder 4-stroke
Fuel	Unleaded gasoline
Transmission	CVT adapted from BMW C1
Final Drive	Toothed belt drive from modified output through differential to rear wheels
Wheelbase	2.508 m
Wheeltrack	0.838 m
Rake angle	18°
Mass (unladen)	310 kg
Front wheel load (unladen)	90 kg
Rear wheel load (unladen)	110 kg each
Tilt limits	51° to left 39° to right

Table 5.1: Specifications of CLEVER development prototype

for crash testing, and as such, were not fully functional completed vehicles: these vehicles did not have any hydraulics (with the exception of filled and closed actuators), and did not include an engine and transmission system.

The fifth prototype, the final show vehicle was a fully functional demonstrator vehicle with a complete hydraulic tilt actuation system, and the internal combustion engine running on compressed natural gas. This vehicle is shown in figure 5.31 on page 152.

This trim vehicle is essentially identical to the development prototype vehicle. Both vehicles are built around the same CAD data and frame design, but there are a few notable exceptions:

- The trim vehicle has a fully trimmed cabin and body panels, which increase the vehicle unladen weight to 396 kg.
- The engine, although based on the 176 cc single cylinder engine from the BMW C1, has an increased swept volume of 230 cc and runs on compressed natural gas. The fuel is stored in two removeable cylinders mounted at the top of the rear frame. The power and torque outputs of the CNG engine are equivalent to those for the smaller gasoline engine used in the development prototype.
- Owing to the placement of the fuelling system in the rear frame, locations

of the hydraulic components differs from the development prototype. The hydraulic reservoir is also a different design to that used in the development prototype, and is positioned between the two compressed natural gas cylinders.

- The speed sensor is an inductive pick up (instead of an optical sensor), mounted to pick up a tooth profile cut on the outer edge of a front wheel brake disc.
- The controller used is based on that used in the development prototype. Differences in calibration values (due to slightly different transducer mounting positions) are taken account of within the software.

This vehicle was constructed by PSW Automotive Engineering, a subcontractor of BMW based in Gaimersheim, Germany. The author was involved with the installation of the tilt electronics and the commissioning of the hydraulic tilt actuation system. The trim vehicle, despite its full functionality, was not used for any measured performance testing of the tilting system.

5.7 Conclusions

The development prototype vehicle was constructed as part of the role of the University of Bath within the CLEVER Project. Following the selection of appropriate chassis systems, design work was conducted to produce manufacturing drawings of the components necessary to make the prototype vehicles.

Following the completion of the design work, the components were manufactured by external suppliers, and off-the-shelf components were purchased. The main vehicle frame was shipped to the University of Bath, and an engine and transmission system was removed from a donor vehicle and installed in the development prototype.

The hydraulic components were installed in the development prototype, and the tilt electronics were also mounted wihtin the vehicle. Safety equipment was also fitted to the development prototype to protect the vehicle frame and the occupant during testing.

The fully functional show vehicle, constructed by a subcontractor of BMW, was essentially identical to the development prototype with a few notable exceptions. The hydraulics and tilt electronics were commissioned and installed by the University of Bath before public demonstration. This show vehicle was not used for any quantitative testing of the tilting mechanism.

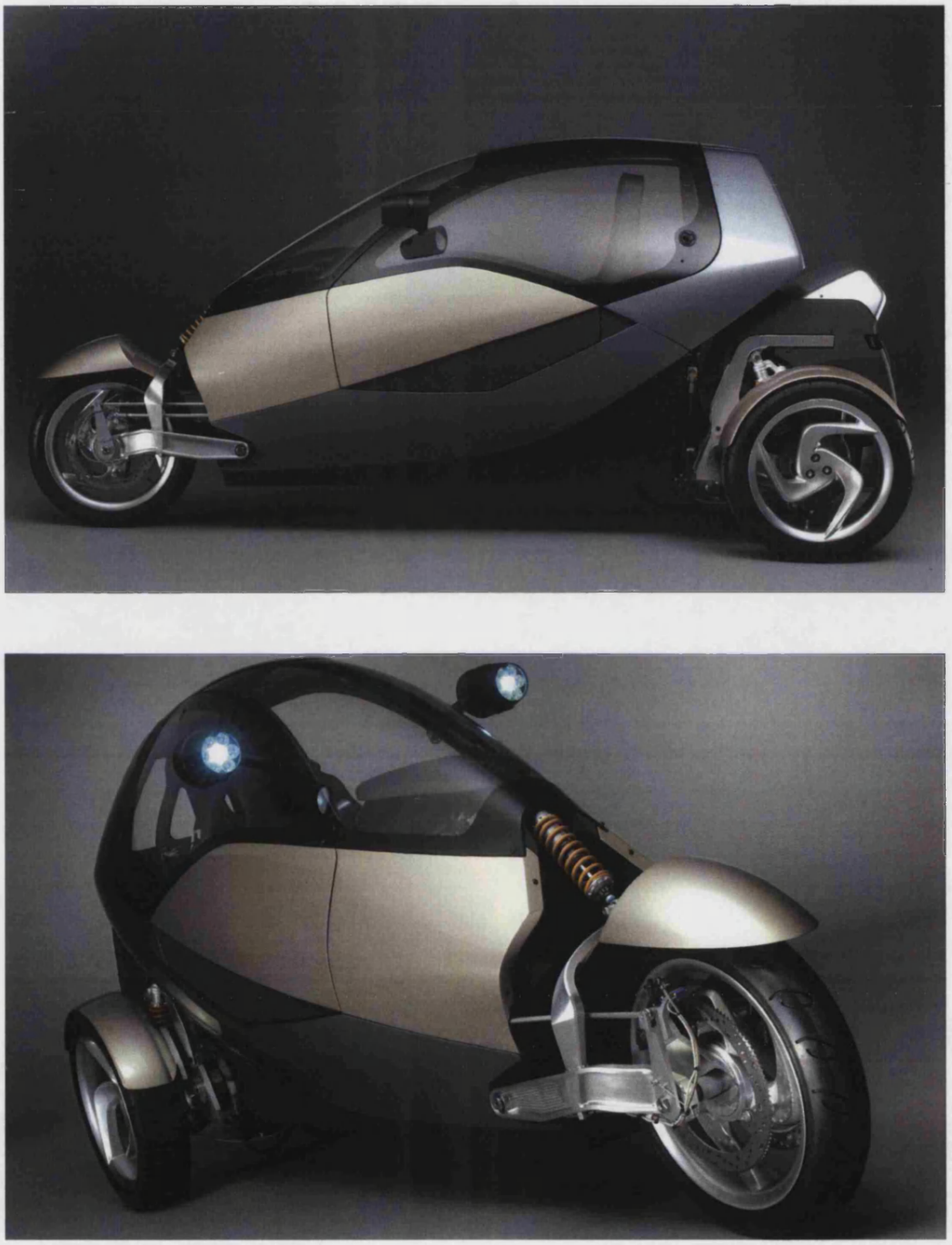

Figure 5.31: Final show vehicle

Chapter 6

Vehicle Testing

6.1 Introduction

One of the University of Bath's principal deliverables in the CLEVER Project was the development of a working prototype vehicle with which to develop the tilting system. To test this development prototype, a testing schedule was undertaken comprising three distinct stages: Systems; Tilt Actuation; and Driving.

The first stage comprised tests to assess the various chassis systems independently of each other. This proved the correct functioning of the engine, transmission and the braking systems, bench testing of the active control system and the hydraulic actuation system.

The second stage of testing examined the combined hydraulic actuation system and active control system and conducting static tests to check that the active tilting system was functioning correctly. A frequency response test of the tilting system was also conducted as part of this stage of testing.

After passing the second stage testing, the vehicle was driven for the first time with the tilting system activated. These initial driving tests were primarily to assess the tilting behaviour, to check reliable operation of the tilting system, and to tune the parameters of the tilting mechanism to provide a safe vehicle that

met the targets of the project. These tests are identified as stage three.

6.2 Stage One: Systems

Following construction of the prototype vehicle, much of the initial testing undertaken was 'shakedown' testing. These tests were run initially to verify that the various systems installed in the vehicle were functioning correctly, independent of any other systems.

6.2.1 Engine, Transmission and Braking Systems

The first tests undertaken were independent tests of the engine and transmission systems. As stated in the rig design and construction chapter (chapter 5), the engine to be used in the vehicle prototype was from a BMW C1 motorcycle. The engine had been removed from the C1 and dismantled in order to modify the transmission casing to accommodate the new transmission output shaft necessary to install it in CLEVER. The engine was reassembled, mounted in the vehicle prototype, and all the engine ancillary systems and electrical systems installed. Once proper functioning of the engine was ensured, the output pulley from the transmission was mounted, and the toothed belt connecting the output pulley to the differential was positioned. With the tilt actuation system deactivated and the vehicle cabin in the upright position, the vehicle was driven a short distance.

The aim of this test was to verify appropriate behaviour of the CVT transmission system, to set the front-rear balance for the braking system, and to check correct functioning of the speed sensor. While the transmission and braking systems performed adequately, the speed signal worked up to approximately 15 kph, but was not producing a robust signal beyond this speed. Further examination revealed that the frequency response of the transducer was not sufficient for the application on this vehicle. This problem was resolved by replacing the speed sensor with a more responsive optical pickup that detected the teeth on the drive pulley.

6.2.2 Controller and Tilt Electronics

The second step of stage one testing was verification of the controller functioning on the bench. With the full software program loaded on the controller, an analogue tilt position input was simulated, and in mode 0 (manual mode), the output position demand and corresponding valve opening was simulated. Mode 1 (normal, automatic mode) was checked by adding simulated analogue speed and steer position inputs, again checking for the correct position demand and valve opening outputs. As recommended in section 3.2.6, the proportional gain in the control code is initially set to be 1.

The controller was then connected to the signal conditioner unit, and again, inputs of tilt and steer position were simulated, and a signal generator was used to simulate speed. Again, the controller was checked for correct calculation of position demand and valve opening. The complete unit was then mounted on the development prototype.

6.2.3 Hydraulics

The third step of the stage one testing was to verify the correct functioning of the hydraulic actuation system. Using the external power-pack first implemented to flush the system (see section 5.4), small valve openings were used to tilt the vehicle slowly from side to side to expel any air entrained in the actuators (it was not possible to flush the single acting actuators using the flush plate). The external power pack was also used to set the pressure relief valve to a suitably low level (40 bar) for this initial static testing. Adjustments were then made to the valve trim (zero point) and ramp on the valve opening using the integrated potentiometers on the valve to ensure prompt response and equivalent valve openings for each side.

The engine driven pump was then connected to the tilting system hydraulic circuit, and at this low maximum pressure setting, the engine had no problem supplying the necessary power to the pump necessary to tilt the vehicle slowly. While ensuring no loose connections, and hence leaks, in the circuit, the maximum pressure was increased to 115 bar. This involved a slight increase in the engine

idle speed to provide the necessary power (this increased idle speed was still considerably lower than the speed necessary to engage the centrifugal clutch in the transmission). With the engine drive pump connected, the vehicle could be manually tilted side to side while under its own power.

6.3 Stage Two: Active Tilt Actuation

The second stage consisted of static testing of the complete tilt actuation system, integrating the active controller and the hydraulic tilt actuation system for the first time.

6.3.1 Manual Control

With the controller in manual mode (mode 0), with the engine pump running, and valve opening limited to 20% (the valve has an overlap of ±15% of spool travel) the vehicle was tilted slowly from side to side using the controller. The sequence of the photographs in figure 6.1 show the vehicle tilting from one side to the other under its own power, while in manual mode.

Figure 6.1: The prototype tilting from full right to full left in manual mode

The behaviour of the tilting system was good, with smooth operation over the full tilting regime. The cabin tilted at a constant rate towards the target tilt position, and arrived at the target smoothly with no apparent overshoot. This was not entirely surprising given the small valve openings and small flow rates.

6.3.2 Normal Control

To test the functioning of the controller in the normal mode (mode 1), a signal generator was connected to the speed input port of the electronics. With the speed input being simulated, the vehicle could be tilted by changing the steering position. See figures 3.28 and 3.29 for the flow chart of the position demand and valve output code. The input AD1 (speed) input was simulated using the square wave output from a signal generator.

In this mode, the valve opening limit was increased from 20% to 45% to achieve good speed during tilting. A 44% opening permits a 10 l/min flow rate with 160 bar pressure drop across the valve (from ports P to T), thus meeting peak flow requirements. It was important to not tilt the vehicle too aggressively in the absence of the 'balancing' lateral acceleration force. In this condition, the hydraulics were able to generate sufficient force to lift either inner wheel with harsh steering inputs.

6.3.3 Other modes

The other controller modes were also briefly tested. These were the control map select mode (mode 2), the calibration mode (mode 3) and the return to centre mode (mode 4). All these modes functioned appropriately.

6.4 Stage Three: Driving

Following these stage two tests, the vehicle was driven and simultaneously tilted under its own power using the controller. Following the frequency sweep tests, the first subjective tests were in general successful but it was immediately apparent that some modifications to the code were necessary before testing could safely continue. As the initial calibration values were determined in the laboratory when the vehicle was stationary, the values for the tilt and steer position were not quite correct—these changes were made before quantitative driving testing started.

6.4.1 Frequency Response

A frequency sweep test of tilt actuation system was performed primarily to establish the effect of rear and front damper settings and tyre pressures on the dynamic response of the vehicle. This test was relevant as it demonstrated the tilt actuation system response to a sinusoidal input of increasing frequency. Additionally, a square wave was also used to assess the step response of the tilting system.

The frequency response testing was conducted on a level laboratory floor with the engine running. A driver was in the vehicle, and was loosely gripping the steering wheel — his eyes were shut to prevent him reacting to the inputs. The vehicle brakes were not applied as this restricts the steering effect of the rear axle when the cabin tilts.

A tilt demand signal of $\pm 0.35\,\mathrm{V}$ was input directly into the controller. This was equivalent to a tilt angle demand of approximately $\pm 7°$. This was deemed as an acceptable level to satisfactorily evaluate the response of the tilt system, and it was suggested that step inputs of amplitudes above this would risk rear-wheel lift off, and possible damage to the vehicle frame. Two signals were used for the tests: a sinusoidal frequency sweep from 0.2–8 Hz and a square wave frequency of 0.2 Hz. Plots of these test signals against time are shown in the figure 6.2.

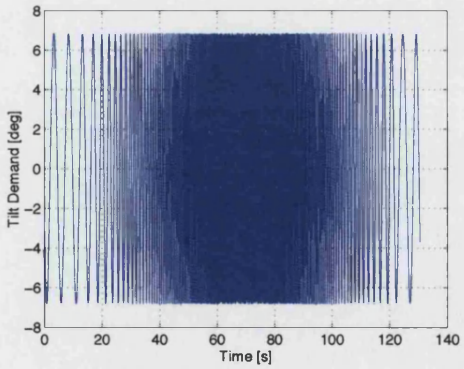

Sinusoidal sweep demand

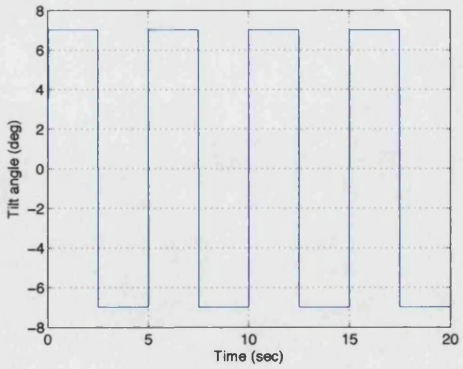

Step Demand

Figure 6.2: Demand signals

Sine Response

The response of the tilting cabin, and hence the tilting system, to the sinusoidal frequency sweep in the time domain is shown in figure 6.3. At the design specification frequency of 0.33 Hz, the response amplitude is 97% of the demand. The major chassis modes observed during the frequency sweep are listed in table 6.1.

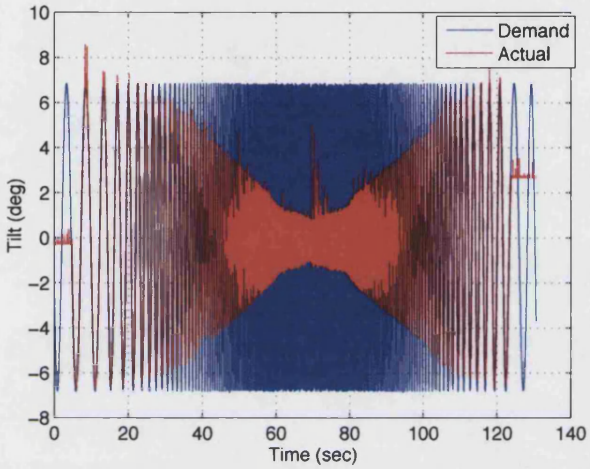

Figure 6.3: Tilting system response to sinusoidal frequency sweep

Frequency Range (Hz)	Observed Mode Description
0–0.8	Vehicle tilting normally, driver inline with vehicle motion
0.8–3	Lateral movement of driver out of phase with tilt
1.2–1.5	Whole vehicle roll on rear suspension
3	Rear frame roll only
4	Cabin lateral movement on front wheel contact patch
5	Increased lateral movement with apparent chassis twisting

Table 6.1: Subjective chassis modes observed during sinusoidal frequency sweep

An estimate of the linearised transfer function for the system was obtained using the TFE (transfer function estimate) function in Matlab. Figures 6.4(a) and 6.4(b) are the amplitude ratio and phase shift for this transfer function estimate. By identifying the frequency at which the phase shift is $-90°$, the bandwidth was calculated to be approximately 2.9 Hz.

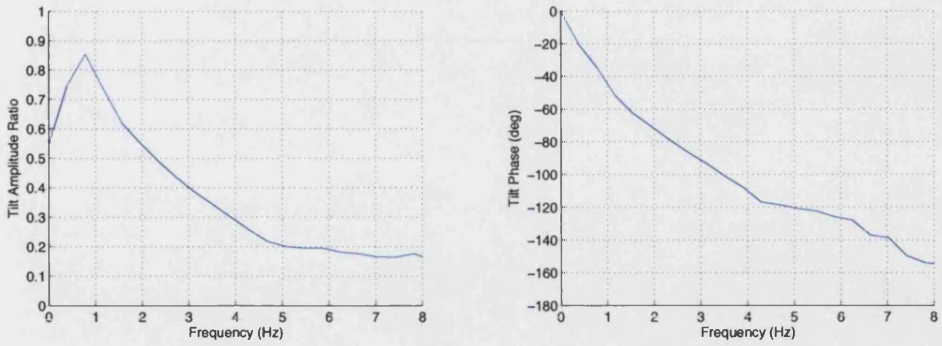

(a) (b)

Figure 6.4: Tilt system transfer function frequency response estimate, amplitude ratio (a) and phase shift (b)

At a tilting frequency of around 0.8 Hz, the cabin tilts normally with the driver remaining in line with the cabin. As this frequency is increased, the driver starts to move out of phase with the cabin until a frequency of 2–3 Hz is reached. At these frequencies, the absolute movement of the cabin (relative to the ground) is reduced; the actuation system is merely rotating the rear unit of the vehicle on its suspension. This is illustrated in figure 6.5 which is a plot of the rear left hand suspension unit displacement versus time. The largest amplitude of suspension travel occurs at approximately 45 seconds, and again at approximately 100 seconds, when the frequency is close to 3 Hz.

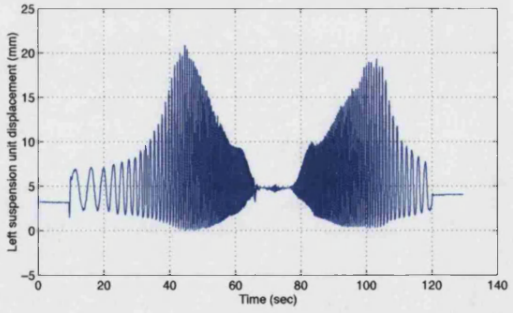

Figure 6.5: Left hand suspension displacement versus time

From 4 Hz upwards, the front end starts to move laterally from side to side, with the front wheel rotating about its steering axis. This indicates that the tilting mode of the front cabin is coupled with the steering mode. This coupling can be visualised through a transfer function estimate between the demand tilt angle and the steering system oscillation. Figure 6.6(a) is the amplitude ratio and figure

6.6(b) is the phase shift. It is worth noting that the point of resonance—where the phase shift is $-90°$—occurs at approximately 4.5 Hz.

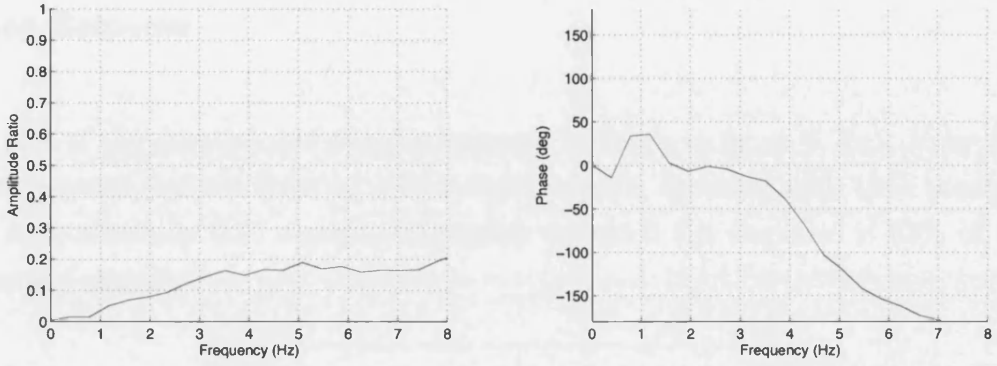

(a) (b)

Figure 6.6: Frequency response estimate relating demand angle to steer angle

As noted in [36], motorcycle handlebar wobble, although usually occuring at higher speeds, is an oscillation around this frequency [79]. If such a situation was encountered, an unstable oscillation in the tilting system could be triggered as steering angle forms part of the demand signal in the controller. As stated in section 6.4.4 later in this chapter, and documented in [80], a low-pass filter was required in the controller which has the added benefit of solving this issue.

At frequencies of 5 Hz and above, the chassis of the cabin appeared to be twisting, but measurements or recordings of this phenomenon were not obtained so this cannot be proved quantitatively. Testing at these high frequencies was limited to restrict any damage that may have been induced by this apparent twisting.

The influence of vehicle setup, with particular focus on suspension settings is covered in further detail in [44].

Comparison between this and the linear analysis of the hydraulics system conducted in section 4.4 indicates significant discrepancies between the results of the real system and the simulation. In particular, the simulation model is heavily damped compared to the real system, and the calculated natural frequency is extremely low. This could be explained by the fact that the linear analysis is conducted operating around a specific operating point, which in turn dictates the flow and flow-pressure gains, which have an effect on the natural frequency and damping ratio of the simulated system. It is possible that this operating

point does not represent the real system conditions.

Step Response

A plot of the demand and the tilt response is shown in figure 6.7(a). Note that the response has the form of a first order transfer function with time constant of approximately 0.15 seconds (the point at which the response is 63% of the demand signal).

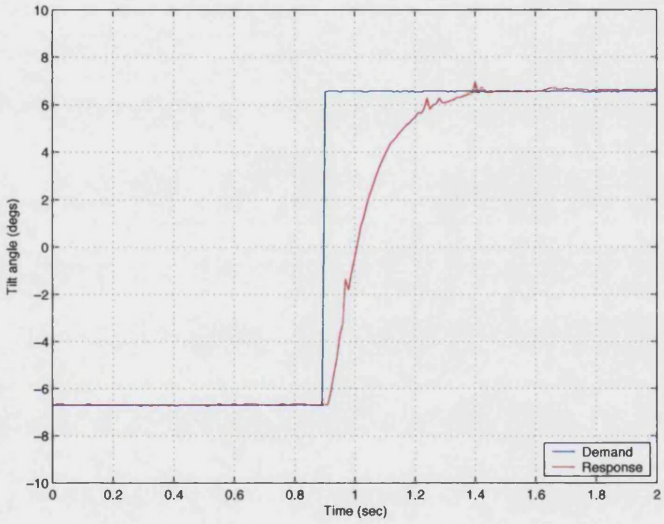

Figure 6.7: Demand and response of a step input

As with the sinusoidal frequency sweep, there is a discrepancy between the experimental results and the simulation results (see section 4.4.7). The time constant determined in simulation was 1.02 seconds, and this is again explained by the large damping ratio and low natural frequency found as a results of the specific operating point used in simulation.

Figure 6.8 is a plot of the left hand suspension displacement during two step inputs (one tilt from $+7°$ to $-7°$ and then another returning to $+7°$). It is evident that two stages exist in the chassis movements: the rear frame rolls outwards and the cabin then moves to the desired position, which locks the actuators. This second stage is coupled with a small change in the rear unit tilt angle (indicated by the shift in suspension displacement).

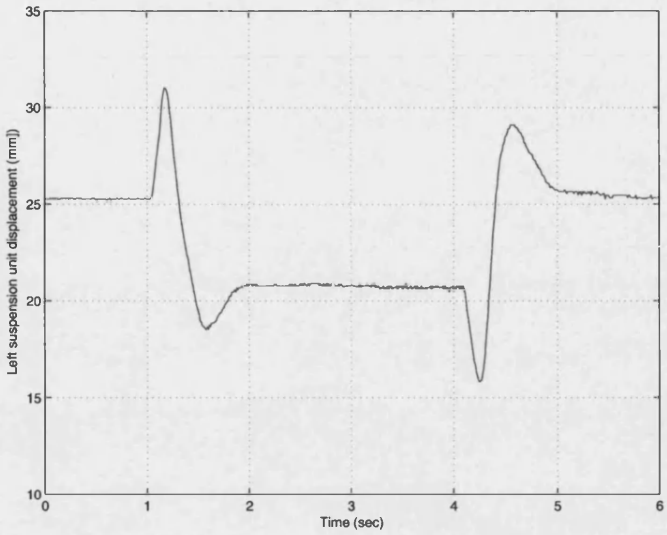

Figure 6.8: Suspension displacement during step input

Again, the influence of vehicle setup on the step response of the vehicle is covered in further detail in [44].

6.4.2 Steady State Behaviour

The first driving tests run as part of stage three were subjective tests to establish a reference tilting behaviour to be used as a basis for improvements. In these first tests, the emphasis was placed on achieving good steady state behaviour.

These tests were conducted on a relatively low friction road surface due to the weather conditions and two coupled issues were highlighted. Firstly, during cornering, there was considerable roll in the rear frame of the vehicle, as can be seen in figure 6.9(a). This outward roll of the non-tilting unit reduced the absolute tilt angle of the front cabin, reducing the balancing effect. The second issue was that there was a significant weight transfer to the outer rear wheel since the inner rear wheel was losing grip, signified by a short rise in engine speed while accelerating out of a corner. This in itself was not a problem with right hand corners (right inner wheel unloaded), but since the optical speed pick up was located to sense the passing teeth of the left drive pulley, when this wheel unloaded, it sped up, sending a false speed command to the tilt controller. This in turn, sent a corresponding command to the valve, causing the vehicle to tilt deeper into the corner.

On one occasion, the rate at which the speed built up caused a large moment to be applied between the base and the tilting cabin, and the inside rear wheel was lifted from the ground resulting in roll over. In this instance, the applied moment exceeded the maximum permissible value of $mgt/2$, as determined in chapter 3.

The first modification made to rectify this issue was to increase the roll stiffness of the rear unit by removing the rubber elements in the stabiliser assembly (see section 5.2.4). The second modification necessary to correct this was to over-lean the cabin with respect to the rear unit to ameliorate the reduction in the balanced position owing to the outward roll of the rear unit. This also transferred some cabin weight to the inside rear wheel. Figure 6.9 (b) shows the improvement made for similar cornering conditions.

(a) (b)

Figure 6.9: Initial testing without (a) and with (b) overlean

To implement over-lean in the controller code, an additional gain was introduced into the postition demand signal. (See figure 3.28 for the flow chart of the position demand code.) Different gains were tried in testing—selection was made using the map select mode in the controller (mode 2)—and it was agreed that a 20% over-lean felt the most natural.

In addition, the speed sensor was moved to the front wheel. This had the advantage that in the event of a locked front wheel under harsh braking, the speed sent to the controller was zero, hence making the vehicle stand upright, the appropriate position with the front wheel sliding: if the front wheel is locked and sliding, no cornering force and hence no lateral acceleration is generated.

Dynamic chassis analysis conducted as part of the work covered in [44] revealed that the CLEVER chassis was unable to achieve a 1 g lateral acceleration owing to the tilt angle limits; the maximum lateral acceleration while having a balanced vehicle was approximately $8\,\mathrm{m/s^2}$. To incorporate this in the code, equation 3.23

becomes:

$$\theta_d = 0.8662 \left(\frac{V^2 \delta}{l a_{\mathrm{y,max}}} \right) \tag{6.1}$$

where $a_{\mathrm{y,max}}$ is the new lateral acceleration limit of $8\,\mathrm{m/s^2}$. (This was implemented in the code by changing the integer value of g_i from 981 to 800.) Using this equation in the controller code also has the effect of increasing the lean angle—a 45° tilt angle command is now associated with a corner that results in $a_y = 8.0\,\mathrm{m/s^2}$.

Following these modifications, further testing indicated good performance in steady state corners. The subjective feeling from the driver was that of a very natural, balanced tilt position, with the combination of gravitational forces and lateral acceleration in line with the occupant's body.

Upon installation of the data-loggers on the vehicle, the good subjective performance was confirmed through objective experimental measurement. The plot on the left in figure 6.10 shows the actual (blue) and perceived lateral (black) acceleration (a_y and a_{per} respectively) during a manoeuvre with constant steer angle and increasing speed. The plot on the right is the GPS absolute position during the manoeuvre. As can be seen, the level of perceived lateral acceleration is very small (maximum of around 0.14 g) compared with the actual lateral acceleration being generated by the corner radius and vehicle speed (up to 0.6 g). The vehicle is turning right (clockwise), and as the GPS plot shows, as speed was increased, the radius of the corner reduced. This indicates oversteer that may be caused by camber thrust at the front wheel, some element of overlean and a rear biased centre of gravity. Clearly the vehicle does not perfectly follow Ackermann steering principles.

Further analysis of the results showed that the steer angle and the Ackermann angle match reasonably well. Figure 6.11 shows steer angle (δ) and Ackermann angles against the lateral acceleration measured in the logger for both left- and right-handed circles (left-handed is indicated by negative values for lateral acceleration).

Despite small variations in the computed Ackermann angles, differences between left- and right-handed circles can be detected from the figure: in left-handed circles, the steering remains neutral throughout the tested lateral acceleration

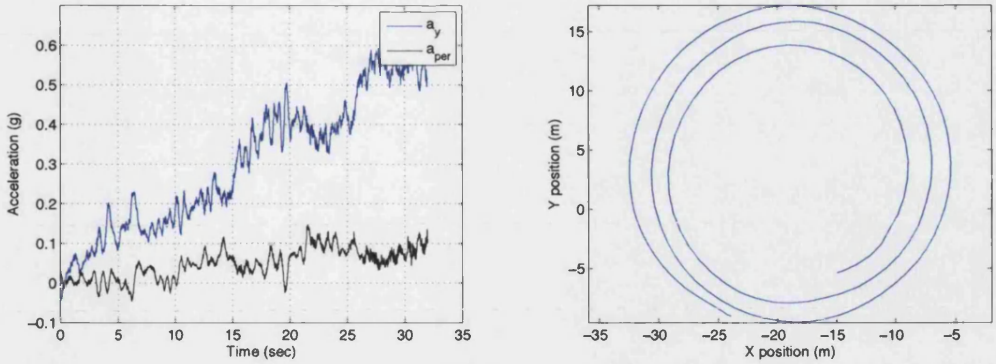

Figure 6.10: Actual (a_y) and perceived (a_{per}) lateral acceleration, and GPS position plot of manoeuvre

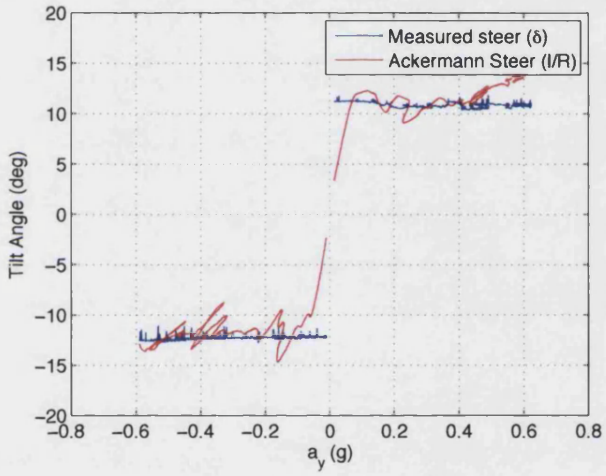

Figure 6.11: Steer angle and Ackermann angles versus lateral acceleration

range, whereas in right-handed circles, the vehicle oversteers above 0.5 g. This is also apparent in the plot of achieved tilt angle versus lateral acceleration, as shown in figure 6.12 (both left and right handed curves are shown, in addition to the theoretical line that should be followed). While the vehicle follows the theoretical tilt angle in left-handed circles, the tilt angle was greater in right-handed circles, which in turn caused an increase in camber thrust generated at the front wheel, which in turn made the vehicle oversteer. This difference in tilting left and right was discovered during calibration of the controller (covered in section 3.4.1) and is due to inadequate manufacturing tolerances during frame construction. More thorough and accurate calibration is required to ensure correct performance in left- and right-hand corners.

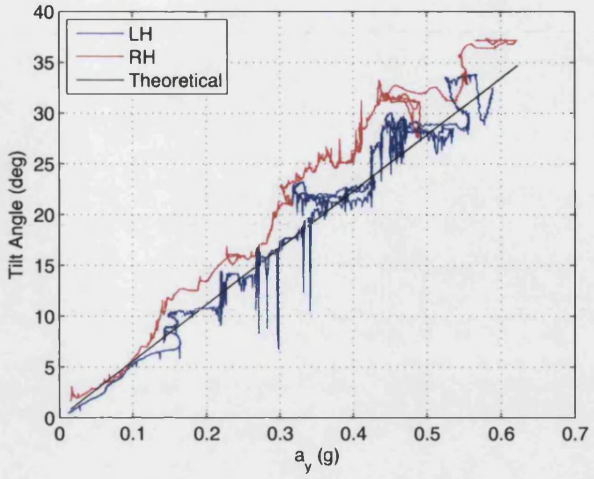

Figure 6.12: Tilt angle versus lateral acceleration for left- and right-handed circles

6.4.3 Transient Behaviour

While good performance had been achieved for steady state corners, the transient response required further improvement. The poor response was particularly apparent with heavier occupants (two drivers weighing 95 kg and 120 kg noted poor response). Due to the higher inertia of the tilting mass with heavy drivers, the slow response meant large lateral accelerations were generated significantly before the tilting cabin could approach the balanced position, and in some cases, the inner rear wheel lifted, as shown in figure 6.13. With lighter occupants—the regular test drivers weighed 65–70 kg—the transient response was still slow, but the lower inertia of the tilting cabin meant the tilting system was able to respond more quickly and was closer to the balanced position when large lateral forces were generated.

To improve the transient response with heavy occupants, the first method implemented was to increase the system pressure. As stated in section 6.2, the maximum system pressure was initially set at 115 bar. The unloading valve threshold settings were modified so that the maximum pressure (at which point the pump was unloaded) was 150 bar, and the minimum pressure (the point at which the pump was loaded) was 130 bar. These points were determined by looking at the worst case scenario of the vehicle failing with a heavy driver (120 kg) at the full tilt position. For a heavy driver, at least 108 bar was required to lift the cabin

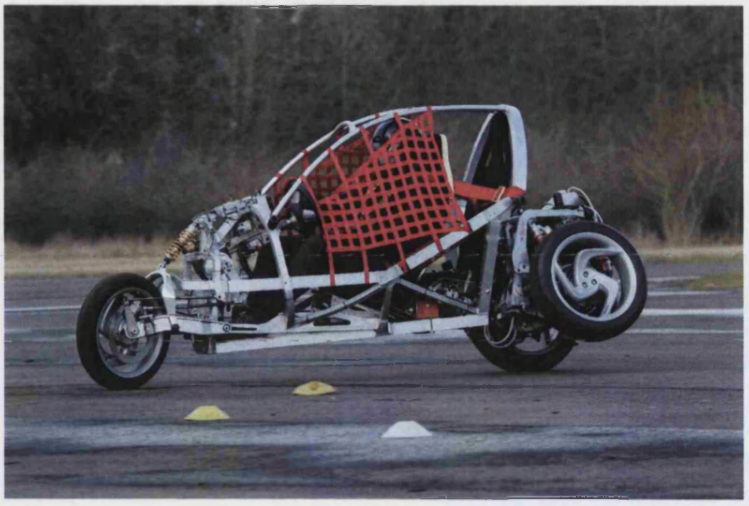

Figure 6.13: Slow response leading to lift of inside inner wheel

back to the upright position. The plots shown in figure 6.14 show the tilt angle during a 'figure-of-8' manoeuvre, and the pressure rising and falling between the lower and upper threshold points. It must be noted that despite concern about the drive-ability of the vehicle when the pump was unloaded and loaded, as noted in section 4.5.4, this issue was not a problem in testing—the changes between the loaded and unloaded state were imperceptible, even with an abrupt transition between the two states implemented in the controller.

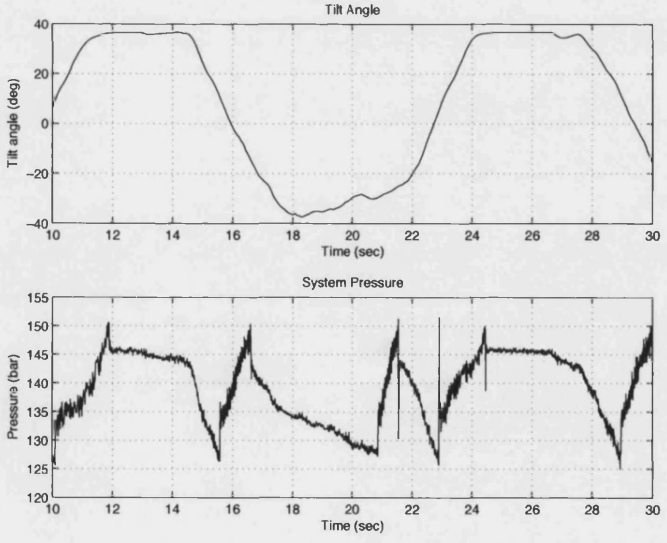

Figure 6.14: Tilt angle and pressure plots during a 'figure-of-8' manoeuvre

Changing these pressure threshold positions improved the response with heavier

occupants, but the system was still slow to respond with all drivers in slalom and 'lane-change' manoeuvres. Any rapid steering input at the steering wheel that resulted in a large change in lateral acceleration resulted in a slow tilt response.

This indicated that an increase in system gain was necessary. Initial trials indicated that a gain of 1 was a suitable starting point for testing, and this gain value resulted in the smooth tilting action seen in stages 1 and 2 of the testing. Simply increasing this value was not directly possible due to noise in the signals while the engine was running. Increasing the gain not only increased the response, but amplified any noise in the system, leading to an uncomfortable and unstable vehicle, impairing drive-ability. With an increased gain, in manual mode, the tilting system was 'juddery' and would appear to jump from one position to another. Despite the 15 Hz filter installed within the signal conditioning box, the cut-off frequency for this filter was too high for it to have a significant effect.

Examining the measured results revealed the cause for the unstable behaviour: the valve position was shuttling across the dead band at high frequency. With the increased gain, the spool was moving faster, and would overshoot the dead-band position, leading to small flows passing through the valve, tilting the cabin. The closed-loop control built into the valve electronics could not ensure that the overshoot did not occur. Adjusting the ramp speed of the valve slowed the valve response, hence eradicating the overshoot of the spool, but as this ramp was applied over the complete valve operating domain, it resulted in very slow valve response when high response was required. The plot on the left of figure 6.15 shows the integer input values into the controller for tilt angle, steer angle and vehicle speed for a typical 'figure-of-8' manoeuvre. The plot on the right is the valve command signal for this manoeuvre. This clearly shows the rapid shuttling of the valve spool across the dead-band.It is clear that the valve was much larger than necessary for this particular manoeuvre and probably too large for this application. Unfortunately, time constraints prevented a smaller valve from being purchased so alternative methods were adopted to overcome this problem.

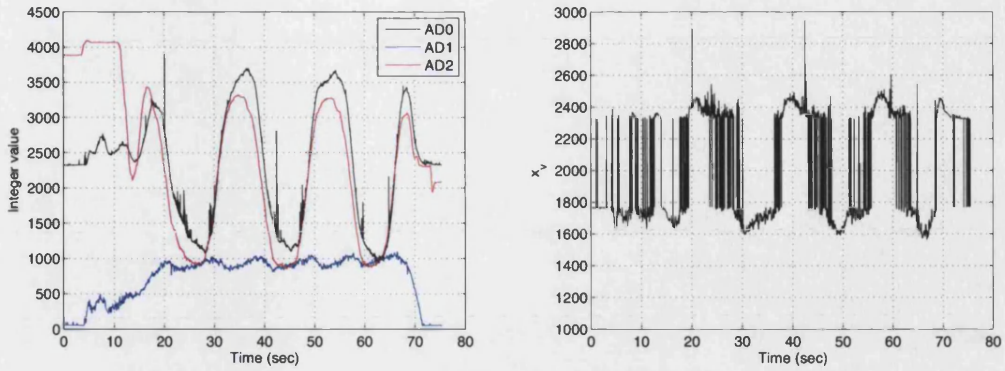

Figure 6.15: Inputs to controller and corresponding valve output

6.4.4 Filter Development For Improved Valve Control

Moving Average Filter

The filter developed to improve the valve spool control around the dead-band was a low-pass filter, allowing low frequency signals to be used, while attenuating those at higher frequencies. The first method of filtering the signal was to implement a moving average filter, where a window, whose size is related to the filter frequency, passes over the signal, averaging the values within the window. With the sample rate of 150 Hz, the window for a 5 Hz filter would consist of 30 elements ($150/5 = 30$). Likewise, for a 3 Hz filter, the window would contain 50 elements, and so on. This filtering method was tested in the controller with the valve disconnected; a sinusoidal frequency sweep was input into the controller, it was then filtered, and the output was logged. Results for a 5 Hz filter are presented in figure 6.16.

As can be seen, this filtering method is not acceptable. While multiples of the cut-off frequency (5 Hz) were suitably suppressed, there was ripple between them. Additionally, this type of filter placed a large number of calculations within the controller loop: with a 1.5 Hz moving average filter, the loop could not be executed within 6.7 ms, as specified in the controller requirement (see section 3.3.3).

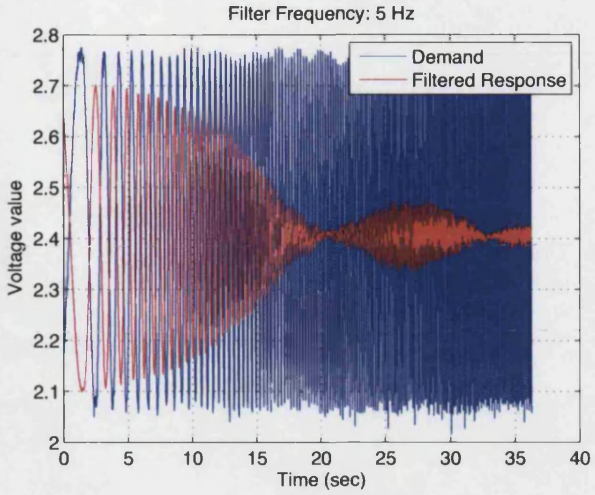

Figure 6.16: Moving average filtering method, 5 Hz filter

First Order Lag Filter

The next filtering method investigated was to implement a simple first order lag filter. This filter has the advantage that there are no ripples in the passband and the response slopes off towards negative infinity with a roll-off of -20 dB per decade. While higher order Butterworth, Bessel, Chebyshev and elliptic filters were considered, these were seen as unnecessary if adequate performance could be acquired from the use of a first order filter. In addition, these more sophisticated filtering techniques required more processor power than that available, and also suffered from gain distortion in the passband. The bode plot of a simple first order low pass filter is shown in figure 6.17.

The filtering function for a first order lag was implemented in the controller code using equation 6.2:

$$\theta_{ief,n} = \frac{b_1\theta_{ie,n} + b_2\theta_{ie,n-1} - a_2\theta_{ief,n-1}}{a_1} \tag{6.2}$$

where a_1, a_2, b_1 and b_2 are filter coefficients based upon results from the `butter` function in Matlab. The `butter` function takes the arguments of order and normalised cut-off frequency and designs a low-pass digital filter, returning the filter coefficients in row vectors b and a. These coefficients were then scaled to

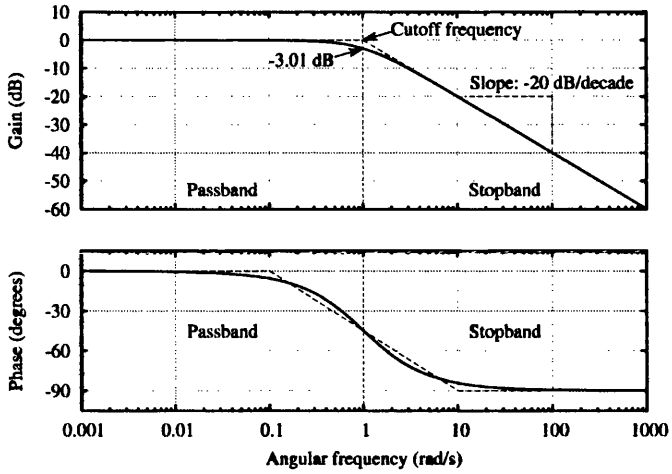

Figure 6.17: Bode diagram of a first order filter with cut-off frequency of 1 rad/s [81]

work with integer values, owing to the way the controller was coded. The current filtered tilt error angle (in integers), $\theta_{ief,n}$, is a function of these coefficients, the current error signal, $\theta_{ie,n}$, and the previous error and filtered error signals (signified by the $n-1$ subscript).

The plots shown in figure 6.18 show the magnitude and phase lag of four filter cut-off frequencies presented here (1, 2, 4 and 6 Hz). The arrows in the figure point in the direction of increasing frequency.

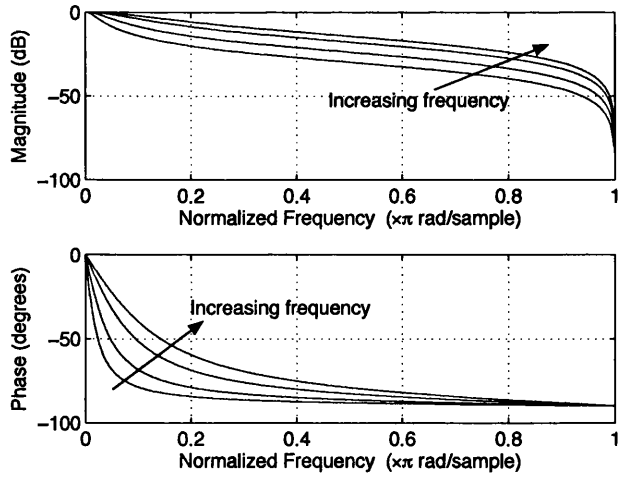

Figure 6.18: Magnitude and phase of filters

This plot demonstrates that with increasing frequency, the phase lag and drop in

amplitude is reduced.

Using the logged results presented in figure 6.15, the filter was developed in simulation before implementation on the controller. Figure 6.19 compares the original valve output command as shown in figure 6.15 with the command filtered with cut-off frequencies of 1 Hz, 2 Hz, 4 Hz and 6 Hz. As can be seen in the figure, the lower the cut-off frequency, the more filtered the command as indicated by the reduced number of excursions across the valve dead-band.

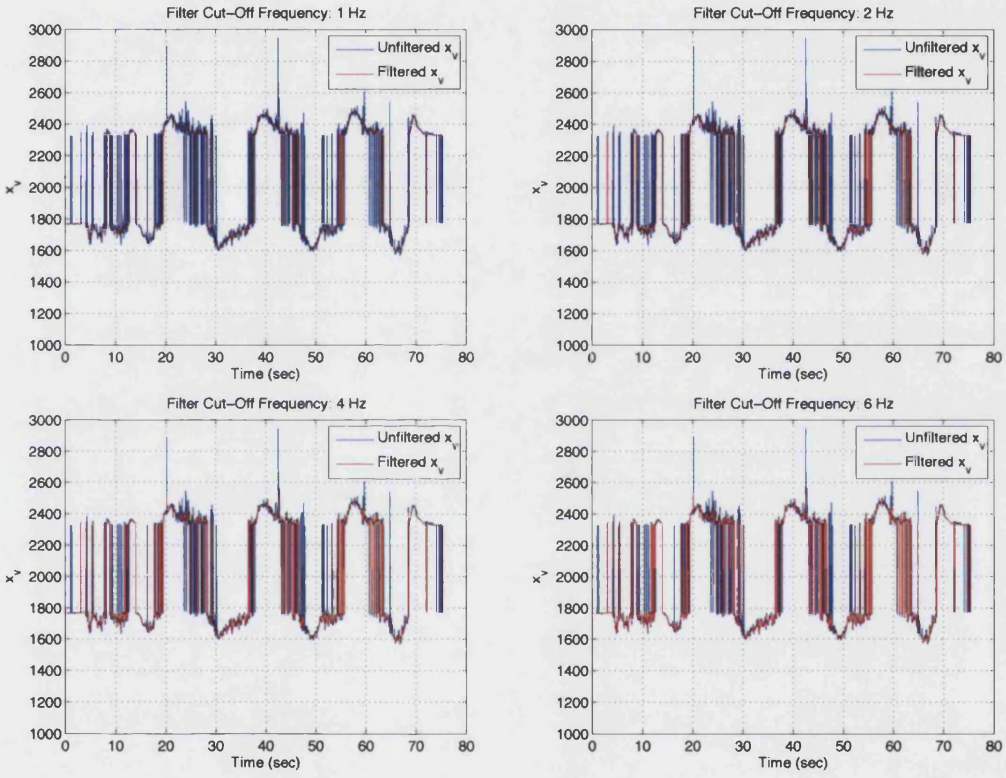

Figure 6.19: Filtered valve output overlaying the original output

The cut-off frequency was initially chosen to be 2 Hz. This was felt to be suitable, as 2 Hz is significantly faster than the maximum tilting frequency of the tilting system (0.33 Hz), but slower than suggested frequencies of instabilities resulting from bump inputs at either rear wheel. In addition, it also resulted in a short phase lag between the unfiltered and filtered demand. Despite this decision, the map select mode (mode 2) of the controller was programmed so that different filter frequencies could be selected during testing such that tilt response and the associated lag could be assessed for varying filter cut-off frequencies.

6.4.5 Results with Increased System Gain

Following implementation of the filter on the position error signal entering the controller, the system gain was increased to improve the transient response. Figure 6.20 shows the two plots of the valve command signal with the increased gain overlaying the original command signal for the run shown in figure 6.15. The plot on the left is for a filter with a 2 Hz cut-off frequency, while the plot on the right is for a filter with a 6 Hz cut-off frequency. As can be seen, with the slower filter, the valve spool has fewer excursions across the dead-band. While with the faster filter, the valve spool has a faster response, large spikes in the command value are apparent indicating that some noise is being amplified.

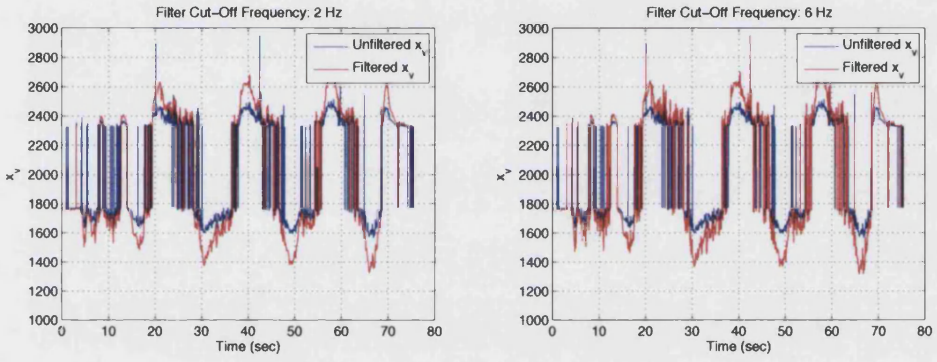

Figure 6.20: Filtered valve output with increased gain overlaying the original output

The filters were implemented in the controller code and tests were run to assess the results. A 'figure-of-8' manoeuvre was used as a means of evaluating the system's transient response; the vehicle undergoes a tilt from one extreme to the other.

Figure 6.21 is a plot of steer angle and the resultant tilt angle during such a 'figure-of-8' manoeuvre with the initial, low gain value of 1 (with a 2 Hz filter on the position error signal). The lag between the input (the steer angle) and the output (the tilt angle) is evident where the signals cross the zero degree position; when the steer angle is zero, the tilt angle should also be zero.

As can be seen from figure 6.21, the lag between the point at which the steer angle crosses the zero position and the tilt angle crossing the zero position is around 0.4 seconds. (This is an average value of the lag for left and right turns—the

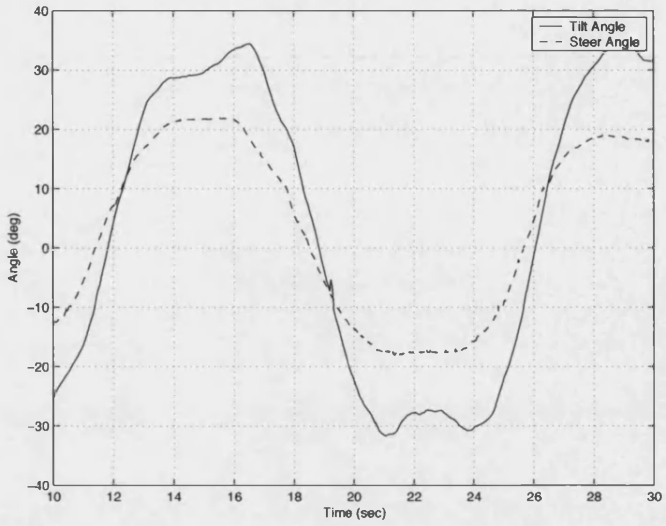

Figure 6.21: Steer and tilt angles: system gain of 1

slight difference in the two is down to small errors in calibration of the sensors.) It must be noted that these results were taken with a relatively light occupant; with heavier drivers, this lag is increased due to the higher tilt inertia.

Doubling the system gain from that used initially results in the plot shown in figure 6.22. Again a 'figure of 8' manoeuvre is used, but now the average lag between the steer angle and the tilt angle at the zero degree position is reduced to around 0.1 seconds. In addition, for a similar steer demand, the tilt rate is faster with the higher gain. The subjective feeling of the vehicle with this improved response was much better; it almost felt as though there was a mechanical link between the steering wheel and the tilting system.

With gains above 2 a faster response was noted, but any noise still in the signal after filtering became more apparent, even with a low cut-off frequency.

6.4.6 Filter Frequency Sensitivity Analysis

Following success in achieving improved response by increasing the system gain, it was necessary to examine the effect of the filter cut-off frequency on the tilt response to harsh ramp inputs at the steering wheel at a constant forward velocity. It must be noted that the implementation of the filter also has the effect of limiting

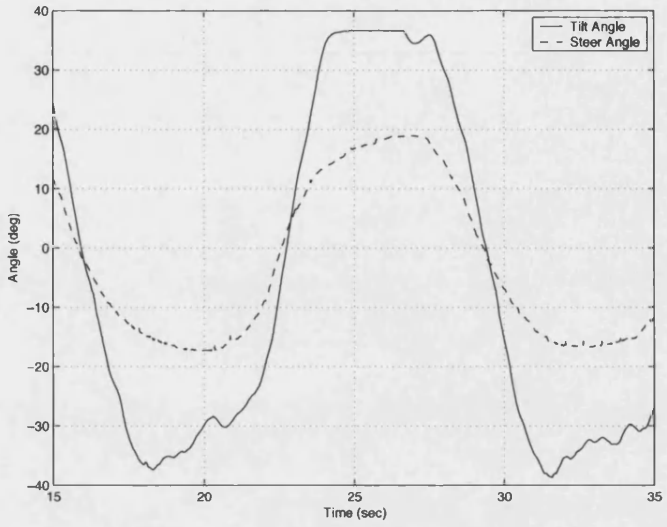

Figure 6.22: Steer and tilt angles: system gain of 2

the rate of change of torque generated by the hydraulic actuators between the front and rear units resulting from harsh step inputs at the steering wheel. As this filter was applied to the tilt position error signal, both the speed and steer inputs into the control system—those used to calculate tilt angle—are effectively filtered.

A series of test runs were conducted where step inputs were made to the steering angle to examine the vehicle response. Results for step inputs with filter cut-off frequencies between 1 Hz and 6 Hz were measured. All six results are shown in figures 6.23, 6.24 and 6.25.

It is clear that the higher cut-off frequency increased the response speed and the tilt rate (in a similar manner to increasing the system gain) due to the reduced filter lag. In addition, the higher cut-off frequency also effectively increased the torque generated in the actuators, necessary to increase the response. This increased the torque availability but had the potential disadvantage that step inputs, as shown in figure 6.25, could cause the inner rear wheel to hop from the ground. This was due to the high cabin inertia—the tilting torque generated by the actuators has an effect on both the front tilt frame and the rear frame. In a harsh avoidance manoeuvre it is possible that a tilt system with a very fast dynamic response could cause the rear unit to tilt out of the bend to such an extent that the inner rear wheel leaves the ground and the vehicle rolls over.

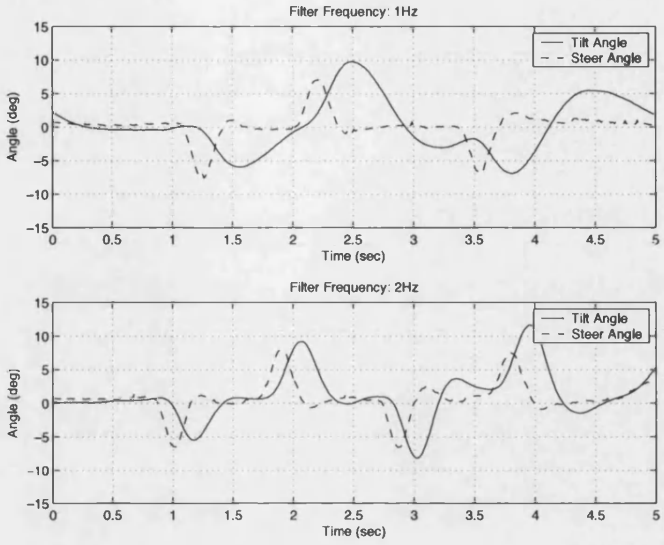

Figure 6.23: Steer and tilt angles, 1 & 2 Hz filter

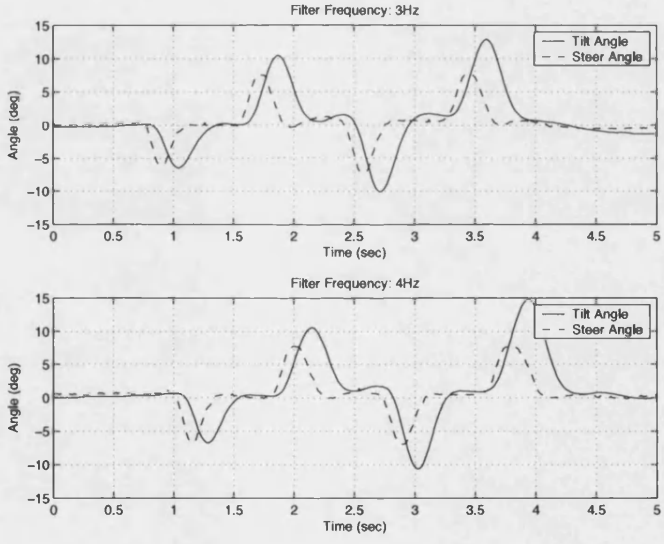

Figure 6.24: Steer and tilt angles, 3 & 4 Hz filter

In addition, the filter cut-off frequencies were influential in how the vehicle dealt with high frequency oscillatory steering inputs at the steering wheel (and consequently at the the front wheel). As expected, with the lower frequency (1–2 Hz) filters implemented, the tilting system did not react to these inputs, but the higher frequency filters (5–6 Hz) resulted in the vehicle tilting. Figure 6.26 shows results for a control system filter with a 6 Hz cut-off frequency. The figure shows that the tilt system responded to the input signal; additional testing

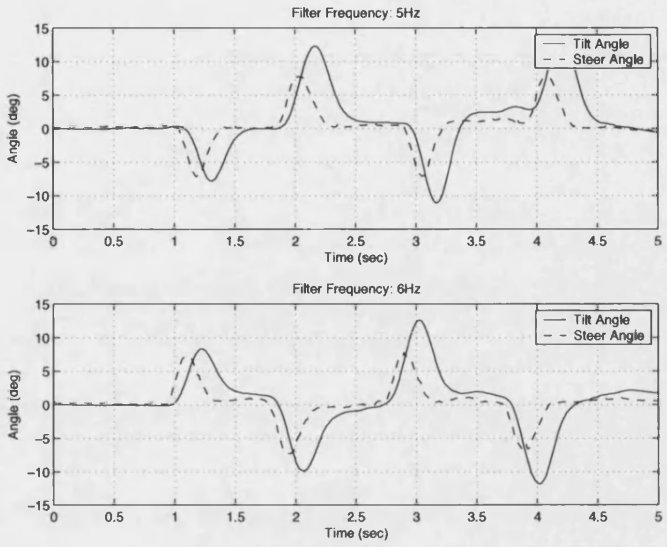

Figure 6.25: Steer and tilt angles, 5 & 6 Hz filter

demonstrated that a control system filter with a 1 Hz cut-off frequency did not respond to similar oscillations at the input. Although no motorcycle 'wobble' and 'weave' instabilities were exhibited during testing, it would be desireable to prevent these oscillations from having an effect on the tilting system.

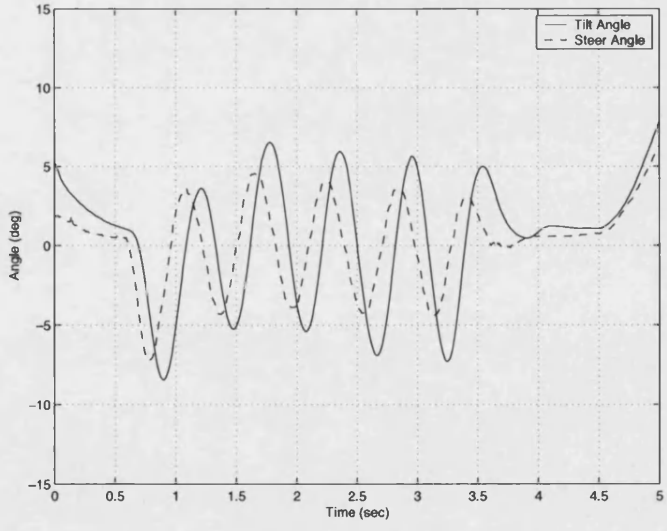

Figure 6.26: Steer and tilt angles, sscillation at steering wheel

This sensitivity analysis demonstrates one of the significant compromises associated with the direct tilt control adopted in the CLEVER Vehicle. This compromise exists between the necessity of having a tilting system that responds

adequately to input signals, but reacts to harsh inputs in a safe and controllable manner. To prevent harsh inputs, a lower frequency filter is required, but this impairs response in 'normal', less harsh manoeuvres. This response is improved by implementing a higher frequency filter, however, as demonstrated, harsh inputs increase the tilt rate and result in the lifting of a rear wheel.

While using higher frequency filters gives a better response compared to using lower frequency filters, their use also means that the tilting moment applied in aggressive manoeuvres can exceed the permitted maximum value, possibly causing roll-over.

6.5 Concluding Remarks

Within the timeframe of the CLEVER project, the development prototype was tested in three stages: systems, tilting actuation, and driving.

Stage one confirmed that the vehicle chassis systems worked well independently of each other, while stage two integrated the tilt controller and tilt actuation systems to verify the correct functioning of the complete tilting system in the static case.

Once these two preliminary stages were completed, stage three was initiated. A frequency response test of the tilting system was undertaken, encompassing a sinusoidal sweep and step inputs, to assess the response of the tilting actuation system. The tilt system responds to frequencies up to 8 Hz (the maximum frequency tested), with the system having an amplitude ratio of 97% at the design specification of 0.33 Hz. A steering mode coupled to the tilting mode was noted at 4.5 Hz, although this was reduced during later testing through the use of filters in the controller.

In the driving condition, initial focus was placed on achieving a suitable steady state response – modifications were necessary to allow the cabin to reach the best absolute tilt angle (with respect to the road), and measured results indicated that the perceived lateral acceleration levels were low compared to a non tilting vehicle, indicating that the cabin is reaching a suitable tilt angle. In addition, the

steer angle input and the theoretical Ackermann angle were comparable, although differences were evident between left- and right-handed circles. Despite this, the integration of a tilting system with a direct steering system was successfully demonstrated.

The transient response, however, was initially insufficient, so the hydraulic system pressure was raised to compensate for the high tilt inertias when the prototype was operated by heavier drivers. It was also necessary to raise the system gain, but due to noise in the signals, this resulted in the valve spool shuttling across the dead-band in the valve and overshooting beyond the dead-band region with increased gains. Software filters were applied to the position error signal to reduce this shuttling, allowing the gain to be increased while suppressing the effects of noise on the output signal.

Both the proportional gain and the cut-off frequency of the software filter are significant factors contributing to the transient tilt response. Higher gains and higher cut-off frequencies allow for a fast tilt response, but also they also increase the effective moment that can be applied between the base and the tilting cabin, such that roll-over is possible when the vehicle is steered aggressively. Lower frequencies prevent this from happening, but provide poorer response in non-aggressive manoeuvres. It was shown that when designing a direct tilt controlled three-wheeled tilting vehicle with the arrangement and physical characteristics used in CLEVER, safe handling can only be achieved at the expense of a fast tilt response. This is a result of the fundamental limitations of the narrow track vehicle design and the use of direct tilt control, and was predicted in section 3.2.6 as a result of the simulation of the direct tilting system.

It must, however, be noted that the testing covered within the project timeframe was very limited, and tests were deliberately not performed at limit conditions or close to rollover. Further testing coupled with in-depth analysis is required to fully appreciate the dynamics of the system, with focus on improving transients.

Chapter 7

Conclusions

7.1 Overview and System Selection

In an attempt to solve the problems of congestion and pollution in urban environments, a novel vehicle with a narrow wheel track of 1 metre was designed and developed as part of the work presented here. This formed part of the EU-funded project, CLEVER (Compact Low Emission VEhicle for uRban transport).

The CLEVER vehicle is targeted at the current drivers of conventional cars used in urban environments. It aims to marry the comfort and safety advantages of conventional cars with the small road footprint, manoeuvrability and efficiency of a motorcycle. The vehicle is fully enclosed to protect occupants from inclement weather, and the plastic bodywork is mounted on a lightweight frame specifically optimised for good crash performance, comparable to conventional city-class cars.

A number of industrial and academic institutions were involved in the CLEVER project. IFP modified a standard gasoline engine to run on compressed natural gas in order to reduce emissions. A novel refuelling system is developed by WEH Gas Technology to facilitate refuelling in areas where an established CNG supply network is not yet implemented. Running on compressed natural gas not only helps to reduce greenhouse gas emissions within urban environments, but is an advantage from a manufacturer's point of view as, depending on proposed

legislation (based upon the results of this project), a vehicle such as CLEVER could be included in the manufacturer's fleet to reduce the average CO_2 output of a manufacturer's complete vehicle range.

In order to maintain stability in corners, vehicles with a narrow track such as the CLEVER vehicle concept, must tilt towards the centre of the corner to maintain stability, in similar manner to that of a motorcycle. The reason this aids stability is that the lateral acceleration force directed away from the centre of the corner is balanced by the gravitational force pointing downwards, so the component force acts along the centreline of the tilting portion of the body, balancing the vehicle.

As CLEVER is aimed at drivers of conventional cars, the vehicle must have a steering wheel and pedals. Due to the subtle but significant counter-steering input involved in balancing a motorcycle with handlebars, a passive tilting system was not possible in CLEVER. An active tilting system that takes inputs from the driver and the vehicle behaviour was therefore implemented to tilt the vehicle automatically.

Tilting vehicles have been studied in the past, with varying success. The objective of CLEVER was to improve on current technology and existing prototypes by employing modern, robust control methods with an efficient tilt actuation system, and prove the function of the tilting system in a development prototype vehicle.

The development of an active tilting system for a narrow vehicle requires the integration of two fundamental attributes: an active tilt control system and an energy efficient actuation system.

Three methods of active tilt control have been assessed in previous literature, primarily in simulation only. Direct tilt control (DTC), whereby the vehicle tilts by positioning an actuator between two components of the vehicle. When a force is applied between these two components, the relative movement between them results in the vehicle, or part of the vehicle banking towards the centre of the corner. A DTC system takes inputs from the driver and the vehicle behaviour in order to calculate the desired tilt angle, and then outputs a command signal to an actuation system to lean the vehicle. The advantages of such a system are relatively simple implementation, intuitive design, the ability to balance at all speeds, and simple, robust control. The disadvantages relate to the large roll

moment required, resulting from the delay between the generation of lateral acceleration forces and the balancing effect of tilting the vehicle, and the maximum moment that can be applied between the components that, when moved relative to each other, tilt the vehicle.

The second method is steer tilt control (STC), whereby the vehicle is balanced in a similar manner to that of a motorcycle, but the driver inputs are those for a conventional car. The system takes the driver inputs and vehicle behaviour, and controls the steering independently of the driver's steering input, necessary to keep the vehicle balanced while following the desired path. The advantages of an STC system are that the tilting motion is generated by tyre cornering forces, thus no moment is required to tilt the vehicle, and it is argued that the feeling of an STC system would result in a more natural feeling than vehicles controlled using DTC. Disadvantages however are that in low speed situations and when stationary, balancing the vehicle becomes impossible since no restoring moment can be provided by steer control alone. In addition, the steered wheel is controlled independently of the driver's input so a complex steer-by-wire or active steering system is required. These technologies have issues associated with legality and safety, and research is required concerning the important aspect of a reaction torque in the steering wheel providing an element of driver 'feel'.

The third method is a dual mode system, which marries a DTC and an STC system together. Such a system provides stability when stationary and at low speeds, yet has a natural feeling at higher speeds and reduces the disadvantages of the moment requirement and moment generation limitations associated with DTC systems. The problems with a dual system are that complex control is necessary to integrate the two systems in one vehicle, two complete tilt actuation systems are required, and the complication of controlling the front wheel independently of the steering wheel remains.

Two possibilities are available for tilt actuation systems: electric and hydraulic. Difficulties arise with electric systems in automotive systems due to the high current demands necessary to provide the high power to tilt the vehicle, while retaining a low voltage automotive electrical system. Hydraulic systems overcome this difficulty, while also offering the advantages of high power density and flexibility of installation.

For the CLEVER vehicle, a direct tilt system was chosen owing to it robust control method, and the ability to reach the project targets within the required timeframe. This system was married to an efficient hydraulic actuation system which provided the necessary moment to tilt the vehicle through the use of actuators positioned between the front tilting portion of the vehicle, and the rear, non-tilting traction unit.

7.2 Active Control

The active control system for the CLEVER vehicle was implemented electrohydraulically, using sensors to measure driver inputs and vehicle behaviour, and a micro-controller to evaluate the measurements, determine the demand tilt position, and calculate the necessary hydraulic valve signal to initiate tilt motion in a closed loop electrohydraulic tilt position control system.

A simple model of a direct tilt control system was developed to evaluate the performance of such a system and determine the appropriate values of different control parameters. The model was also used to develop the control logic that formed the structure of the control system, and calculations are presented that outline the procedure required in order to determine the position demand value and hydraulic valve control signal. Most importantly, however, the model highlighted specific issues associated with direct tilt control, in particular the limitations of moment generation between the non-tilting base and the tilting body.

To implement the control system on the development vehicle, the necessary hardware components—the micro-controller, signal conditioning cards, and transducers—were identified. The software for the controller was developed in two stages: the first step was to develop the program structure to set up the different functions, enable interaction between the user and the software through the interface, and to access measured data and output command signals. The second step was to implement the code necessary to calculate the position demand value and determine the valve opening to achieve the required tilt angle. Limitations due to the lack of a floating point processor in the chosen controller hardware meant that additional effort and time was required for controller code development, re-

ducing available testing time and limiting the refinement and sophistication of the controller code.

7.3 Hydraulic Actuation

A hydraulic system was identified as the best solution for tilt actuation for the CLEVER vehicle prototype. A hydraulic circuit was designed including the general specification of necessary components.

To establish the dynamic characteristics of the hydraulic system, a linearised valve-actuator model was developed from basic principles, and the operating conditions necessary to ensure proper functionality of the model were determined. Values for natural frequency and damping ratio for the valve actuator system were determined, and the the closed loop system approximated as a first order system produced a time constant.

In order to evaluate the expected system performance, and to select and size components, a fully non-linear model of the complete system was constructed. This model presented promising simulation results, indicating the performance that could be expected from the tilt actuation system. A series of input demands were used and the resulting behaviour was assessed, looking specifically at the system response, the torque load on the engine, the force in the cylinders, and the resulting system pressure. Acceptable performance was achieved for all input demands using the final component specifications. Following this specification list, the necessary hardware was selected and acquired for the development prototype.

7.4 Prototype Construction and Testing

Following the development and simulation of the active controller and the hydraulic actuation systems, a vehicle prototype was designed and constructed with which to assess the performance of the complete tilting system.

The detailed design of the chassis systems was undertaken as part of the Univer-

sity of Bath's role in the CLEVER Project. This involved modelling of components, conducting design analysis using finite element methods, and producing manufacturing drawings and 3D models that were used by component manufacturers to produce the chassis parts.

A donor vehicle was supplied, from which the engine was removed, dismantled, and modified for the application in the CLEVER development prototype. Following the modifications, it was reassembled and installed within the CLEVER vehicle frame along with the ancillary systems. The donor vehicle electrical system was also implemented on the CLEVER vehicle, ensuring reliable engine function. Hydraulic components and active tilt control electronics were installed and commissioned.

Testing was conducted in three stages. Stage one successfully tested the engine, transmission, tilt actuation and active control systems independently of each other, while stage two focused on static testing of the complete tilting system (control and actuation). In stage three, the vehicle was driven to develop, tune and refine the tilting system.

Testing the hydraulic and control system using a frequency sweep demonstrated good response, with the amplitude ratio in the 'worst case' scenario being very close to the demand signal in both amplitude and phase. With the step response, the time constant was 0.15 seconds, which was deemed adequate for preliminary driving tests. Discrepancies were found between these results and the simulated results of the linear analysis in the hydraulics chapter. These differences were associated with the limitations of simulating the system around a specific operating point using the small perturbation technique. Slight differences in this operating point would change the damping ratio and natural frequency values found in simulation, and the associated time constant when approximating the system as a first order lag.

Following some initial modifications, adequate steady state tilt performance was obtained. The transient tilt response, however, was poor, and this issue was exacerbated with heavier occupants.

Increasing the hydraulic system pressure helped alleviate the slow response with heavier drivers, but to improve this further, an increased system gain was neces-

sary. In order to implement this higher gain, a filter was applied to the position error signal to reduce the influence of noise in the command signals. Further testing revealed considerable improvements in response and increased tilting rate.

It was shown through both simulation and experimental testing of the prototype vehicle that roll-over problems can still arise with a direct tilt control narrow track vehicle. This problem is associated with the dynamic tilt torque input that can occur during severe transient manoeuvres. The tilt toque is applied to both the front tilting body and the rear 'non-tilting' chassis but can result in the rear unit rolling out of the bend. A sensitivity of different filter cut-off frequencies revealed that safe handling can only be achieved at the expense of a fast tilt response—a fast tilt response allows the hydraulics to generate enough force to lift either rear wheel instead of tilting the vehicle cabin. The solution of having a safe handling vehicle while providing fast response is ultimately constrained by the *direct tilt control* method employed in CLEVER. Modifications to the chassis may improve the stability at the expense of the advantages offered by a narrow wheeltrack.

This limitation is a fundamental flaw in providing a safe, stable vehicle using the direct tilt control system. To achieve the goal of good tilt response without compromising the stability of the vehicle, an element of steer tilt control should be included to properly synchronise the application of lateral acceleration with tilt angle. Alternatively, an Electronic Stability Programme (ESP) type system could be used to limit the vehicle yaw acceleration and associated tilt torque demand. Using steer and speed as the input signals to the control system means that the tilting system always lags behind the vehicle lateral acceleration, and while smooth steering inputs result in a balanced, stable, and comfortable vehicle in the steady state, the tilt response required for aggressive steering inputs, such as high speed slaloms or emergency obstacle avoidance, seriously compromise the stability of the vehicle. Attempts to limit the moment application between the base and the tilting cabin do not prevent roll over, as the lag between the lateral acceleration and the balanced tilt angle is increased.

In conclusion, this work presents the design and development of a unique narrow track direct tilt control three-wheeler. Simulation studies are presented alongside experimental results from a development prototype vehicle and demonstrate good performance from this highly unusual vehicle, and highlight some of its

limitations.

7.5 Further Work

Within the constraints of a direct tilt control tilting three-wheeled vehicle, there are limitations on improvements that can be made solely in software due to the fundamental issues raised within this research in controlling a tilting three-wheeled vehicle using direct tilt control. It is reasonable that with further development and testing work, and increased controller sophistication, finite improvements could be made. These improvements, however, must lie within the limitations of the technology and control methods employed.

To make significant improvements, modification of the active tilt control strategy is required to improve transient behaviour of the CLEVER vehicle. The solution should focus on development of more sophisticated control strategies, based on a dual mode control method, where an element of steering tilt control is combined with the existing direct tilt control system.

The initial approach could be to assess the effectiveness of applying a lag between steering command and the steered wheel response, thus providing an element of lead for the tilting system, such that the application of lateral acceleration and tilt angle achieve better levels of synchronisation. Another possibility would be to slave the steering control to the tilt system, so that it would not be possible to generate high lateral accelerations before the tilt system was balanced. If the steering wheel command actually actuates the tilting system instead of directly steering the vehicle, similar logic could be used as currently employed to calculate the necessary steer angle based on tilt angle and vehicle speed. (The current vehicle uses steer angle and vehicle speed to calculate the tilt angle – this system would use tilt angle and speed to calculate steer).

In addition to this modification of the tilt control strategy, the active control system requires additional sophistication in order to function appropriately at limit conditions, on low friction surfaces and while traversing cambered surfaces. Through simulation work, proposed improvements such as the use of perceived lateral acceleration as a control signal as well as the implementation of a dual

mode tilt control system could be assessed and evaluated.

Narrow, tilting vehicles possess many advantages over current conventional personal transport options, and the CLEVER vehicle offers a tangible glimpse of technology that could be employed to vehicles of the future, both within, and beyond urban environments. Further research and development is required to ensure that the tilting technology is foolproof, safe, and offers good response while maintaining stability in all situations. The work presented in this thesis, combined with the results of the CLEVER Project, represent the first step of achieving this goal.

Bibliography

[1] EU Funded research project CLEVER, 2002. Contract no. G3RD-CT-2002-00815. `http://tinyurl.com/ naarg`.

[2] The CLEVER Project. `http://www.clever-project.net/`.

[3] B. Sampson. "Lean Machine". *Professional Engineer*, page 39, March 8 2006.

[4] Annex 1 "Description of Work" for CLEVER Project proposal, 2004. Proposal no. GRD2-2001-50079, Revised 22 October 2004.

[5] Ford Focus: Fuel, Performance and Emissions. `http://tinyurl.com/fnd6w`.

[6] S. Hanzl, A. Neumann, J. Stark, and G. Sammer. "CLEVER Deliverable D9: Benefits for Urban Traffic". Technical report, Universität für Bodenkultur Vienna, Institute of Transport, 2005. Internal Report for European Commission.

[7] CO_2 Emission Agreement. `http://ec.europa.eu/environment/co2/co2_agreements.htm`.

[8] University of Bath Press Office, 30 August 2006. `http://tinurl.com/otnbk`.

[9] H. Heisler. *Advanced Vehicle Technology*. Butterworth-Heinemann, Oxford, second edition, 2002.

[10] Vandenbrink Carver One. `http://www.carver-europe.com/`.

[11] Smart fortwo coupé. `http://tinyurl.com/msnrd`.

[12] V. Schindler *et al.* "CLEVER Technical Report Deliverable 2: Technical Product Guideline", May 2003. Internal Report for European Commission.

[13] A. Raman, J. S. Rao, and S. R. Kale. "Overturning Stability of Three Wheeled Motorized Vehicles". *Vehicle System Dynamics*, 24:123–144, 1995.

[14] M. Hall. "GM Lean Machine". Obtained from: `http://www.maxmatic.com/ttw_leanmachine.htm` on 12/10/2003.

[15] D. Karnopp and R. Hibbard. "Optimum Roll Angle Behavior for Tilting Ground Vehicles". *ASME, Dynamic Systems and Control Division (Publication) DSC, Transportation Systems*, 44:29–37, 1992.

[16] P. G. Van Valkenburgh and R. H. Klein. "Three-Wheel Passenger Vehicle Stability and Handling". *SAE Paper 820140*, 1982.

[17] R. S. Rice. "Rider Skill Influences on Motorcycle Maneuvering". *SAE Paper 780312*, 1978.

[18] R. Hibbard and D. Karnopp. "Twenty First Century Transportation System Solutions - a New Type of Small, Relatively Tall and Narrow Active Tilting Commuter Vehicle". *Vehicle System Dynamics*, 25(5):321–347, 1996.

[19] Anon. "Tilting Train". Obtained from: `http://en.wikipedia.org/wiki/Tilting_train` on 13/6/2006.

[20] A. Harrison. "Practical Alternatives for the ZEDIS Tilting System". Technical Report 11/98, University of Bath, 17 March 1998.

[21] M. Hall. "Tilting Three-Wheelers". Obtained from: `http://www.maxmatic.com/ttw_index.htm` on 12/10/2003.

[22] Anon. "The Calleja three wheeler, the future of motorcycling?". Obtained from: `http://www.motobykz.co.uk/3wheel/Calleja_3_wheeler.htm` on 7/1/2004.

[23] D. Karnopp. "The Dynamics of Narrow, Automatically Tilted Commuter Vehicles". In *Proceedings of the 1997 EAEC Congress: Lightweight and small cars: the answer to future needs*, pages 13–19, 1997. Paper number 97A2KN08.

[24] Anon. "The Calleja three wheeler, the future of motorcycling?". Obtained from: `http://www.bat-motorcycles.co.uk/gyrocanopy.asp` on 7/3/2003.

[25] C. van den Brink and H. Kroonen. "Dynamic Vehicle Control for Enclosed Narrow Vehicles". In *Proceedings of EAEC 6th European Congress: Lightweight and Small Cars—The Answer to Future Needs*, 2–4 July 1997. Paper number 97A2I22.

[26] C. van den Brink and H. Kroonen. "Slender Comfort Vehicles: Offering the Best of Both Worlds". *AutoTechnology*, pages 56–59, 1/2004.

[27] H. Andreae. "Pure Leanius". *Autocar*, pages 58–61, February 19 2003.

[28] J. P. Pauwelussen. "The Dynamic Behaviour of Man-Wide Vehicles With An Automatic Active Tilting Mechanism". In *Proceedings of the 1999 EAEC Congress: Vehicle Systems Technology for the Next Century: Conference II — Vehicle Dynamics and Active Safety*, pages 50–58, 30 June–2 July 1999. Paper number STA99C206.

[29] M. Booth. "The tip of a lifetime". *The Independent on Sunday: Motoring*, page 59, 25 April 2004.

[30] C Van den Brink and H. Kroonen. "DVC — The banking technology driving the CARVER vehicle class". In *Proceedings of the 7th International Symposium on Advanced Vehicle Control (AVEC04)*, 13–20 Aug 2004.

[31] J. Voelcker. "Three Wheels Good". *ROVE*, 2006.

[32] Anon. "The F300 Life Jet". Obtained from: `http://www.mercedes-benz.com/com/e/home/innovation/laboratory/researchvehicles/f300lifejet/intro/index.html` on 7/1/2004.

[33] Anon. "Mercedes-Benz F300 Life Jet". Obtained from: `http://www.supercars.de/singlecar/98/59.html` on 7/1/2004.

[34] F. Puhn. *How to Make Your Car Handle.* HP Books, New York, USA, 1981.

[35] J. Reimpell and H. Stoll. *The Automotive Chassis: Engineering Principles.* Arnold, London, UK, 1996.

[36] J. Robinson. *Motorcycle Tuning: Chassis.* Butterworth Heinemann, Oxford, 2001.

[37] J. Robinson. *Pass Your Motorcycle L Test.* Elliot Right Way Books, Kingswood, 1992.

[38] H. Imaizumi, T. Fujioka, and M. Omae. "Rider model by use of multibody dynamics analysis". *JSAE Review*, 17:65–77, 1996.

[39] M. Yokomori, T. Oya, and A. Katayama. "Rider control behavior to maintain stable upright position at low speed". *JSAE Review*, 21:61–65, 2000.

[40] R. Sharp. "Stability, Control and Steering Responses of Motorcycles". *Vehicle System Dynamics*, 35(4–5):291–318, 2001.

[41] D. Karnopp and C. Fang. "A Simple Model of Steering-Controlled Banking Vehicles". *ASME, Dynamic Systems and Control Division (Publication) DSC, Transportation Systems*, 44:15–28, 1992.

[42] V. Cossalter, R. Berrita, F. Biral, and S. Garbin. "Analysis of the Dynamic Behaviour of Actual and New Design Solutions for Motorcycles using the multibody codes of MSC.visualNastran". Obtained from: `http://www.atnet.it/lista/paper83.pdf` on 12/3/2003.

[43] B. Drew, K. Edge, M. Barker, J. Darling, and H. Johannsen. "Review of Tilting Three Wheeled Vehicle Chassis Design". In *Proceedings of FISITA 2004*, 23–27 May 2004. Paper number F2004F382.

[44] M. Barker. *Chassis Design and Dynamics of a Tilting Three Wheeled Vehicle.* PhD thesis, University of Bath, Bath, UK, 2006.

[45] Y. Li, J. L. Meiry, and W. G. Roesler. "An Active Roll Mode Suspension System for Ground Vehicles". *Journal for Basic Engineering*, pages 167–174, 1968.

[46] R. Gohl, R. Rajamani, L. Alexander, and P. Starr. "The Development of Tilt-Controlled Narrow Ground Vehicles". In *Proceedings of the American Control Conference*, 2002.

[47] A. Snell. "An Active Roll Moment Control Strategy for Narrow Tilting Commuter Vehicles". *Vehicle System Dynamics*, 29:277–307, 1998.

[48] J. Golten and A. Verwer. *Control System Design and Simulation.* McGraw-Hill, Maidenhead, 1991.

[49] EC Directive 70/311/EEC. "Steering equipment for motor vehicles and their trailers". Obtained from: `http://europa.eu.int/comm/enterprise/automotive/directives/vehicles/` on 12/2/2004.

[50] W. Kimberley. "Focus on Safety". *Automotive Engineering*, pages 19–36, October 2003.

[51] M. Rösth, J-O. Palmberg, and J. Pohl. "Active Pinion – A Cost Effective Solution for Enabling Steering Intervention in Road Vehicles". In *Proceedings of the Bath Workshop on Power Transmission and Motion Control (PTMC 2003)*, Bath, UK, September 2003.

[52] M. Krenn and T. Richter. "Active Steering — BMW's approach to modern steering technology". In *Proceedings of Braking 2004: Vehicle Braking and Chassis Control*, pages 3–14, Jul 7–9 2004.

[53] S. So and D. Karnopp. "Active Dual Mode Tilt Control for Narrow Ground Vehicles". *Vehicle System Dynamics*, 27:19–36, 1997.

[54] S-G. So and D. Karnopp. "Switching strategies for narrow ground vehicles with dual mode automatic tilt control". *Int. J. of Vehicle Design*, 18(5):518–532, 1997.

[55] R. Hibbard and D. Karnopp. "Methods of Controlling the Lean Angle of Tilting Vehicles". *ASME, Dynamic Systems and Control Division (Publication) DSC, Transportation Systems*, 52:311–320, 1993.

[56] D. Bortoluzzi, R. Lot, and N. Ruffo. "Motorcycle steady Turning: The Significance of Geometry and Intertia". In *Proceedings of the 7th International Conference and Exhibition, Florence ATA*, 23–25 May 2001. Paper number 1A1025.

[57] PML Flightlink. `http://www.pmlflightlink.com/`.

[58] Anon. "Soft, Pilot operated, balanced poppet, Relief valve". Obtained from: `http://www.sunhydraulics.com/cmsnet/cpp.aspx?model_id=709` on 9/3/2004.

[59] Anon. "The Digital-Displacement Pump-Motors – A New Generation of Hydraulics". Obtained from: `http://www.mech.ed.ac.uk/research/wavepower/ddpm.html` on 29/9/2003.

[60] TERN Inc. TD40 Controller. `http://www.tern.com/td40.htm`.

[61] H. Johanssen *et al.* "CLEVER Technical Report: CLEVER Powertrain Report", March 2006. Internal Report for European Commission.

[62] M. Barker. "Simulation of CVT Transmission for the CLEVER Vehicle", November 2004. CPTMC, University of Bath. Internal Report.

[63] 4/2 and 4/3 proportional directional valves direct operated, with electrical position feedback: Types 4WRE and 4WREE, 2003. Rexroth Bosch Group. Catalogue Number RE 29 061/02.03.

[64] P.J. Chapple. *Principles of Hydraulic System Design.* Coxmoor Publishing Company, Chipping Norton, UK, 2003.

[65] M. Sokola. "Fluid Power 3: Hydraulic System Design. Section 4.5.2: Hoses", Nov 2000. CPTMC, University of Bath. Course Notes.

[66] D. Tilley. "Systems and Control". University of Bath. Undergraduate course notes.

[67] Hydraulic Blockset produced by ExpertControl GmbH. `http://www.expertcontrol.com/`.

[68] A. Almondo. "Active Tilting System", February 2004. CPTMC, University of Bath. Internal Report.

[69] Gear pumps, 1998. Rexroth Bosch Group. Catalogue Number 1 987 760 1000/01.98.

[70] A. Filippone. "Aerodynamics Database: Drag Coefficients". Obtained from: `http://aerodyn.org/Drag/tables.html` on 25/8/2004.

[71] Jason hydraulics hydraulic cylinder catalogue. Obtained from `http://www.jasonhydraulics.co.uk/`.

[72] Hydro-pneumatic accumulators, 2003. Rexroth Bosch Group. Catalogue Number 1 987 761 403/06.03.

[73] Sun hydraulics cartridge valves. Obtained from `http://www.sunhydraulics.com/`.

[74] Bimota Tesi 2D. `http://www.bimota.it/scheda_tesi2d_1_eng.htm`.

[75] M. Barker. "Simulation of CVT Transmission for the CLEVER Vehicle", November 2004. CPTMC, University of Bath. Internal Report.

[76] Curvilinear synchronous belt drive systems, 1999. ISO 13050:1999.

[77] C. Matthews. *Engineers' Data Book.* Professional Engineering Publications, Ltd., London, UK, 1998.

[78] M. Dietzen. "Description and Simulation of the Brake System of the CLEVER-Vehicle", April 2004. CPTMC, University of Bath. Internal Report.

[79] D. Limebeer, R. Sharp, and S. Evangelou. "Motorcycle Steering Oscillations Due to Road Profiling". Technical report, Imperial College of Science, Technology and Medicine, UK, 2001. Given as a seminar on 22/2/2002 at University of Cambridge, Dept of Mechanical Engineering.

[80] B. Drew, M. Barker, K. Edge, J. Darling, and G. Owen. "Experimental Evaluation of a Hydraulically Actuated Tilt System for a Narrow Track Three-Wheeled Vehicle". In *Proceedings of the ASME International Mechanical Engineering Congress and Exposition*, 4–11 Nov 2006. Paper number IMECE2006-14606.

[81] Anon. "Butterworth filter". Obtained from: `http://en.wikipedia.org/wiki/Butterworth_filter` on 04/7/2006.